Master Thesis

Pumpability, rheological behaviour and temperature stability of colloidal lignin suspensions and their applications

carried out for the purpose of obtaining the degree of
Diplom-Ingenieur_in (Dipl.-Ing.in)

submitted at TU Wien
Faculty of Mechanical and Industrial Engineering
by

Theresa MAYR

Matr.Nr. 01616731 (033 273)

under the supervision of
Ao.Univ.Prof. Dipl.-Ing. Dr.techn. Michael Harasek[1]
Dipl.-Ing.in Julia Tomasich[1,2]
Ass.Prof. Dipl.Ing. Dr.techn. Walter Wukovits[1]
Dipl.-Ing. Dr.techn. Stefan Beisl[2]

[1]Institute of Chemical, Environmental and Bioscience Engineering, E166
[2]Lignovations GmbH

Wien, September 2023 Signature: _____

Declaration

This work has been supported by the FFG within the framework of FEMtech internships.

I confirm, that the printing of this thesis requires the approval of the examination board.

I declare, that I wrote this thesis and performed the associated research by myself, using only the cited literature. If text passages from sources are used literally, they are marked as such. I confirm that this work is original and has not been submitted elsewhere for any examination, nor is it currently under consideration for a thesis elsewhere. I acknowledge that the submitted work will be checked electronically using suitable and state-of-the-art means (plagiarism detection software). This ensures, on the one hand, that the high-quality standards within the scope of the issued rules for the assurance of good scientific practice - "Code of Conduct" (Mitteilungsblatt 2007, 26. Stück, Nr. 257 idgF.) at the TU Vienna were adhered to. On the other hand, a comparison with other student theses will avoid infringements of my personal copyright.

Theresa Mayr
Wien, September 2023

Signature: _____

Acknowledgements

I would like to express my sincere thanks to some people for their support during my diploma thesis.

This work was made possible by a FemTech grant from the Austrian Research Promotion Agency (FFG) and implemented in cooperation with the Vienna University of Technology and Lignovations GmbH.

Special thanks go to my supervising professor Univ.Prof. Dipl.Ing. Dr.techn. Michael Harasek and thesis adviser Ass.Prof. Dipl.Ing. Dr.techn. Walter Wukovits at TU Wien as well as my thesis supervisors at Lignovations Dipl.Ing. Julia Tomasich and Dipl.Ing. Dr.techn. Stefan Beisl. I am grateful for their guidance, help and constant support during the whole research work.

I would also like to thank all my colleagues at Lignovations not only for their professional input but also for their personal support and help. Johannes, Maria, Stelyiana and Thomas made for incredible lab partners.

At this point, I would also like to thank my parents, family and friends for their continuous support during all my years of studying.

Abstract

Lignin in the form of Colloidal Lignin Particle (CLP) suspensions has gathered significant attention in recent years due to its interesting qualities and wide range of possible applications. The downstreaming of the produced suspensions, as well as their further processing, is dependent on various properties. This thesis encompasses the study of colloidal lignin suspensions, combining two distinct yet interconnected domains: the fundamental investigation of pumpability and temperature stability and the importance of rheology and temperature in their applications.

For the first part, this work focuses on colloidal lignin suspensions. The suspensions' flow behaviour was investigated through rheological measurements, allowing to shed light on their pumpability. Different influences on the rheological behaviour were analysed, such as various CLP concentrations, elevated temperatures, the particle size of the CLPs and the presence of additives and contaminations. Different suspensions' viscosity and flow curves were analysed and brought into context with Dynamic Light Scattering (DLS) and Scanning Electron Microscope (SEM) measurements. The flow curves at higher concentrations and temperatures revealed the non-newtonian character of the suspensions, particularly their shear thinning behaviour. In contrast, suspensions at low concentrations of 3 wt% showed nearly Newtonian behaviour similar to water. The measured dynamic viscosity values were converted into kinematic ones, allowing the highest concentrated suspension C220523 to be analysed and evaluated in terms of pumpability. The rheological measurements at different temperatures also revealed the necessity for temperature control during the pumping process, as elevated temperatures increase the suspensions' viscosities. While the primary particle size could be identified as a lesser influence on the rheological behaviour, the presence of additives and charged particles such as salts were revealed to be a crucial parameter that needs to be controlled. Additionally, the temperature sensitivity was rigorously examined through controlled heating experiments, providing crucial insights into the thermal limits and behaviour of the lignin particles within suspension systems. The results revealed the temperature sensitivity of the CLPs, since temperatures of up to 90°C lead to an increase in the particle size and the appearance of visible precipitating agglomerations. Different heating patterns and raw lignins led to varying amounts of agglomerates, while qualitative UV absorption and Fourier-Transform-Infrared (FTIR) measurements were used to show that the chemical structure remained unchanged.

In the second part of this work, the focus shifts towards applying colloidal lignin suspensions in the production of Pickering emulsions, focusing primarily on personal care and cosmetic applications. By capitalising on their stabilising and anti-oxidative, and UV-blocking properties, the colloidal lignin suspensions were used to create emulsions with varying concentrations and pH levels. Rheological shear controlled and oscillatory measurements of emulsions with different amounts of CLPs revealed their shear thinning properties and increased yield stress with increasing concentration, allowing their characterisation regarding their stability, spreadability and skin feel. Since personal care products often contain various ingredients, the influence of pH on the Pickering emulsions rheology was also evaluated, with the results indicating higher emulsion stabilities for the emulsions with pH values between 3 - 7. Furthermore, the influence of temperature in the production methods on the efficacy of CLP applications is examined through a comparative study of hot and cold production processes for Pickering emulsions. *In vitro* Sun Protection Factor (SPF) measurements were used to evaluate the varying production conditions on their performance impact of the resulting emulsions as a UV blocker.

Kurzfassung

In den letzten Jahren hat Lignin in Form von Suspensionen kolloidaler Ligninpartikel (CLP, colloidal lignin particles) aufgrund seiner interessanten Eigenschaften und vielfältigen Anwendungsmöglichkeiten große Aufmerksamkeit erlangt. Das Downstreaming der hergestellten Suspensionen sowie deren Weiterverarbeitung ist von verschiedenen Eigenschaften abhängig. Diese Arbeit umfasst die Untersuchung von kolloidalen Ligninsuspensionen und kombiniert zwei unterschiedliche, aber miteinander verbundene Bereiche: die grundlegende Untersuchung der Pumpbarkeit und Temperaturstabilität der Suspensionen und die Bedeutung von Rheologie und Temperatur in ihren Anwendungen.

Im ersten Teil dieser Arbeit geht es um kolloidale Ligninsuspensionen. Durch rheologische Messungen wurde das Fließverhalten der Suspensionen untersucht, was Aufschluss über deren Pumpfähigkeit gibt. Es wurden verschiedene Einflüsse auf das rheologische Verhalten analysiert, wie unterschiedliche CLP-Konzentrationen, erhöhte Temperaturen, die Partikelgröße der CLPs sowie das Vorhandensein von Zusatzstoffen und Verunreinigungen. Sowohl die Viskositäts- als auch die Fließkurven der verschiedenen Suspensionen wurden analysiert und mit Messungen der dynamischer Lichtstreuung (DLS, dynamic light scattering) und mittels Rasterelektronenmikroskop (SEM, scanning electron microscope) in Zusammenhang gebracht. Die Fließkurven bei höheren Konzentrationen und Temperaturen zeigten den nicht-newtonschen Charakter der Suspensionen auf, insbesondere ihr strukturviskosem (scherverdünnendem) Verhalten, während Suspensionen bei niedrigen Konzentrationen von 3 Gew.% ein nahezu newtonsches, wasser-ähnliches Verhalten zeigten. Durch Dichtemessungen wurden die dynamischen Viskositätswerte in kinematische umgewandelt, so dass die höchstkonzentrierte Suspension C220523 analysiert und hinsichtlich ihrer Pumpbarkeit bewertet werden konnte. Die rheologischen Messungen bei verschiedenen Temperaturen zeigten auch die Notwendigkeit einer Temperaturkontrolle während des Pumpvorgangs auf, da erhöhte Temperaturen zu einer erhöhten Viskosität der Suspensionen führten. Während die primäre Partikelgröße einen geringeren Einfluss auf das rheologische Verhalten zeigte, erwies sich das Vorhandensein von Additiven und geladenen Partikeln wie Salzen als ein entscheidender zu kontrollierender Parameter. Darüber hinaus wurde die Temperaturempfindlichkeit durch kontrollierte Erhitzungsexperimente eingehend untersucht, was wichtige Erkenntnisse über die thermischen Grenzen und das Verhalten der Lign-

inpartikel in Suspensionssystemen lieferte. Die Ergebnisse zeigten die Temperaturempfindlichkeit der CLPs, da Temperaturen von bis zu 90°C zu einer Zunahme der Partikelgröße sowie zum Auftreten von sichtbaren Ausfällungsagglomerationen führten. Verschiedene Erhitzungsmuster und Roh-Lignine führten zu unterschiedlichen Mengen an Agglomeraten, während qualitative UV-Absorptions- und Fourier-Transformations-Infrarot (FTIR, foureir transformed infrared) Messungen zeigten, dass die chemische Struktur unverändert blieb.

Im zweiten Teil der Arbeit liegt der Schwerpunkt auf der Anwendung kolloidaler Lignin-suspensionen bei der Herstellung von Pickering-Emulsionen, besonders im Bereich der Körperpflege- und Kosmetikanwendungen. Unter Ausnutzung ihrer stabilisierenden sowie antioxidativen und UV-blockierenden Eigenschaften wurden die kolloidalen Ligninsuspensionen zur Herstellung von Emulsionen mit unterschiedlichen Konzentrationen und pH-Werten eingesetzt. Scherraten kontrollierte und oszillatorische Messungen des rheologischen Verhaltens von Emulsionen mit unterschiedlichen Mengen an CLP zeigten deren strukturviskose Eigenschaften und eine Zunahme der Fließspannung mit zunehmender Konzentration, was ihre Charakterisierung in Bezug auf ihre Stabilität, Verteilbarkeit und ihr Hautgefühl ermöglichte. Da Körperpflegeprodukte häufig verschiedene Inhaltsstoffe beinhalten, wurde auch der Einfluss des pH-Werts auf die Rheologie der Pickering-Emulsionen untersucht, wobei die Ergebnisse auf eine höhere Stabilität der Emulsionen bei pH-Werten zwischen 3 und 7 hindeuteten. Darüber hinaus wurde der Einfluss der Produktionstemperatur auf die Wirksamkeit von CLP-Anwendungen untersucht, indem ein Vergleich von heißen und kalten Produktionsverfahren für Pickering-Emulsionen durchgeführt wurde. Mit Hilfe von *in-vitro*-Messungen wurden die unterschiedlichen Produktionsbedingungen hinsichtlich ihrer Auswirkungen auf die Leistung der resultierenden Emulsionen als UV-Blocker bewertet.

Contents

Abbreviations

CLP Colloidal Lignin Particle

CP Cone-Plate

DLS Dynamic Light Scattering

DLVO Derjaguin Landau Verwey Overbeek

DMC Dry Matter Content

FTIR Fourier-Transform-Infrared

HD Hydrodynamic Diameter

IUPAC International Union of Pure and Applied Chemistry

LVE Linear Visco-elastic

LVR Linear Visco-elastic Region

MCT Medium-chain triglyceride

PP Plate-Plate

SEM Scanning Electron Microscope

SPF Sun Protection Factor

UV Ultraviolet

Nomenclature

Symbol	Description	Unit
a	Radius of particle	m
BP	Power consumption of the pump	W
D	Diameter	m
D_p	Pipe diameter	m
F	Force	m
F_L	Durand factor	$-$
g	Gravitational acceleration	m/s^2
G'	Storage modulus	Pa
G''	Loss modulus	Pa
$G*$	Complex modulus	Pa
η	Dynamic viscosity	Pas
η_m	Dynamic viscosity of the medium	Pas
η_O	Total pump efficiency	kW
γ	Shear strain	$\%$
γ_{crit}	Critical strain	$\%$
γ_f	Flow point	Pa
$\dot{\gamma}$	Shear rate	s^{-1}
$\dot{\gamma}_w$	Shear rate at pipe wall	s^{-1}
H	Head of the pump	m
K	Power law coefficient	$kg/(m * s^{2-n})$
k_B	Boltzmann constant	J/K
m	Mass	kg
n	Power law index	$-$
ν	Kinematic viscosity	m^2/s
ϕ	Volume fraction	$-$
ψ	Potential	V
ψ_{DLVO}	DLVO potential	V
Q	Flow rate	m^3/s

Continued on next page

– continued from previous page

Symbol	Description	Unit
ρ	Density	kg/m^3
ρ_l	Density of liquids	kg/m^3
ρ_m	Density of medium	kg/m^3
ρ_p	Density of particle	kg/m^3
ρ_s	Density of solids	kg/m^3
R^2	Coefficient of determination	$-$
σ	Stress	Pa
τ	Shear stress	Pa
τ_0	(Apparent) Yield stress	Pa
ζ	Zeta potential	V
T	Temperature	$℃$
v	Velocity	m/s
v_{cr}	Critical velocity	m/s
V	Volume	m^3
ω	Angular frequency	s^{-1}
$\tan\delta$	Loss factor	$-$

Chapter 1

Introduction and motivation

In recent years, the growing concerns over climate change highlighted the acute need for sustainable alternatives to fossil fuels [10]. As a result, the focus has shifted towards using renewable and environmentally friendly resources. As the second most abundant natural polymer after cellulose in plants [31], lignin has emerged as a promising candidate in this quest for a greener future [93]. It is a complex phenolic polymer found abundantly in dry-land plant cell walls [31] and holds immense potential for a wide range of applications [24, 22, 93]. Forming colloidal lignin particles expands the possible high-value utilisation of lignin [63], as the micro-size opens up new properties while keeping the antimicrobial, UV-filtering and other advantageous characteristics of lignin [22].

The ability to pump and handle fluids is vital for optimising industrial processes' overall efficiency and operational cost [2]. Furthermore, the rheological characteristics significantly influence their pumpability [60], and therefore also the processing of colloidal lignin suspensions. Understanding the rheology of colloidal suspensions is crucial for designing efficient pumping systems, preventing clogging sedimentation, and minimising energy consumption [60, 2, 58]. Properties such as concentration and morphology of particles and the addition of ions can significantly alter the process-relevant rheological characteristics [88]. Also, the temperature has a significant impact on the handling of suspensions, not only in terms of rheology but the stability of the suspension itself. Research by Leskinen et al. and Fritz et al. showed different reactions of CLP suspensions to rising temperatures, underlining the need to further study the temperature stability of CLPs [41, 23].

In addition to suspensions, colloidal lignin emulsions, which are mixtures of immiscible liquids stabilised by lignin particles, called Pickering emulsions [83], have also gained attention due to their potential as green alternatives in various applications [64, 4, 67]. The properties of lignin make the colloidal lignin emulsions an exciting system for cosmetic products such as sunscreens [94, 85, 28], as the use of fossil-fuel-based surfactants are avoided [64]. The rheological properties of these emulsions are critical for long-term stability, texture, and the desired spreadability of the final product [86, 39]. However, since the production process of

cosmetic products typically involves high temperatures [12, 17], the usage of temperature-sensitive CLPs in Pickering emulsions can have an influence on the functionality of the Pickering emulsions.

Therefore, this thesis aims to explore the pumpability and rheology of colloidal lignin suspensions and emulsions, as well as their temperature stability. By investigating these fundamental properties, valuable insights can be identified into the handling and processing of lignin-based materials. Essential influences on rheology are analysed and evaluated and brought into the context of the pumpability of suspension. Simple heating experiments were used in order to determine the temperature stability of the suspensions. This can contribute to the development of sustainable high-value lignin applications, such as colloidal lignin emulsions, whose rheological behaviour and temperature sensitivity were also investigated.

The work is expanding on the research on the handling of the downstream processing to increasing the CLP concentration in colloidal lignin suspensions [54], as well as the application of CLPs in Pickering emulsions [85].

Chapter 2

General theoretical background

2.1 Biorefinery

The challenges posed by climate change have led to a growing interest in the use of renewable resources in recent years. Biorefineries have emerged as a promising solution to this demand [35]. The International Energy Agency (IEA) defines the biorefinery concept as "the sustainable processing of biomass into a spectrum of marketable products and energy" [8]. Currently, most chemical products are produced by oil refineries, in addition to oil being the primary energy source for the transport sector. As the use of fossil resources by humans and the subsequent emission of greenhouse gases are tied to the earth's changing climate, the search for alternative production chains in the transport and chemical industries led to biomass in order to realize a sustainable economy [10]. Using biomass such as crops or algae not only offers a renewable source of raw materials for a wide range of products but can also positively affect agricultural jobs and rural spaces [32].

Biorefineries can be seen as analogous to crude oil refineries, where multiple products are produced from petroleum [15, 10]. They can be classified according to four main features: (1) platforms, (2) products, (3) feedstocks and (4) processes [32]. (1) Platforms include intermediate products that can be transformed further, linkages between different biorefinery concepts or the final product. In contrast to oil-based platforms, bio-platform molecules contain more oxygen, allowing a shift from harsh oxidation chemistry to one of reduction [10].(2) The biorefinery products can be grouped into two main categories: materials and energy products [10]. Examples of the first include chemicals, organic acids, polymers and biomaterials, while the latter includes biogas, pellets and biofuels for transportation. (3) The raw materials or feedstocks can be extracted from agriculture, forestry, or aquaculture like crops, short rotation forestry and algae [32]. Also, residues from these sectors and trade and industry can be the basis for biorefinery processes. The primary biomass feedstocks are carbohydrates, lignin, and triglycerides [10]. Like petroleum, biomass's composition is complex, making it necessary to separate and process it further to produce an extensive

product palette [35]. (4) These conversion processes include biochemical, thermochemical, chemical and mechanical processes [32]. Depending on the feedstock, platform and product processed in the biorefinery specific technologies are used. Similar to oil refineries, the biorefinery concept represents an integrated system where waste production is minimized, and all resources are used[10].

Lignocellulose biorefineries are just one of the various advanced biorefinery concepts designed to use a wide range of feedstock to produce a spectrum of different products [32]. It is an up-and-coming concept since the conflict between food and energy production for the biomass used as raw material is reduced. Lignocellulose encompasses cellulose, hemicellulose and lignin and is a widely available, renewable and inedible raw material for biorefinery processes [89, 66]. The distribution of the components in lignocellulosic biomass can be seen in Figure 2.1. The content of each component is 35 to 50%, 20 to 35% and 15 to 30% respectively[8].

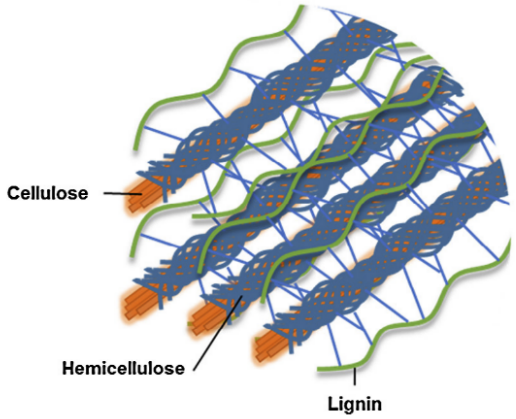

Figure 2.1: Schematic figure of the distribution of lignin in lignocellulosic biomass, taken from [22].

The realizable products are marketable in both traditional petrochemical and future biobased markets. Possible intermediate products include furfural and hydroxymethylfurfural, which are platform chemicals for a range of different end-products, as well as glucose and xylite [35]. Currently, most lignocellulose biorefineries focus on the valorization of cellulose and hemicellulose, while lignin is used as fuel, adhesive or binder. In order for future biorefineries to be cost-effective on an industrial scale, the processing of lignin to value-added products is of interest, like the sustainable production of aromatics due to lignin's naturally occurring phenolic rings [89, 66]. Difficulties in obtaining this valorization of lignin are mainly due to its complex structure and the high reactivity of lignin fragments [89].

2.2 Lignin

As described in the previous section, lignin is one of the components of lignocellulose. After cellulose, lignin is the second most abundant biopolymer in lignocellulosic biomass and accounts for around 30 % of the organic carbon in the biosphere [22]. Its central role in plants is structural, strengthening and supporting the cell wall. Still, it also enables the transport of water and solutes through the vascular system and protects the plant against environmental stresses, like UV radiation. In lignocellulosic biomass, it is arranged around the cellulose strands together with hemicellulose throughout the primary and secondary cell wall, linked through covalent bonds to the cellulose structure [22]. The function of lignin in plants is strongly linked to these covalent crosslinks [63].

Lignin is an amorphous polymer comprising three different methoxylated phenylpropane building blocks: sinapyl, coniferyl and *p*-coumaryl alcohols. These building blocks are linked through ether and carbon-carbon bonds [27] and differ in the substitution at positions 3 and 5 [31]. The aromatic rings of these building blocks are referred to as syringyl or S (two methoxy groups), guaiacyl or G (one methoxy group) and *p*-hydroxyphenyl or H units (no methoxy group), respectively and contain a phenyl group and propyl sidechain [27]. Depending on the origin, the makeup of the lignin differs: the primary building block for softwood lignins is coniferyl alcohol (G-type). For hardwoods, it is coniferyl and sinapyl alcohols (GS-type) and *p*-coumaryl is most prominent in grasses (HGS-type) and compression wood (HG-type) [31, 27]. Figure 2.2 shows a schematic figure of the lignin building blocks. Generally, two-thirds of lignin bonds are ether bonds, while the rest are carbon-carbon bonds. More than half of the bonding structures comprise β-O-4' ether linkages, bonding the monomers together [22]. The characterization of the bonds is determined by the carbon atoms on the aliphatic side chains (α, β, γ) and those in the aromatic moieties, which are numbered from 1 to 6 [27].

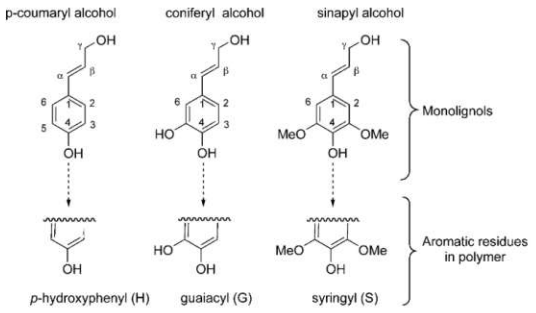

Figure 2.2: Schematic figure of the lignin building blocks, adapted from [24].

The extraction of lignin is difficult as depolymerization of the lignin is necessary to separate it from carbohydrates. Due to the tendency of lignin and its fractions to re-polymerize, new C-C bonds are formed during extraction leading to different intermediates with various properties [89]. The extracted product differs depending on the lignin source and the extraction process used [22]. Currently, there are four main industrial extraction processes for pure lignin:

kraft, sulfite, organosolv and soda process. The primary process to extract lignin from lignocellulosic biomass is the kraft process, where the lignin is dissolved at high temperatures and pH values in sodium hydroxide and sodium sulfide. After that, the dissolved lignin is precipitated using acid. Kraft lignin contains small amounts of sulfur groups and is usually sulfonated to make it soluble in water. The process is responsible for 85 % of the world's lignin production. However, it is also highly integrated into the pulp and paper industry, which relies on the produced lignin as fuel for process heating [27]. The sulfite process encompasses the production of lignosulfonates by extracting lignin using several salts of sulfurous acid [24]. Calcium, magnesium and sodium act as counter ions [22]. The sulfur content in the lignosulfonates is higher than those from the kraft process, and they are soluble in water. Lignin from non-wood feedstocks is usually extracted using the soda process, where it is solubilized at higher temperatures using an aqueous solution of sodium hydroxide in the presence of a catalyzer. The extracted lignin is difficult to recover but is sulfur-free, making it a valuable starting material for high-value lignin products. The organosolv process is another method to obtain sulfur-free lignin [24]. Here, lignin is extracted from lignocellulosic biomass using a mixture of organic solvent and water at high pressure and temperature. Common organic solvents include various alcohols with reagents. Then, the lignin is precipitated using acids [24] or recovered by evaporating the organic solvent [22]. The lignin from organosolv processes is sulfur-free, still has its native structure and has higher purity. However, the method has the disadvantage of equipment corrosion and lower pulp quality. Other extraction methods for lignin include steam explosion [24] and ionic liquids as green solvents for biomass processing [27].

Lignin shows antioxidant, antimicrobial and antifungal properties and can absorb UV radiations [22]. Other interesting properties include the fire-retardant character of lignin, hydrophilic or hydrophobic features, good rheological characteristics and broad compatibility with various chemicals. Lignin can be described as moderately stable at higher temperatures because of the presence of aromats in its chemical structure [76]. Thermogravimetric analyses are often used to study the properties of lignin by measuring the weight-loss of the sample during thermal degradation [93]. Lignin starts to decompose at temperatures from 150° to 275°C, where the breakage of α- and β-ether linkages occurs [53]. At 300°C the aliphatic side-chains split off from the aromatic ring, at 370° to 400°C the carbon-carbon bonds are broken and at temperatures higher than 500°C the measured thermogravimetric curve flattens out as volatile pyrolysis products are released and char is formed. The temperature when decomposition occurs depends on the structure of the lignin. The thermal behaviour of lignin shows thermosetting as well as thermoplastic characteristics [76]. The chemical structure and the present hydrogen bonds give cause to the thermoplastic behaviour, meaning it can be repeatedly brought into new shapes with the application of heat. The poor flow behaviour often prevents the use of lignin as such a material. Thermoset materials on the other hand build a cross-linked structure at elevated temperatures, which was shown to be the case for lignin. Research showed that softwood kraft lignin showed a dramatic increase in its molecular weight after reaching 20°C above its glass transition temperature of 153°C. At temperatures above 100°C [42], lignin also undergoes condensation reactions in aqueous

medium [41].

For the valorization of lignin, new transformation processes must be developed to obtain lignin with the necessary properties for a specific application [93]. Two main paths for the functionalization of lignin can be identified. The first is the direct use of lignin without chemical modifications or selective functionalization of the macromolecule. Possible products include lignin in composites, copolymer materials, adhesives, resins and carbon fibres. The second path involves the production of low molecular weight chemicals that can replace fossil fuel-based building blocks. For this, the lignin is de-polymerized by thermochemical or biotechnological processes. This makes it possible to obtain low-value carbon sources for energy production and high-value products like vanillin. Lignin embodies the largest renewable reservoir of aromatic compounds. However, the current separation techniques for lignocellulosic materials lead to a heterogeneous raw feedstock, which should be improved for more efficient and economic lignin extraction [24]. Another challenge in the valorization of lignin is the difficult selective conversion of lignin caused by its natural degradation resistance and heterogeneous structure [89]. A novel approach to lignin valorization is the preparation of colloidal or nano-sized lignins [63]. The colloidal particles could solve the aforementioned heterogeneity issues and the poor solubility of lignins due to the well-defined surface chemistry and shape. The size and shape of the particles also open up new possible applications in drug delivery or sunscreen formulations.

2.3 Colloidal lignin particles

In recent years there has been an increased interest in colloidal lignin particles. As mentioned in the section above, lignin has considerable potential for high-value applications. However, using it for applications is a significant challenge due to its heterogeneity and complexity after extraction [94, 5]. Producing nano- or micro-sized lignin particles provides an exciting opportunity to face these challenges. Particles, especially in the range of 1 to 100 nm, have an increased surface area [5]. The phenomenon of gaining new attractive properties in nanoscale materials is called the "quantum effect", which occurs due to either the expanded surface area to volume ratio or the possibility for new tunable properties at this scale [94]. At the same time, the interesting properties of lignin, such as non-toxicity, anti-UV, antimicrobial and oxidation resistance, are still present [9]. Also, most lignins are only soluble in water at alkaline pH, but with micro and nanosized particles, it is possible to prepare aqueous dispersions, making it possible to overcome industrial scale limitation of poor water solubility [5]. The nomenclature for smaller-sized lignin particles in the literature is not always compatible with the IUPAC definition for nanoparticles, which only ranges up to 100 nm [37]. The size range for most published particles go from 10 to 1000 nm, thus making the term CLPs more appropriate for this size range.

2.3.1 Production

The preparation of CLPs includes various methods such as anti-solvent precipitation, mechanical methods, emulsion inversion [94] as well as biological methods [9].

Anti-solvent precipitation This method is based on the insolubility of lignin in water and acidic solutions while showing good solubility in organic solvents [94]. The process of dissolving lignin in an aqueous organic solvent, followed by precipitation in a non-solvent (usually water), can also be referred to as solvent shifting, solvent exchange or nanoprecipitation [64]. Typical solvents include tetrahydrofuran (THF), ethanol, acetone/water and dimethyl sulfoxide [5, 94]. Independent of which solvent is used, the precipitation is based on the tendency of lignin to assemble in spherical particles when in contact with the non-solvent phase to reduce the surface area [64]. In addition to water, acidic solutions can be used as anti-solvent. Frangville et al. proposed using aqueous HCl as an anti-solvent to precipitate lignin particles from ethylene glycol [5]. While the addition of acid to an alkaline lignin solution shifts the pH value so that precipitation also occurs, the particles produced this way are not as colloidally stable as those produced by solvent shifting [64] and the method is referred to as pH-shifting [5].

Emulsion inversion The emulsion inversion method is based on the dissolution of two monomers or polymers with different active groups in two unmixable solutions, respectively. At the interface of the solutions, an emulsion inversion occurs when one solution is disperged in the other [94]. Beisl et al. [5] describe several cross-linking methods. One possible setup is the solution of lignin in NaOH and adding the solution to an oil phase made up of octane and surfactants and gently turning it upside down to prepare the emulsion. The cross-linking was then achieved by adding epichlorohydrin under gentle stirring. The oil removal was accomplished by adding excess water and centrifugation.

Mechanical methods The preparation of CLPs by mechanical methods based on mechanical force or ultrasound avoids using chemicals and, therefore, the environmental impact is reduced [94]. Possible preparation strategies include ultrasonication, high-shear homogenization, or a combination of multiple mechanic means. When using ultrasonication, the molecular bonds of lignin are broken down under ultrasonic energy resulting in smaller lignin particles. For high-shear homogenization, the bond breakage is achieved by high shear forces during the dispersing and homogenizing of lignin particles in a suspension or emulsion. Generally, CLPs prepared by ultrasonication have less sedimentation and are more stable than those prepared by high-shear homogenization [9].

Biological methods The biological methods include the use of microorganisms as well as enzymes to prepare CLPs [9]. The microbial method includes the degradation of lignin through specific microorganisms. Compared to the mechanical methods described above, the yield is lower. However, the dispersibility of the CLPs increases. The enzymolysis method

can obtain dry or wet particles using specific enzymes to decompose and remove substances other than lignin.

Other methods Other preparation methods reported in the literature include ice segregation, aerosol processing, CO_2 antisolvent and electrospinning methods [5].

The chemical methods above result mostly in wet particles, while the mechanical and biological methods lead to the production of powdered products [9]. Wet particles are typically formed in aqueous media and have a hydrophilic surface, allowing for easy surface modifications that can benefit different applications [64]. Particles prepared with the solvent exchange or the inversion emulsion method can be obtained by freeze- or spray-drying of the dispersed particles. However, the drying process has to be controlled, or the formation of aggregate structures and irregular powder will occur. Generally, higher temperatures affect the inter-particle forces in colloidal suspensions as well as the interactions of particles with the suspending medium, which in turn, can impact the particle aggregation, stability and rheology of the suspension [6]. According to Fritz et al. who studied the self-association and aggregation of kraft lignins using turbidity measurements, an increase in temperatures from 25° to 70°C lead to the aggregation of lignins [23]. Leskinen et al. used thermal treatments up to 191°C to induce cross-linking in aqueous lignin suspensions to reinforce spherical CLP particles showing higher stability against dissolution in known solvent systems [41]. Also, the thermal treatment led to a darkening of the colour of the suspensions.

2.3.2 Applications

As already described, CLPs hold the same exciting properties as lignin, and the nano- and micro-sized particles can provide additional potential for high-value applications. Table 2.1 was adapted from Beisl et al. [4] and shows an overview of possible lignin applications, either through direct usage or after further processing steps. As the usage of CLPs is possible in various applications, this work limits its effort to give only a short overview of some. For a more detailed description, Beisl et al. [4] and Österberg et al. [64] provided a more detailed account of possible applications.

One of the first reported applications of the particles is as dispersants or, to be more precise, surfactants [64]. Typical industrial dispersants, like polystyrene, are often of synthetic origin, not biodegradable and are produced from non-renewable materials. Surfactants stabilise emulsions, consisting of two or more immiscible liquid phases dispersed in each other by mechanical shearing [9]. CLPs provide a more sustainable alternative to common surfactants by forming Pickering emulsions [64]. Here, the emulsion is stabilised by any colloidal solid particles at the surface of emulsion droplets, where they are adsorbed [67]. A later chapter will provide further information on Pickering emulsions (subsection 3.1.2). Pickering emulsions have received increased attention from the cosmetics and pharmaceutical industry due to their higher biocompatibility, stability against coalescence and reduced Ostwald ripening phenomena. According to Österberg et al., [64] this was also confirmed for Pickering emul-

Application	Direct usage	Further processing	Possible applications
Surfactant	Pickering emulsions		
Reinforcement	In Polymer blends		
Carrier		Carbonization Protein coating Agent infusion	Fertilizer Pesticides Nanomedicine
Antioxidant	Food additive Food packaging		
Biocide		Epoxydation Silver infusion	Food packaging Impregnating agent Membrane additive Substitute for silver particles
UV-Blocker	Sunscreens Food packaging Impregnating agent		
Carbon Materials and Energy Storage		Carbonization	Anode materials Adsorbent Supercapacitors

Table 2.1: Overview of the applications of colloidal lignin particles, adapted from [4] and [9]

sions stabilised by colloidal lignin particles. While not only bringing environmental benefits over common Pickering emulsion particles due to their compostability, CLPs also bring the additional benefit of UV-shielding and anti-oxidation properties.

Precisely these properties also open up other applications for the colloidal lignin particles. The functional groups such as phenol and ketone present in the chemical structure of lignin can absorb a wide range of ultraviolet light and reduce ultraviolet radiation [94]. Yearla and Padmasree [92] compared the potential of lignin nanoparticles in protecting *Escherichia coli* against UV-induced mortality. They showed that nanoparticles were more efficient in protecting the bacteria from UV-induced mortality compared to bulk lignin. This opens up possible applications of colloidal lignin particles in the food, pharmaceutical and cosmetics industries [22], for example, in food packaging films or sunscreens [94].

While CLPs show a wide range of potential applications from pharmaceuticals to energy storage, these are dependant and determined by particle morphology, colloidal particle production method as well as the source of the raw lignin [4]. In biorefinery processes, it is crucial to determine suitable products to reach the potential lignin valorisation possible with CLPs.

Chapter 3

Specific theory

This chapter serves as a brief introduction to the key aspects investigated in this work, explaining the most relevant theoretical concepts and giving definitions to the relevant terminology.

3.1 Colloidal systems

There are two main colloidal systems investigated in this work: Colloidal suspensions and Pickering emulsions. According to IUPAC, colloidal systems are dispersions were particles of colloidal size of any aggregate state are dispersed in a continuous phase [19]. Disperse systems where the disperse phase is solid and the disperse medium is liquid are refered to as suspensions, while an immiscible liquid in a liquid dispersion medium is called emulsion [82]. The term colloid generally refers to the dispersed phase of a two component system, that is too small to be easily observed by a microscope [50]. The size range encompassing colloidal systems extends from 1 nm to 1000 nm for the dispersed particles or droplets [82]. The lower size limit of 1 nm allows for the dispersion medium to be considered as a continuum since the mass of the colloid is significantly larger than the molecule mass of the medium [50]. The upper limit ensures that the dispersed phase does not settle under the gravitational forces acting on it but remains suspended in the dispersion medium.

3.1.1 Colloidal suspensions

The key theoretical concepts of colloidal systems will be explained using colloidal suspensions as an example but also apply to the other types of colloidal dispersions. Three forces are acting on the individual colloidal particles: Brownian force, hydrodynamic force and gravitational force [50]. The Brownian force (Equation 3.1) results from the random thermal collisions of the particles and the suspension mediums' molecules, leading to diffusive motion. The thermal energy unit $k_B * T$ consists of the Boltzmann constant k_B and the

absolute temperature T and the denominator of the equation is the particle radius a.

$$F_B = \frac{k_B * T}{a} \tag{3.1}$$

The hydrodynamic force or Stokes drag (F_h) is shown in Equation 3.2, with η_m being the viscosity of the medium and v being the velocity of the particle.

$$F_h = 6\pi\eta_m a v \tag{3.2}$$

Lastly, colloidal particles are subject to the gravitational force F_g, which acts on a particle with density ρ_p in a medium with density ρ_m (Equation 3.3). The typical gravitational force on a colloidal particle is often comparable to or less than the Brownian force, resulting in the suspension of the particles in the medium [50].

$$F_g = \frac{4}{3}\pi a^3 g(\rho_p - \rho_m) \tag{3.3}$$

To understand the properties of colloidal suspensions such as the rheology, one must look at the inter-particle interactions [82, 65]. The interaction of colloidal particles in water is best described by the Derjaguin Landau Verwey Overbeek (DLVO) theory. [72]. The DLVO theory describes the relation between repulsive electrostatic forces and attractive forces, mainly Van der Waals forces [72], and can help to explain the dispersion or coagulation of colloidal systems [65].

At this point, some definitions regarding the de-stabilized form of dispersions should be given. These definitions can be used for both emulsions and suspensions. The IUPAC manual on Definitions, Terminology and Symbols in Colloid and Surface Chemistry [19] defines a suspension as colloidally stable when "the particles do not aggregate at a significant rate". Aggregation describes the formation of aggregates, which are structures formed by colloidal particles being held together. The terms flocculation and coagulation are often used synonymously for aggregation when talking about fluid colloidal systems. The term flocculation is often used for the formation of a loose network, while coagulation describes the formation of compact aggregates.

The electrostatic interactions considered in the DLVO theory arise due to the formation of an electrical double layer. The particles generally have a surface charge, which attracts counter ions and co-ions at some distance from the surface that compensate this charge [82]. The particle surface charge can arise due to the suspending of the particles in liquid by surface acids or bases, by adsorption of free ions or by adsorption of charged surfactants [50]. The thickness of the double layer is described by κ^{-1}, the so-called Debye length [65], which increases with a decrease in electrolyte concentration [82]. The potential Ψ decreases over the

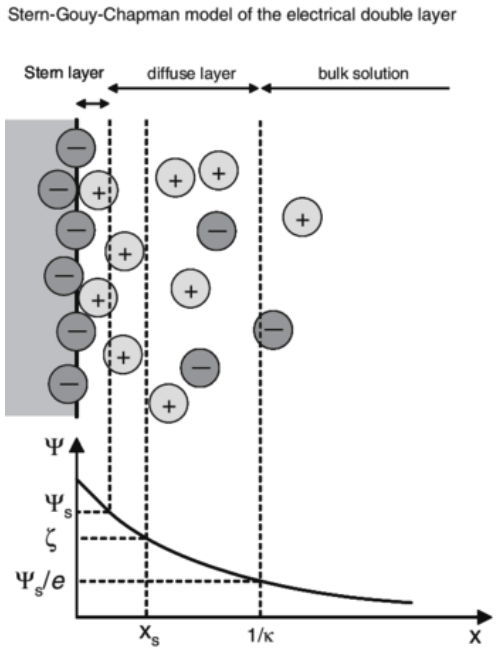

Figure 3.1: Schematic figure of the electrical double layer as described by Stern-Gouy-Chapman, taken from [30]. The figure shows the arrangement of the ions around the particle surface as well as the potential Ψ over the thickness of the double layer

thickness of the electrical double layer. Close to the surface of the particle, there is a non-diffusive layer of specifically absorbed ions, the so-called Stern-layer, where the potential decreases linearly. This layer can be further divided into the inner Helmholtz plane (for chemically adsorbed ions) and the outer Helmholtz plane (for physically adsorbed ions with a hydration shell). After the Stern layer, the ions are diffuse in nature and the potential decreases exponentially. Figure 3.1 provides a schematic overview of the electrical double layer and potential Ψ. ζ is the so-called zeta potential, which indicates the electrokinetic potential and is the potential drop across the mobile part of the double layer [19]. A high zeta potential is a good indicator for a stable suspension in combination with a low electrolyte concentration and ion valency [82]. When two charged colloidal particles interact, the double layers begin to overlap and the particle separation becomes less than twice the Debye length. The resulting repulsion arises mostly due to the osmotic repulsion because of the large number of ions in the double layer [50].

The second type of forces considered by the DLVO theory are van der Waals forces, which are short-range attractive forces between particles due to the fluctuations in the electron density distributions [82]. In the DLVO theory the two forces, electrostatic force and van der Waals forces are added to form the combined DLVO potential Ψ_{DLVO} [50]. The resulting curve presents a primary minimum, an activation energy barrier and a secondary minimum. This is shown in Figure 3.2a. When the total potential interaction energy is stronger on the repulsive side, the potential remains positive [13]. Thus, the suspension can be regarded

as stable as it is unlikely for aggregation to occur. If the potential is negative or has a small positive value, the particles attract each other [65]. Three possible energy potentials are shown in Figure 3.2b. If a colloidal system shows a deep secondary minimum, the particles can flocculate as there is long-range attraction [82]. However, this flocculation is reversible for example by shear or sonication. For particles to reach the primary minimum, an activation energy barrier has to be overcome. If the barrier is not high enough, Brownian motion can lead particles to overcome the barrier and move to a distance where the van der Waals attraction is prominent [72]. This can lead to aggregation and the particles form secondary structures. Due to the resulting size increase, the energy balance may change, and the system re-stabilizes as this secondary structure. Since the double-layer thickness is dependent on the concentration of electrolytes and the valency of the counter-ions [82], manipulating the ionic strength of the suspension medium can reduce the activation barrier enough so that coagulation occurs [13]. Also, the pH can influence colloidal stability [50]. It plays a role in the surface charge of the colloid as the latter may be determined by the dissociation of acids and bases on the particle's surface.

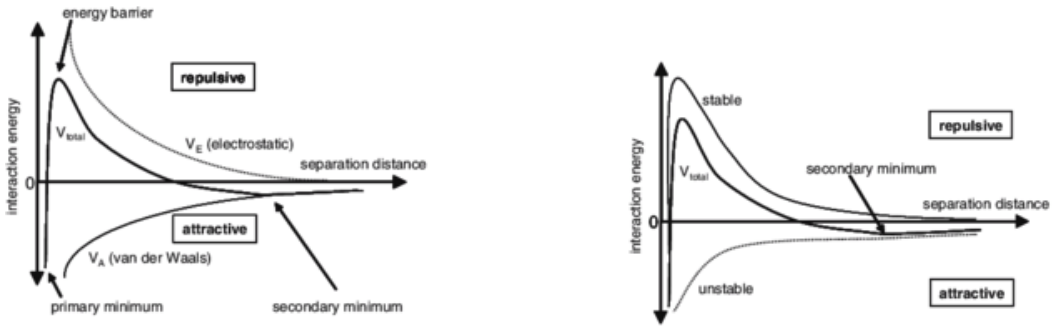

(a) (b)

Figure 3.2: Schematic diagram of the DLVO interaction energies, taken from [30]. The left side shows how the combination of electrostatic interaction and van der Waals forces results in a curve with a primary and secondary minimum and an activation barrier. The right-hand side shows three possible situations: a stable system, one with a primary and secondary minimum and an unstable system.

The conventional DLVO theory only considers the electrostatic and van der Waals forces [65]. However, there might be additional forces to consider such as steric forces that originate due to the adsorption of polymers onto the particle. A colloidal system can be stabilized using electrostatic stabilization, where the van der Waals attraction is overcome due to the addition of ionic surfactants, or it can be sterically stabilized due to the addition of non-ionic surfactants or polymers [82].

Colloidal lignin particles in water can form an electrical double layer due to the phenolic hydroxyl groups and possible carboxyl groups [43], which are also the cause for the negative charge of lignin [11]. Both Lievonen et al. [43] and Riviere [73] showed that CLPs have a

negative surface charge since the zeta potential was sufficiently high/negative to ensure an electrostatic repulsion and therefore a stable suspension. According to Lievonen et al., this is due to the adsorption of hydroxyl ions on the particle surface. The addition of a high enough salt concentration can lead to the reduction of the zeta potential, resulting in the reduction of the electrical double layer thickness and therefore the aggregation of particles [43]. Also, the lowering of the pH value can lead to a reduction of the zeta potential as the charged groups are protonated. This can lead to aggregation and sedimentation [73].

3.1.2 Pickering emulsions

The concept of Pickering emulsions was already introduced in subsection 2.3.2. An emulsion is generally defined as a liquid-in-liquid dispersion [19]. The suspended fluid takes a droplet form in the suspending medium. If the latter is an aqueous solution, the emulsion can be denoted as an "O/W" ("oil in water") emulsion. If the continuous phase is an organic liquid this changes to "W/O". For the formation and long-term stability of emulsions a third component, namely the emulsifier is needed [83]. In the case of Pickering emulsions, the emulsion is stabilized by solid particles which accumulate at the oil and water interface and are wetted by both liquid phases. While this type of emulsion was already discovered in 1907, it gained renewed interest in the last years [91]. This is due to the fact that particles can bring about higher stability and lower toxicity compared to common emulsifiers. The particles might also carry interesting and useful characteristics. Pickering emulsions can be used for a variety of applications in various fields such as biomedicine, food and cosmetics.

The particles for Pickering emulsions should be wetted by both liquid phases forming the emulsion [1]. Which type of emulsion (O/W or W/O) is produced depends on which phase the surface of the particle is preferably wetted by [83]. If the particle is wetted more by the oil phase, the particle is hydrophobic and a water-in-oil emulsion is formed. For the oil in water emulsions, it is the opposite. This can be quantified using the three-phase contact angle θ, which is the angle at the boundary of the solid particle and the two liquid phases [91]. It is measured in the aqueous phase and determined using the Young equation (Equation 3.4) [1]. The two types of emulsion, as well as the corresponding contact angle for two different particles, are shown in Figure 3.3. When the contact angle is smaller than 90°C, the particles are mostly hydrophilic, can stabilize O/W emulsions and are mostly immersed in the aqueous phase [1]. Contact angles larger than 90°C represent the opposite: the particles are hydrophobic and W/O emulsions are stabilized by them. If the particles are too hydrophobic or too hydrophilic, no stabilization can occur, since the particles remain dispersed in the respective phase [91].

$$cos\theta = \frac{\gamma_{PO} - \gamma_{PW}}{\gamma_{OW}} \tag{3.4}$$

As mentioned in subsection 2.3.2, colloidal lignin particles can be used for the formation of Pickering emulsions. This is not only due to the advantages of Pickering emulsions over

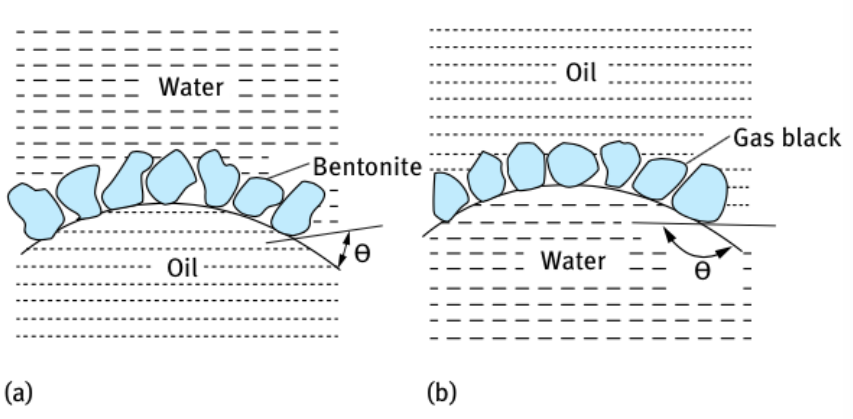

Figure 3.3: Schematic figure of O/W (a) and W/O Pickering emulsions (b), with hydrophilic and hydrophobic particles respectively, taken from [83].

general emulsions, like the higher stability against coalescence and reduced Ostwald ripening phenomena, but also because of the antioxidant and UV-resistance properties of CLPs. Coalescence and Ostwald ripening represent two types of emulsion breakage [83]. During coalescence, emulsion droplets fuse into larger ones and the liquid film between them becomes thinner. Ostwald ripening also leads to larger droplets, but here it is due to the mutual solubility often present in the two emulsion liquids. As lignin is a heterogeneous polymer, the type of lignin can influence its hydrophobic and hydrophilic characteristics [11]. Depending on the CLP production method, the extraction method of the lignin as well as the origin of the raw material the contact angle of the CLPs can change. Farooq et al. [20] showed the more hydrophilic character of CLPs originating from a solvent-shifting process and traces it back to the formation of the particles, where the hydrophobic groups present in lignin are oriented inward, while the hydrophilic functional groups are oriented outward to interact with water. This is also shown in the research conducted by Tomasich et al. [85], where contact angle measurements of CLPs produced with the solvent-shifting method from lignin extracted by different methods displayed the CLPs hydrophilic character. CLPs with mostly hydrophilic character lead to the formation of O/W emulsions [85, 11].

3.2 Pumpability

Merriam-Webster defines pumpability as "the quality, state, or degree of being pumpable" [70]. A pump is used to transport fluids from one location to another [68]. The movement results due to the increase of the total energy content of a fluid with mechanical work, either by velocity acceleration, pressure increase or both [2]. Pumps are used in nearly all industries, from petroleum refineries to water pipelines. As the pump requirements vary significantly from process to process, many pump designs are available [61].

Two pump classes can be distinguished based on how energy is added to the fluid: dynamic

and displacement pumps [2]. Dynamic or rotodynamic pumps constitute one or more impellers with vanes, which rotate and are surrounded by a pump casing [61]. The energy conversion process harnesses the forces generated as liquid flows around the vanes. Inside the impeller, the velocity of the fluid is increased to speeds higher than at the exit velocity. Due to velocity reductions in or after the pump, a pressure drop is created [2]. Depending on the liquid flow direction, one can distinguish between radial, or so-called centrifugal, and axial pumps (propellers) [61].

In displacement pumps, the higher fluid energy is reached by a force that moves the fluid from the low to the high-pressure side [2]. Here, two sub-types can be distinguished as well [61]. Plunger pumps move a particular volume by a reciprocating motion. Gear pumps, on the other hand, squeeze the enclosed liquid and expel it into the outlet.

Centrifugal pumps are the most used type of pump in the chemical industry and are available in various sizes, discharge heads and capacities [68]. They are suitable for about 80% of all pump requirements [60] and have the advantage of low investment and maintenance costs, simple design and adaptability [68]. Displacement pumps are commonly used for high pressure, small flow and viscous fluids, but can also be more advantageous for low pressure uses [60].

The performance of pumps is commonly characterized by the total head H, the power consumption of the pump BP, the total pump efficiency η_O and the flow rate Q [2]. The head H represents the energy added to the fluid between the suction and delivery nozzles of a pump per unit weight of fluid. Equation 3.5 shows how the head can be calculated. h_d represents the delivery head, while h_s is the suction head at the pump suction nozzle. v_s and v_d are the velocity at the suction and delivery nozzles, respectively, and z_s and z_d represent the elevation.

$$H = (h_d - h_s) + \frac{v_d^2 - v_s^2}{2g} + (z_d - z_s) \tag{3.5}$$

The pump's power consumption BP is the pump input power and can be calculated by multiplying the driving torque with the angular velocity [2]. The overall efficiency η_O is the output power divided by the input power. The output power of a pump represents the energy added to the fluid per unit of time, which is the product of the total head and the mass rate of the liquid. The overall efficiency is given by Equation 3.6. The pump performance characteristics can be presented graphically as iso-efficiency curves.

$$\eta_O = \frac{\rho Q H}{BP} \tag{3.6}$$

The selection of a pump for a process depends on the operating conditions of the process, such as flow, temperature, head, pressure, viscosity and fluid properties [60]. The liquid properties of the fluid, such as viscosity or corrosiveness are especially critical for selecting

the correct type of pump and need to be considered in the specifications when purchasing a pump. To reach an economic operation, optimal pump performance should be achieved to minimize operational and energy costs [2].

3.3 Basic concepts of rheology

In simple terms, rheology is the science of the deformation and flow of a material resulting from a force exerted on it [88]. Knowledge of the relationship between stress and deformation is essential in industrial applications, for example, when planning and constructing transfer systems or obtaining structural information about a material.

Before describing more advanced rheological concepts, it is necessary to define some key terminology, focusing on fluid and fluid-like materials. Generally, two types of exemplary rheological behaviour of a material can be distinguished [88]. An ideally fluid or viscous material deforms as long as stress is applied, retaining the form it had at the moment as the stress is removed. Ideal solid or elastic materials deform to an extent at once and regain their original shape after the applied stress is removed. Fluids exhibiting viscous and elastic properties are called visco-elastic [68].

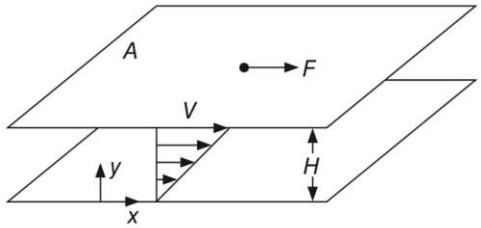

Figure 3.4: Schematic figure of a fluid subjected to shear stress, taken from [68]

In general, stress describes the force per unit area which causes deformation [82]. To explain simple shear flow, a basic set-up of a fluid between two parallel planes with an area A and a separation distance h can be considered [68], as shown in Figure 3.4. The bottom plate remains fixed while a force is applied to the upper plane, causing it to move with a defined velocity v, leading to fluid movement. The shear stress τ is the force per unit area A [68] and has the unit Pa [82]. Due to the no-slip condition, the velocity at the lower plate is zero, and a velocity profile over the height is established [68]. The velocity gradient for this profile is the shear rate $\dot{\gamma}$ and has the unit s^{-1}. Fluid flow is usually more complex than this simplified case. However, this approach allows for the classification of fluids into rheological types using the relationship between shear stress and shear rate. The graphic depiction of this relationship is called rheogram [68] or flow curve [82]. An exemplary rheogram is shown in Figure 3.5.

Newtonian flow behaviour or ideal-viscous flow can be described by the so-called Newtonian

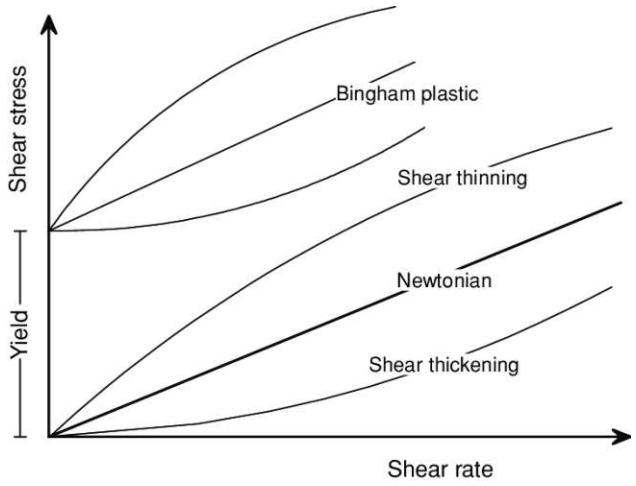

Figure 3.5: Schematic figure of flow curves for different types of flow behaviour, taken from [55]

viscosity law shown in Equation 3.7 [52]. Liquids that follow this law are called Newtonian liquids. The viscosity η is a material constant for these fluids at a constant temperature. The shear stress is proportional to the shear rate, resulting in a linear curve in the rheogram. The slope of the flow curve gives the viscosity and is not influenced by the magnitude or time of shearing [88]. The viscosity is usually displayed in so-called viscosity curves, where the viscosity derived from the flow curve is depicted over the shear rate [52]. The curve results in a straight line for a Newtonian fluid, as the viscosity does not change with the shear rate. Water is a typical example of a Newtonian fluid [55].

$$\tau = \eta\dot{\gamma} \tag{3.7}$$

For non-Newtonian liquids, the shear stress is not proportional to the shear rate, and the viscosity resulting from the relationship between τ and $\dot{\gamma}$ is not necessarily constant [46]. If the slope of the flow curve is decreasing, the fluid can be described as shear-thinning or pseudo-plastic [52]. For a shear-thinning fluid, the viscosity decreases with an increasing shear rate [88]. However, if the viscosity increases with the shear rate, the fluid is described as shear-thickening. The slope of the flow curve is then increasing [52]. Examples of shear-thickening fluids include starch dispersions, paper coatings and natural rubber, while polymer solutions and melts, organic binders and shampoos are usually shear-thinning.

The fourth type of flow curve shown in Figure 3.5 is Bingham plastic or Bingham fluid. The Bingham model is a fitting function for flow and viscosity curves that allows the user to quickly characterize and compare the fluids measuring data [52]. The Bingham model extends the Newtonian law by adding a yield stress and is described by Equation 3.8 [55]. The yield stress τ_0 is the stress value required before continuous deformation occurs [68]. The existence of an actual yield stress τ_0 in a fluid is still debated by scientists, as some

consider it as left-over stress resulting from a very high Newtonian viscosity at low shear rates. However, this viscosity is so high for many fluids that yield stress is an engineering reality in practical uses. Therefore, the term apparent yield stress is used [79]. Typical Bingham fluids include margarine, tomato paste and chocolate paste [55].

$$\tau = \tau_0 + \eta\dot{\gamma} \tag{3.8}$$

In addition to the Bingham model, various other curve fitting models exist to approximate flow behaviours [52]. The behaviour of non-Newtonian fluids can be modelled using a power law shown in Equation 3.9 [68]. The coefficient K shown in the equation is the power law coefficient, and the exponent n is the dimensionless power law exponent. As the model applies to non-Newtonian fluids, the dimensionless power law exponent can indicate which flow behaviour the fluid displays. If $n < 1$, the fluid is shear-thinning, while $n > 1$ implies shear-thickening behaviour. With an exponent of $n = 1$, the power law is synonymous with Newton's law.

$$\tau = K * \dot{\gamma}^n \tag{3.9}$$

Various measurement systems to investigate rheological properties are available [88]. Generally, two measurement principles can be differentiated: Either the fluid is set in motion or 'dragged' along by the moving of one of the walls, or it passes through a pipe through pressure [51]. The viscosity and flow curves in the industry are often derived from rotational tests [52] performed by rheological measuring systems belonging to the first category [51]. The device should create a simple shear flow with a laminar flow field and constant shear rate throughout the sample. There are various measurement geometries available, with the coaxial cylinder, the Cone-Plate (CP) and the Plate-Plate (PP) configuration being among the most frequently used [88]. They are shown in Figure 3.6.

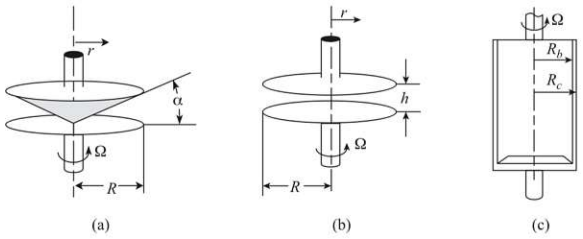

Figure 3.6: Schematic figure of the measuring geometries (a) Cone-Plate, (b) Plate-Plate and (c) coaxial cylinder, taken from [51]

In the coaxial cylinder set-up, the sample is sheared between the two cylinder surfaces, with one of the cylinders moving. The system consists of an inner cylinder, the bob, and an outer cylinder, the cup, with the fluid confined between the two [52]. In the Couette system, the

external cylinder moves, while in the Searle system, the inner cylinder is set in motion [88]. This geometry is often used for low-viscosity fluids, as they cannot flow out the measuring gap between the cylinders [52]. The CP and PP measuring set-up consist of two plates, where the upper plate is in motion while the lower plate is stationary. As the name suggests, the moving plate is cone-shaped for the first geometry, with cone angles up to 5°, while the latter is flat. The CP measurement geometry has the advantage of a constant shear rate in the measurement gap. However, for fluids containing solid material, the particle size is limited. The measurement gap is set automatically depending on the geometry of the cone used, and the particles present should not be larger than 20% of the gap height. The PP geometry does not have this size limitation. Here the gap setting should be adjusted to a value at least five times larger than the largest particles present [52]. It is, therefore, often used for samples containing larger particles and highly visco-elastic materials. The disadvantage of the plate-plate set-up is the inconstant shear rate across the measurement gap, which can influence the measurement results.

The described measurement geometries can be used to perform rotational tests to determine the flow and viscosity curves as well as the time-dependent behaviour, if present, of samples [52]. In addition, they can be used to perform oscillatory tests, which allow the quantification of visco-elastic behaviour [55]. They are based on small, sinusoidal amplitude deformations in a simple shear field performed on the sample. The measurement allows the determination of many visco-elastic properties, with the storage modulus G' and loss modulus G'' being among the most relevant. The storage modulus represents the elastic component of a visco-elastic material and indicates the amount of energy stored. On the other hand, the loss modulus stands for the dissipated energy and, therefore, the viscous component. The moduli can be brought into relation via the Cox-Merz analogy Equation 3.10 and used to calculate the complex modulus $G*$ [50]. The complex modulus defines the overall stiffness of the sample [55].

$$G^* = \sqrt{(G')^2 + (G'')^2} \tag{3.10}$$

The oscillatory tests consist of two parts: Amplitude sweeps and frequency sweeps [52]. During amplitude sweeps, the period of time of each oscillatory cycle, indicated by the frequency, is kept constant, while the amplitude of the measurement geometry in motion varies. Values for the storage modulus G' and loss modulus G'' can be obtained during these tests as well as the limiting value of the Linear Visco-elastic Region (LVR). The LVR represents a range where material properties remain unaffected by stress magnitude, deforming strain magnitude, or strain application rate [55]. When the critical strain value, which represents the end of the LVR, is surpassed, the structure of the sample has been changed, and micro-structural properties can no longer be related to it [52]. For the frequency sweeps, the amplitude of the oscillation is set to a value inside the LVR and remains constant while the frequency is changed. Frequency sweeps can be used to investigate the time-dependent deformation of a sample.

3.3.1 Rheology of colloidal dispersions

The rheology of colloidal dispersions, such as colloidal suspensions and emulsions, depends on the interplay of three main forces: hydrodynamic, Brownian and colloidal (inter-particle) forces [82]. Hydrodynamic forces occur in all flowing suspensions and are the result of the relative particle motion to the surrounding fluid [26], where the flow causes energy to be dissipated [49]. As mentioned in section 3.1, Brownian motion results due to the thermal movement of the particles and the surrounding fluids' molecules [26, 50]. The colloidal or inter-particle forces are a kind of potential force and result in an elastic response [26], meaning they return to the non-deformed state after the stress is lifted [50]. The rheological behaviour of suspensions containing particles in size ranges from 1 to 10000 nm results from the combination of these three forces [26].

Generally, the viscosity of the colloidal system is dependent on the viscosity of the continuous phase, which would be the liquid medium in the case of suspensions [26]. The addition of particles to a liquid leads to an increase in viscosity [59, 88, 26]. The viscosity for a dilute suspension of hard, non-aggregated round particles can be approximated using Einstein's equation (Equation 3.11), which is dependant on the viscosity of the liquid medium η_L, volume fraction ϕ and the intrinsic particle viscosity $[\eta]$ [26]. $[\eta]$ is determined by the particle shape and is 2.5 for rigid round particles. This shows the dependence of the rheology on parameters such as the viscosity of the continuous medium, the particle concentration and morphology.

$$\eta = \eta_L(1 + [\eta]\phi) \tag{3.11}$$

When the particle concentration is higher than $\phi > 0.05$, the interactions between the particles are considerable, and the Einstein equation can no longer be used to calculate the viscosity [49]. This is due to increased hydrodynamic interactions and random particle collisions with increasing particle concentration [26]. Consequently, adding particles can also lead to a deviation in the flow behaviour [14]. Aqueous colloidal suspensions at moderate particle volume usually show non-Newtonian, shear-thinning behaviour, where the viscosity decreases with increasing shear rate. Brownian motion and particle interactions keep the particles in a random arrangement at low shear rates, which is then disturbed as hydrodynamic effects become more prominent with increasing shear. On the other hand, highly concentrated suspensions often do not start to flow until a finite stress is reached and the developed structural network breaks down. In addition to the concentration, particle size, morphology, and size distribution can influence the rheology. Electrostatically stabilized systems are also sensitive to the addition of electrolytes or pH change, which can lead to aggregation and undesirable rheological behaviour [51]. At lower concentrations of particles, the formation of aggregates can lead to increased viscosities but still liquid-like behaviour, while at higher concentrations, it may lead to the appearance of a yield stress and elasticity.

Vliet and Lyklema [88] summarized the main characteristics of colloidal suspensions which influence the rheological properties. This was adapted for Table 3.1.

Type of interactions		Factors of importance	
Between	**Nature**	**Of the particles**	**Of the liquid phase**
Particles and liquid phase	Hydrodynamic	Volume fraction Size distribution Surface smoothness Deformability	Viscosity Elasticity Yield stress
		Flow situations such as: laminar or turbulent flow	
Particles	Hydrodynamic	Hydrodynamic interaction between particles and the liquid phase, insofar that the particles affect the flow pattern around each other	
	Interparticle	Size Van der Waals forces Zeta potential Charge and charge distribution Steric forces due to adsorbed substances	Ionic strength Type of ions pH Dielectric permittivity Solvent quality

Table 3.1: Main characteristics of colloidal suspensions which influence the rheological properties, adapted from [88]

While similar to some aspects of suspension rheology, the flow behaviour of emulsions demonstrates three main distinctions [84]. One, due to the stabilization with a surfactant, the two liquid interfaces now respond to deformation. Also, the viscosity of the dispersed phase affects the emulsion's rheology relative to the viscosity of the medium. Lastly, the emulsion droplets are deformable, which can influence the rheology of emulsions, especially at a high volume fraction. When the emulsion droplets are deformed, the interfacial energy is stored, resulting in elastic properties [86]. After considering these three differences, the bulk rheology of emulsions can be measured and examined the same way as suspensions [84]. Changes in the particle concentration, volume fraction, pH or ionic strength can influence the size distribution of the emulsion droplets, which in turn affects the texture, shelf-life and appearance. Rheological measurements such as steady-state shear flow and oscillatory measurements can be used to determine the physical stability of emulsions [86], as well as the consistency and skin-feel (for cosmetic applications) [39].

3.4 *In-vitro* SPF measurement

"The SPF value of a sunscreen is defined as the ratio of the energy required to produce a minimal erythema dose (skin reddening or minimal sunburn) through the sunscreen compared with the energy required to produce the same reaction in the absence of the sunscreen" [47]. Sunscreens protect the skin from ultraviolet radiation by either absorbing, reflecting and or scattering it [62]. Light with wavelengths from 290 to 320 nm is called UVB radiation, which can be absorbed by DNA, cause mutations and is a tumour promoter. UVA radiation, on the other hand, causes the skin to age with wavelengths of 320 to 400 nm. Two types of sunscreen can be distinguished: chemical absorbers and physical blockers. Chemical sunscreens absorb ultraviolet radiation and can be further divided into UVA or UVB filters depending on the wavelength they absorb. Physical blockers also scatter UVA and UVB radiation in addition to absorbing it. Common physical sunscreens include titanium dioxide (TiO_2) and zinc oxide (ZnO) as active agents [56]. They are often used in the form of nanoparticles, as they do not cast a strong whitening effect on the skin, however, agglomeration of the particles can decrease the effectiveness as a sunblock and consumer acceptance. Both physical and chemical sunscreens come with disadvantages such as controversial studies regarding the toxicity of the nanoparticles [56] and the environmental concerns and bio-accumulation in organisms for synthetic filters [28]. Because of this, there is a growing interest in natural UV filters such as colloidal lignin particles, as mentioned in subsection 2.3.2. With its aromatic structure, lignin can act as an absorber for UV radiation [28] in a light range from 250 to 400 nm [74]. Lignin has shown great potential in enhancing sun protection when mixed with lotions and creams, as well as with other commercial sunscreens, which results in a synergistic effect boosting SPF even at low doses of 1-3 wt% [74]. Micro- and nano-size lignin offer even higher UV-blocking properties compared to unprocessed lignin.

The determination of the SPF is carried out using a standardized, in vivo methodology set by the norm ISO 24444:2022-07 [18]. The test method is a laboratory procedure where a xenon arc lamp is used as a sun simulator. The evaluation of the SPF is carried out on skin sections on the back of the chosen ten to twenty test subjects. One section is left without protection, one is smeared with the to-be-tested sunscreen and a third section is protected by a standard sunscreen with a fixed SPF. All three sections are exposed to radiation and are visually assessed for the presence of erythemas after sixteen to twenty-four hours. The SPF is then calculated as a mean value from all the valid individual SPF results of each test subject. The drawbacks of this method are high costs, long duration and ethical questions since the test subjects are deliberately subjected to radiation [78]. However, the ISO 24444:2022-07 standard is the only regulatory-approved method to determine SPF values.

An alternative, especially for research purposes, are *in vitro* methods [78]. The difficulties herein mostly lay in the choice of an alternative substrate to human skin and the process application control, which are the main reasons for the not fully successful reproducible *in vivo* results, still there is an increasing interest in alternatives to the current tests. *In vitro* methods are based on the transmittance of UV light through a layer of sunscreen applied

to a quartz slide prepared with a suitable substrate. Qian et al. [71] and Gordobil et al. [28] used such a method to evaluate the application of lignin as a sun-protecting agent by mixing it into commercial sunscreens. The samples were measured over a wavelength range encompassing both the UVA and UVB radiation (290-400 nm) and the transmittance was recorded. The final *in vitro* SPF can be calculated using Equation 3.12, where E_λ is the CIE erythemal spectral effectiveness, S_λ is the solar spectral irradiance and T_λ is the measured transmittance of the sample.

$$SPF = \frac{\sum_{290}^{400} E_\lambda S_\lambda}{\sum_{290}^{400} E_\lambda S_\lambda T_\lambda} \tag{3.12}$$

Chapter 4

Materials, instruments and methods

The goal of this thesis is to investigate the pumpability, rheological behaviour and temperature stability of both CLP suspensions and their application as a Pickering emulsion. For the suspensions, general influences on the pumpability of colloidal suspensions were identified based on the literature research described in subsection 3.3.1. This knowledge was then applied to investigate the impact of the concentration of the suspensions, the temperature, the particle size of the CLPs and the addition of salt. For this, viscosity measurements provided by another research project were analyzed and correlated to the pumpability of the suspensions. In addition to the rheological examinations, the suspensions were also analyzed in regard to their particle size using DLS and SEM. To investigate the temperature stability of CLP suspensions, they were heated at various temperatures and lengths. The treated fluids and resulting aggregates were then analyzed using different methods such as DLS, UV spectroscopy, FTIR and dry matter content measurements.

As described in chapter 2.3.2, CLP suspensions have a wide range of possible applications. Especially for uses in cosmetics, the ability to form and stabilize emulsions, not only the resulting rheological behaviour is relevant, but also the temperature stability due to the production process. Research by Tomasich et al. compared Pickering emulsions stabilised by CLPs produced from various bulk lignins using steady shear stress and oscillatory tests [85]. Expanding on this work, the rheology of emulsion-based CLP applications and the influence of varying CLP concentrations in emulsions were investigated. Additionally, the influences of pH changes accomplished by the addition of acid and base on the viscosity and stability were studied and analyzed. The temperature stability of the CLPs in an application was examined by producing lignin Pickering emulsions similar to sunscreen at higher and lower temperatures and the subsequent comparison of their *in-vitro* SPF values.

4.1 Materials

4.1.1 Suspensions

Different colloidal lignin suspensions were examined for their pumpability and temperature stability, as well as that of Pickering emulsions. All are listed in Table 4.1. The different raw lignin sources were processed to a colloidal form by solvent shifting, where the lignin was first dissolved in an ethanol and water mixture and then precipitated using water. The production of the CLP suspensions was not carried out by the author of this work and will not be explained in greater detail. Further information on the production method can be found in Beisl et al. 2020 [3]. After the suspension production, membrane separation methods as described by Miltner et al. [54] were applied to increase the CLP concentration in the suspension and remove impurities and solvent background. After production, 5 wt% of preservative was added (Pentylene glycol, Innometics) to a part of the product (C220601PG).

Batch No. #	Dry matter wt%	Source of raw material
C220329	9.06	Enzymatic hydrolysis of hardwood
C220523	21.10	Enzymatic hydrolysis of hardwood
C220601	15.40	Enzymatic hydrolysis of hardwood
C220601PG	14.63	Enzymatic hydrolysis of hardwood
C220712	14.26	Enzymatic hydrolysis of hardwood
C210803	4.850	Enzymatic hydrolysis of softwood
C211005	5.700	Soda lignin from wheat straw

Table 4.1: Overview of the colloidal suspensions used, their corresponding dry matter content and the source of the CLP raw material.

4.1.2 Emulsions

To investigate the rheological behaviour and temperature stability of CLPs in applications, two types of Pickering emulsions were produced: One similar to commercial sunscreen containing a Ultraviolet (UV) filter and one based on a simple oil phase.

To produce an emulsion similar to sunscreen, a mineral-based sun-protectant was added to an emulsion with shea butter and babassu oil. The UV-dispersion HallBrite® EZ-FLO ZDX by Hallstar Beauty consists of ZnO (60%), Butyloctyl Salicylate, Tricetеareth-4 Phosphate and Triethoxycaprylylsilane. Shea butter, also known as Butyrospermum Parkii butter, and the babassu oil (Orbignya Oleifera oil) were acquired from Naturkosmetik Werkstatt (Product number SW10440.1 and SW10578.3) and used to prepare the sunscreen like emulsion. The fat phase for each of the emulsion was made up of 17.5 g of babassu oil and 17.5 g of shea butter. To this, 15 g of the mineral sunscreen filter containing ZnO (Hallbrite EZ FLO ZDX) was added. This mixture was then heated up to reach 80°C while stirring with a magnetic

stirrer rod. After keeping it at this temperature for 5 minutes, the mixture was left to cool down to 55°C while being stirred. Then, 50g of CLP suspension was slowly mixed into the hot fat phase with the UltraTurrax® at 8000 rpm until a homogeneous cream is formed.

For the second type of emulsion, Medium-chain triglyceride (MCT) oil by Naturkosmetik Werkstatt (Product number: SW10555), consisting of Caprylic/Capric Triglycerides, was mixed with the CLP suspension. The original CLP suspension was diluted with deionized water to receive 50 g of a solution with a concentration of 4.85wt%. The diluted CLP suspension was then mixed for 2 minutes with an UltraTurrax® T25 digital by IKA (Dispersing Tool S 25 KD – 25G) at 8000 rpm. Then, 50 g of MCT oil was slowly added to the suspension while mixing with the same velocity for at least two minutes or until the emulsification was completed. The resulting emulsion has a 1:1 ratio of water and oil phase. The concentration of CLPs in the emulsion is therefore half of the concentration of the suspension used for the preparation. The emulsions were filled into disposable 50 ml containers. A smaller sample amount was also stored in a 10 ml centrifugation tube for 24 hours at room temperature. After the waiting period, the stability of the emulsions was optically assessed.

4.1.3 Chemicals

Salt To investigate the influence of salt on the suspension viscosity, NaCl was added. For this, simple table salt by Salinen Austria AG with a purity of 98.3% was used.

Acid and base To reach the different pH-values in the emulsions, NaOH and H_2SO_4 were used. For the base and acid, one l of 0.1 M stock solution was prepared. The NaOH by Sigma Aldrich has a purity of $\geq$98%. Using the molar mass of NaOH of 39.9970 g/mol, the necessary amount of base to reach a 0.1 M solution can be calculated to 3.9997 g of NaOH. This amount was weighed and filled to 1 litre in a volumetric flask. The H_2SO_4 by Honeywell had a purity of 97%. Using the molar mass of 98.08 g/mol, the 0.1 M stock solution was prepared accordingly.

4.2 Instruments

Rheometer The rheological measurements were carried out with an MCR300 rheometer by Anton Paar. The temperature was regulated using the built-in Peltier element. The rheometer was used to measure the dynamic viscosity of all suspensions and both types of emulsions over a shear rate range as well as additional oscillatory tests for the emulsions containing ZnO. Two measuring geometries were used: a 25 mm PP (PP25-1; Cat. No. ; Anton Paar) and a 50 mm CP (CP50-1; Cat. No. 79040; Anton Paar) system. The measuring gap size between the measuring plates can be set by the user. The setup of the used rheometer with a Plate-Plate measuring system is shown in Figure 4.1.

To start a measurement, a sample amount of the examined suspension or emulsion was put on the lower plate with a disposable pipette. Then the upper plate was lowered and

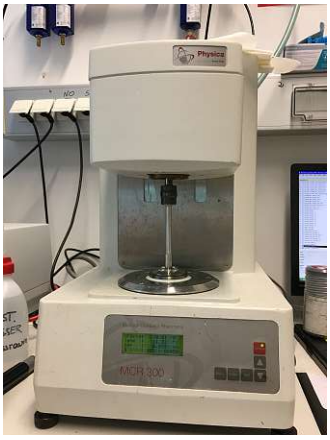

Figure 4.1: Set-up of the rheometer MCR300 by Anton Paar with a Plate-Plate measurement system

the excess sample on the plate border was cleaned off. The measurement started with a resting period of 50 seconds, to ensure the settlement of the sample between the plates after exposing it to shear by withdrawing the sample from the container. During the steady shear measurements, the shear stress, dynamic viscosity, speed and torque were recorded. For oscillatory tests, an amplitude sweep followed by a frequency sweep was carried out. For each sample, three measurements were taken and the mean values were calculated. After the end of the measurement, both plates were cleaned with acetone. The measurements were not carried out by the author of this work but were made available for analysis and discussion by Lignovations GmbH.

Particle size The particle size of the colloidal lignin suspensions was determined via dynamic light scattering measurements with the Particle Analyzer Litesizer 500 by Anton Paar. The particle size was expressed as the Hydrodynamic Diameter (HD) in nanometers. The samples were diluted in polystyrene cuvettes (Nr. 67.754) by Sarstedt to reach a transmission of at least 60%. All samples without added salt were diluted with deionized water.

Solvents	**Molar concentration** *mM NaCl*	**Refractive index** -	**Viscosity at 25°C** μPas
water	0	1.3303	890.308
0.0001 g NaCl / g water	1.7	1.3303	890.231
0.001 g NaCl / g water	17	1.3305	891.409

Table 4.2: Parameter settings for the solvents during the dynamic light scattering measurements with the Particle Analyzer Litesizer500 by Anton Paar

The samples where NaCl was added were diluted with a solution with the corresponding

salt concentration. The measurement temperature was set to 25°C. The refractive index and absorption coefficient of lignin was fixed at 1.530 and 0.100, respectively. The parameter settings for the solvents are listed in table 4.2. The data for water was adopted from the available information in the Litsizer program. The viscosity of the salt solutions was obtained by interpolation from data by Kestin et al. [36]. The refractive index was respectively interpolated and extrapolated from the data available for 10 mM and 154 mM NaCl in the solvent library of the Litesizer.

pH The pH was measured with a pH probe (IDS-pH-Sensor, WTW) connected to a universal multi-parameter pocket instrument Multi 3430, by WTW. The sensor was put into the sample for 3 minutes. Then, the measurement value was read off. Afterwards, the pH probe was cleaned with ethanol and distilled water before the following sample was measured.

Density The density was measured using a glass pyknometer. For this, the exact pyknometer volume was first determined using water. The pyknometer was first weighed out when completely dry. Then, it was filled with deionized water, closed with the stopper and warmed to 20°C using a tempered water bath. After reaching the temperature and making sure the capillary was still filled to the brim, the pyknometer was dried of on the outside and weighed using an analytical balance. Equation 4.1 shows the calculation of the volume using the known density of water at 20°C: 998.1875 kg/m^3 [68]. This process was repeated three times.

Pyknometer mass		**Water mass**	**Density water**	**Volume pyknometer**
Empty	**Full**			
g	g	g	$g\ /\ cm^3$	cm^3
36.0092	85.8851	49.8759	0.9982	49.9665
36.0092	85.8833	49.8741	0.9982	49.9647
36.0075	85.8819	49.8744	0.9982	49.9650

Table 4.3: Results for the pyknometer measurements with deionized water to determine the pyknometer's volume

The final pyknometer volume was then calculated forming a mean value from all three measurements and resulted in 49.965 cm^3.

$$V_P = \frac{m_{filled_{H2O}} - m_{empty}}{\rho_{H2O}} \tag{4.1}$$

The procedure was repeated three times for the suspension. The density for each measurement was calculated using Equation 4.2 and the final density was calculated using the mean of the three single measurement results.

$$\rho_{C220523} = \frac{m_{filled_{C220523}} - m_{empty}}{V_{P_{final}}} \tag{4.2}$$

Dry matter content The determination of the Dry Matter Content (DMC) was carried out in a 105°C drying cabinet. Dry glass containers were weighed out, the sample was added and the full container was weighed out agian. After leaving the sample in the drying cabinet for at least 24 hours, it was weighed out again. The dry matter content can then be calculated using Equation 4.3.

$$DMC(\%) = \frac{m_{after\,drying} - m_{empty}}{m_{before\,drying} - m_{empty}} * 100 \tag{4.3}$$

Fourier-transform infrared spectroscopy The temperature-treated samples were analyzed using a FTIR spectrometer VERTEX 70 by Bruker. For this, the samples were first frozen at -15° in a freezer for at least 24 hours and then freeze-dried in a lyophilizer Alpha 1-4 LSCplus by Christ. For the measurement, the dried sample was thinly loaded onto the spectrometer and measured over a range of 400 to 4000 nm. After the measurement, the apparatus was cleaned with ethanol and a baseline correction was carried out for the obtained raw data.

Absorption measurement The UV absorption of dissolved lignin was measured in fused quartz glass cuvettes in a spectrophotometer UV-1800 by Shimadazu. The measurement was carried out over a light range of 190 - 600 nm. The suspension samples were dissolved to roughly 0.0036 wt% with distilled water and dissolved in 60 wt% ethanol in the cuvettes, while the reference cuvette was filled with just 60 wt% of ethanol. Before the first measurement, the UV spectrophotometer was auto-zeroed and then a baseline measurement with 60% ethanol was performed. After five consecutive measurements, the reference with 60% ethanol was changed and the baseline was newly determined. The measured absorption values in the wavelength range of 240 to 400 *nm* were area normalized using Equation 4.4, in order to minimize the effect of concentration differences between the samples since the absorption measurements were only used qualitatively.

$$x_{i,Areanormalized} = \frac{x_i}{\sum_{240}^{400} x} * 160 \tag{4.4}$$

***In vitro* SPF measurement** The determination of the *in vitro* SPF of a sunscreen as described in section 3.4 was carried out using the spectrophotometer UV-1800 by Shimadazu. Six fused quartz glass plates were taped with fixation plasters (Blenderm® Fixierpflaster, 1525-2, 5 cm x 4,5 m by 3M®) along the short end of the plate, resulting in a square taped area of 6.25 cm^2. Before the first measurement, the UV spectrophotometer was auto-zeroed and a baseline measurement with two taped plates was performed. For the measurement, 0.0012 g of sunscreen sample were weighed out on the taped part of the plate. Then, the sample was spread with the finger following a specific motion pattern to ensure the equal distribution of the sample: The sample was first spread using circular motions for 15 seconds, then the plate was turned 90° and the sample was spread for another 15 seconds. Then, the

same procedure is repeated using a straight spreading motion, resulting in a total spreading time of 1 minute. The plate is then set into the spectrophotometer, and measured over a light range of 190 - 600 nm two minutes after starting the sample distribution. The resulting absorption values were then interpreted using the formula presented in section 3.4.

SEM The primary particle size and the morphology of the CLPs were analysed with a Quanta 200 FEG SEM by Fei. The acceleration voltage was set to 5 kV and the samples were sputtered 2 times with 4 nm of a gold/palladium mixture (60:40 wt%) before the measurement. The primary particle size was manually evaluated with ImageJ software. From 150 counts, a mean value and standard deviation was calculated.

4.3 Methods

4.3.1 CLP suspensions

Pumpability

Steady shear measurements were used to analyze the pumpability of CLP suspensions. The suspensions C220329, C220523, C220601 and C220601PG were measured in undiluted form. Additionally, all solutions were diluted to 3wt%, 6wt% and 9wt% dry matter with de-ionized water. Since the suspension C220329 only had a dry matter content of 9.06, only two dilutions were carried out. For C220523, an additional dilution to 15wt% was carried out.

Batch No.	**Dry matter**	**Dilutions suspensions**
#	*wt%*	*wt%*
C220329	9.06	6 / 3
C220523	21.10	15 / 9 / 6 / 3
C220601	15.40	9 / 6 / 3
C220601PG	14.63	9 / 6 / 3

Table 4.4: Overview of the colloidal suspensions used, their corresponding dry matter content and the performed dilutions.

Steady shear measurements were carried out for each suspension listed in 4.4 at 20°C, 40°C and 60°C, except for C220601PG with 14.3 wt% as it was unstable at 60°C. The same suspensions were also measured at 20°C after adding salt. Two salt concentrations of salt were chosen: 0.0001 and 0.001 g NaCl per 1 g of suspension. The samples were mixed thoroughly with a vortex mixer before measuring.

Since the viscosity of the samples varied largely, both measurement systems were used: CP and PP. The cone-plate was used for most samples if not otherwise indicated, since, as suggested by Mezger [52], the larger diameter of 50 mm is favourable for suspensions with

low viscosity. The gap size between the plates was automatically set to 0.098 mm for this setup. Some samples showed a too high viscosity to make it possible to reach this gap size: C220523 at 20 wt% and 15 wt% as well as C220601PG at 14.6 wt% and 9 wt% with added salt and C220601 at 15.4 wt% with both salt concentrations and at 9 wt% with 0.001 g NaCl added. Here the plate-plate stamp was used. The gap size was set to 1 mm, as Mezger recommends setting it at a value at least five times larger than the biggest present particle [52]. The viscosity and shear stress was measured over a shear rate range of 0.01-1000 s^{-1} with 50 measurement points distributed logarithmically.

As the suspension C220523 showed the highest CLP concentration with around 20 wt%, the density at 20°C of this suspension was also measured using a pyknometer.

Temperature stability

As discussed in section 2.2, lignin is sensitive to higher temperatures and this behaviour is also noted in colloidal lignin particles. Based on preliminary experiments, the temperature stability of CLPs was first investigated by heating a CLP suspension to 90°C, with differing heating speeds. For this, a 100 ml round-bottomed flask was filled with 50 g of suspension C220329 and a small magnet stirrer was added. Then, the flask was closed with a stopper and fixed inside an oil bath at a height so the whole height of the suspension is covered. The temperature of the suspension as well as of the bath was recorded using a thermometer with two PT100 probes attached (Thermometer T 390 by PCE). The bath is heated with a magnetic heating plate (C-MAG HS 7 digital by IKA®) and continuously stirred. The basic experimental setup is shown in Figure 4.2. Three different heating patterns were chosen and are listed in Table 4.5.

Trial No.	Heating pattern	Heating time (h:m:s)
S_1	The suspension is slowly heated together with the oil bath to 90°C	00:48:00
S_2	The suspension is put into a 90°C oil bath	00:17:00
S_3	The suspension is put into a 160°C oil bath	00:04:20

Table 4.5: Overview of the heating patterns chosen for the short-term temperature trials with C220329.

First, a slow heating of the suspension was chosen, where it was heated together with the oil bath until 90°C was reached (Trial S_1). Then for Trial S_2, the suspension was heated faster by putting the flask in an already heated 90° C oil bath. Lastly, the suspension was heated even faster by placing it in a 160°C oil bath (Trial S_3). The heated suspensions were then evaluated using optical means as well as measuring the UV absorption, DLS measurements and determination of the dry matter content.

After determining the fast heating in a 90°C oil bath as the temperature exposure method as the worst-case in industrial practice, this heating pattern was repeated for CLP suspensions obtained from different lignin raw materials: C220329, C210803 and C211005. As for the

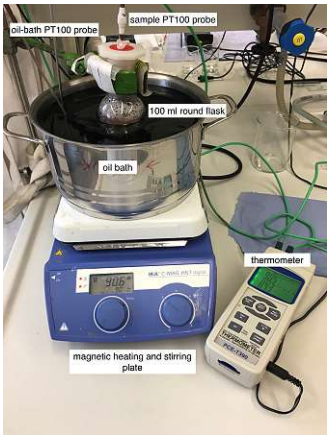

Figure 4.2: Set-up of the temperature exposure experiments

preceding experiments, the heat-treated suspensions were evaluated optically, as well as using DLS, UV and FTIR analysis methods.

4.3.2 CLP applications

Rheology

Two different influences on the rheological behaviour of CLPs applied in cosmetics were examined: varying concentrations and changes in the pH.

Emulsions with varying concentrations To produce the emulsion with varying concentrations, 50 g of the CLP suspension C220601 with 5 wt% of pentylene glycol at three different concentrations was used. The initial concentration of the suspension starts at 14.63 wt%, and was diluted to 4.85 wt% and 9.7 wt% with deionized water. To reach a concentration of 9.7 wt% in 50 g of solution, 33.15 g of C220601PG was weighed out and filled up with deionized water. For 4.85 wt%, 16.58 g of the initial suspension was used. To ensure a homogeneous mixture, the solutions were mixed with an Ultra Turrax® T25 digital by IKA (Dispersing Tool S 25 KD – 25G) at 8000 rpm for 2 minutes. The emulsions were then produced as described in subsection 4.1.2. As a reference, a fourth emulsion was produced where the 50 g of diluted CLP suspension was replaced with water. Table 4.6 shows the concentrations of the three CLP suspensions and the emulsions produced from them.

The rheometer MCR300 was used to carry out steady shear rate measurements for the emulsions, using the plate-plate stamp at a temperature of 25°C. The gap size was set to 1 mm and the measured shear rate range was 0.1-500 s^{-1}.

The produced emulsions were also subjected to oscillatory tests. The set-up of the rheometer and the temperature of 25°C remained the same for these tests. First, an amplitude sweep was carried out to determine the linear visco-elastic border of each emulsion. For this, 25

CLP concentration	
suspension wt%	**emulsion wt%**
14.6	7.3
9.7	4.85
4.85	2.425

Table 4.6: Concentration of the suspension and the respective concentration in the emulsion

measuring points were taken over a logarithmic amplitude range from 0.01-10 % at a set angular frequency of 10 rad/s. This was repeated three times for each emulsion and the mean values of the measured storage modulus G' and loss modulus G" were calculated. The data from the amplitude sweep was then used to determine the critical strain value, marking the end of the linear-viscoelastic region, inside which the frequency sweep should be performed. The oscillation frequency test was carried out in a logarithmic frequency range from 0.01-100 Hz at a set amplitude strain value of 0.01%. The storage modulus G' and loss modulus G" for 21 measurement points were recorded. This was repeated three times for each emulsion.

Emulsions with varying pH The emulsions with MCT oil were produced as described in subsection 4.1.2. For this, the original CLP suspension C220712 was diluted with deionized water to receive 50 g of a solution with a concentration of 4.85wt%. Then the necessary amount of 0.1 M NaOH or H_2SO_4 was added in small volumes with a pipette while continuously measuring the pH to ensure the correct value was reached. The added volumes can be found in Table 4.7. To determine the resulting weight percent of CLPs in the suspension, these volumes were converted to masses using literature values for the density from Perry [68] at 20°C.

pH	**Volume of added 0.1 M base/acid**	**Mass of added 0.1 M base/acid**	**Final concentration of CLPs in the emulsion**
-	*ml*	*g*	*wt%*
2.5	2 ml H_2SO_4	2.0103 g H_2SO_4	4.75
3.4	-	-	4.85
5.5	0.3 ml NaOH	0.3008 g NaOH	4.84
7.2	1 ml NaOH	1.0027 g NaOH	4.80

Table 4.7: Overview of the examined pH values of CLP emulsions and the necessary amounts of added acid and base to reach them, as well as the final amount of CLPs in the suspension after the addition.

The viscosity of the produced emulsions with MCT oil was determined the same way as for the emulsions with varying concentrations with the rheometer MCR300 using the Plate-

Plate stamp at a temperature of 25°C and over a shear rate range of 0.1-500 s^{-1}. The gap size was also set to 1 mm. As the rheological measurements were carried out approximately two weeks after the production of the emulsions, each emulsion was homogenized with the UltraTurrax® for a minute at 8000 rpm before starting with the measurements. The stability assessment and emulsion production was not carried out by the author of this work and the data was provided by Lignovations GmbH.

Temperature stability

To determine the influence of temperature on suspensions when used in an application, emulsions similar to commercial sunscreen were produced. For three emulsions, the production method was the same as described in subsection 4.1.2, however the concentration of the suspension C220329 was kept at 4.85 wt%. To investigate the influence of temperature, three emulsions were produced using a "hot" production method. Here, the oil phase was heated to 80°C and the suspension was mixed in at this temperature. The produced emulsions were then left to cool down, and analyzed after 24 hours using *in vitro* SPF tests. As a control sample, three emulsions without CLPs were produced using a hot production process.

Chapter 5

CLP suspensions

5.1 Results and Discussion

This chapter presents the results for the experimental works described in section 4.3.1 and includes a discussion of these results in terms of the pumpability and temperature stability of the suspensions.

5.1.1 Pumpability

In order to evaluate the pumpability of the CLP suspensions different influences on their rheology were analyzed: the concentration of the CLPs, the temperature, the particle size and the presence of additives and contaminations.

Influence of CLP concentration

The following section explores the influence of the CLP concentration on the pumpability by analyzing the rheological data available for suspensions C220329, C220523 and their dilutions.

Figure 5.1 shows the results for the viscosity measurements for the suspension C220329, its dilutions and water at 20°C. All measured viscosity values decrease with the shear rate. For shear rates $\leq$10 s^{-1}, the viscosity decreases significantly stronger than for higher shear rates. For example, the viscosity of the 9 wt% suspension sinks from a value over 10^4 mPa*s to one below 10 mPa*s over the range of $\dot{\gamma}$ from 10^{-1}-$10s^{-1}$. After this, the viscosity declines less markedly for all samples. The viscosity values seem to increase with the concentration of CLPs present in the liquid, as water shows the lowest and the 9 wt% suspensions the highest values.

The vertical error bars show the standard deviation as the depicted values result from the mean of three single measurements. One can see that the standard deviation for the lower

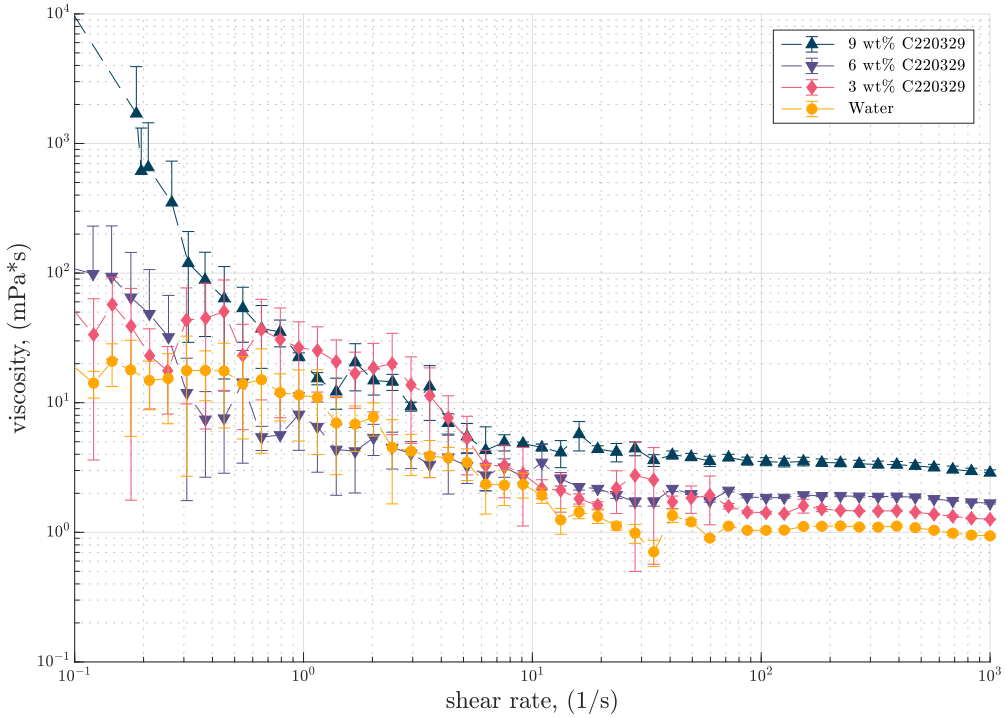

Figure 5.1: Dynamic viscosity η as a function of shear rate $\dot{\gamma}$ for the suspension C220329, its dilutions and water at 20°C

shear stress is far higher than for the last 15 measurement points. This scatter in the experimental data at low shear rates is typical for steady shear measurements with PP and CP measurement geometries, as stated by the International Union of Pure and Applied Chemistry (IUPAC) report on rotational rheometers [40]. The measurement can be improved by increasing the diameter of the measurement geometry. However, the distinct scatter at low shear rates, the so-called error trumpet, cannot be fully avoided as it arises from exceeding the practical measuring limits [40]. For low-viscosity fluids such as water, this limit is determined by the minimum reliably measurable torque created by the sample. A sample with higher viscosity might have a larger measuring range [40].

As water is a Newtonian liquid, the viscosity of the measured water sample should remain the same for all shear rates, which is not true in Figure 5.1. However, the IUPAC technical report [40] places the overall error of viscosity measurements using rotational rheometers at 1-10 % since various parameters like the measurement geometry and sampling process influence the measurements. The deviation of the viscosity values from the literature data (viscosity of water at 20°C is 1.002 mPa*s [36]) is ≤ 12 %, meaning the measured values are primarily of a similar order of magnitude as the inaccuracy of the measurement.

When focusing on the values at higher shear rates, particularly the last 15 measured viscosity values, the viscosity values for the measured suspension are relatively close to water, a

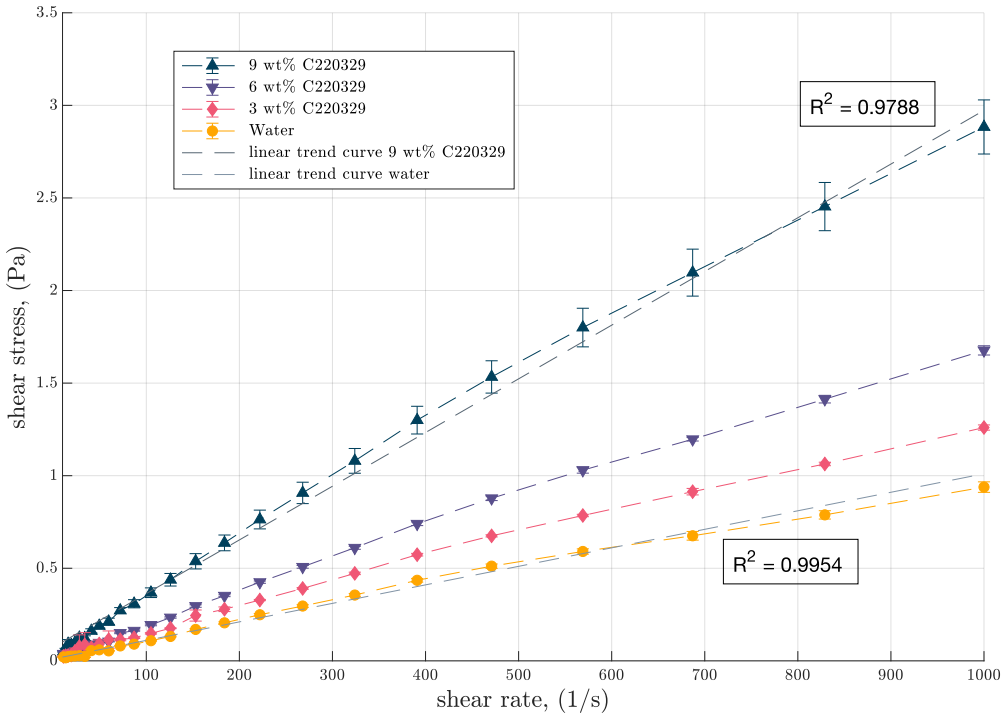

Figure 5.2: Shear stress over the shear rate range 10-1000 s^{-1} for the suspension C220329 and its dilutions at 20°C

Newtonian fluid. The similarity to Newtonian behaviour of the suspension C220329 and its dilutions can also be observed in Figure 5.2, which shows a typical flow curve where the shear stress is plotted over the shear rate. Here, the curves show a mostly linear course. Depending on the concentration, the shear stress increases more or less strongly with the shear rate. The suspension with 9 wt% displays the most substantial increase, followed by 6 wt%, 3 wt% and water. As mentioned in section 3.3, a linear relationship between the shear stress and the shear stress in a flow curve indicates a Newtonian fluid, where the viscosity remains constant and follows Newton's law [52]. In a Newtonian flow curve, a straight line passes through the origin, and the viscosity is indicated by the slope of the line [68]. In the case of water, the viscosity at 20°C should be 0.001 Pa*s. Adding a linear trend curve to the measured values with the equation $y = 0.001 * x + 0.0104$ and an accuracy of $R^2 = 0.9954$ results in a slope of 0.001. Therefore, the measured values allow for the correct determination of water as Newtonian. The shift from the origin can be neglected. While a linear trend curve can also be fitted to the curve for the suspension with 9 wt%, resulting in the equation $y = 0.0029 * x + 0.073$ with $R^2 = 0.9788$, the viscosity can not be modelled as accurately with Newton's law. For example, the measured viscosity at a shear rate of 569 is 0.0031667, which is higher than the slope would indicate. Still, the suspensions can be considered nearly Newtonian. Also, looking back at Figure 5.1, the viscosity of the suspension C220329 with 9wt% does not show significant deviation in the course of the curve in comparison to water

when considering shear rates above 100 s^{-1}.

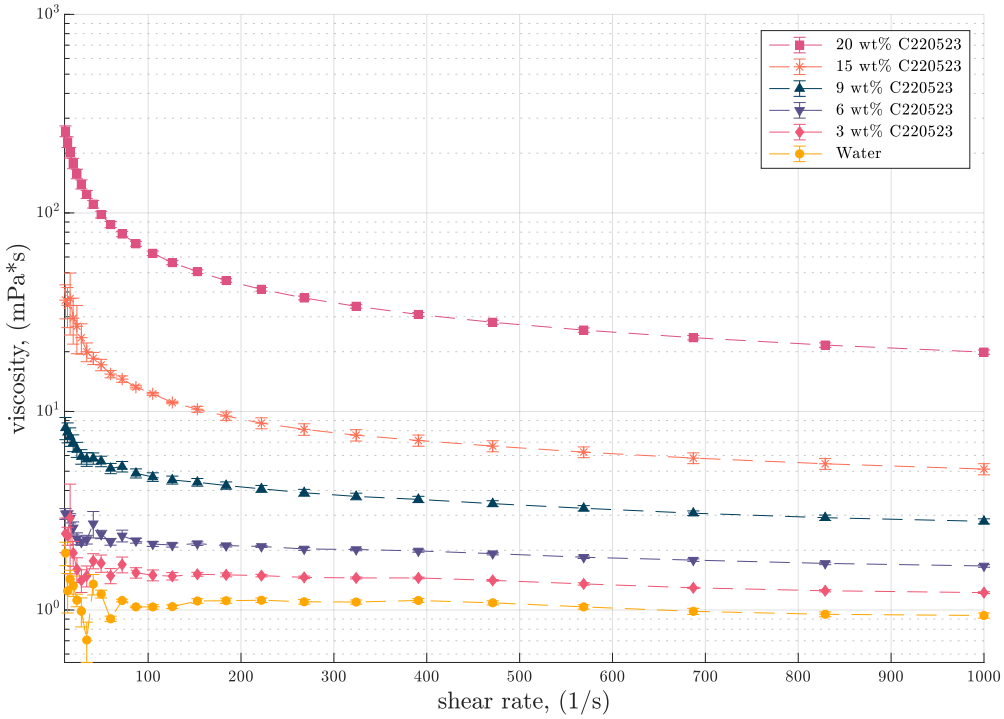

Figure 5.3: Dynamic viscosity η over the shear rate range 10-1000 s^{-1} for the suspension C220523 and its dilutions at 20°C

The results displayed in Figure 5.1 allow for the assumption that viscosity declines with decreasing particle concentration in the sample. This trend can also be observed for the suspension C220523 (Figure 5.3). The suspension with 20 wt% CLPs has the highest viscosity, followed by 15 wt%, 9 wt%, 6 wt% and 3 wt%. Like suspension C220329, the lower concentrated dilutions show higher standard deviations at lower shear rates, while the most concentrated suspension displays fewer deviations over the whole shear rate range. As mentioned above, it would be best to consider only the higher shear rate values for the less concentrated suspensions. Focusing on shear rates $\dot{\gamma}$ $\geq$100 s^{-1}, the suspensions with 20 wt%, 15 wt% and 9 wt% show an apparent decrease in viscosity with increasing shear rate. Looking at the 20 wt% suspension, the viscosity at $\dot{\gamma} = 100s^{-1}$ is around 60 $mPa \cdot s$ and falls to around 20 $mPa \cdot s$ at a shear rate of 1000. The lower concentrated dilutions, 6 wt% and 3 wt% show a more or less even course of their curves, comparable to the one of water.

Figure 5.4 confirms this observation. It shows the flow curves for all dilutions from 1 to 200 s^{-1}. The full measurement curve can be found in Appendix A (see Figure A.1). The flow curve for the suspensions with 20 wt% shows a clear deviation from a linear curve and matches the exemplary flow curve for a shear-thinning fluid in Figure 3.5. This indicates that the viscosity decreases with increasing shear rate as the flow curve shows a decreasing curve slope [52]. While not as pronounced, the suspensions with 15 and 9 wt% of CLPs

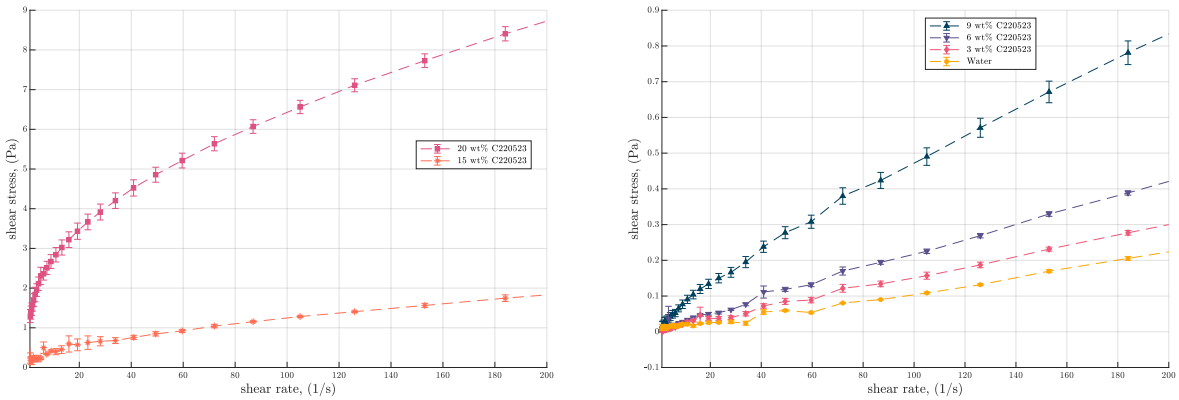

Figure 5.4: Shear stress over the shear rate range 1-200 s^{-1} for the suspension C220523 and its dilutions at 20°C

also show this trend. The lower concentrated dilutions, however, show a more or less linear increase and, therefore, nearly Newtonian behaviour. The behaviour of non-newtonian fluids can be modelled using a power law shown in Equation 3.9 [68]. The dimensionless power law exponent should be less than 1 for shear-thinning fluids. For Newtonian fluids, it is one and for shear-thickening, it is bigger than 1 [68]. Table 5.1 shows the results for K, n and the coefficient of determination R^2 derived from an exponential curve fitting. For this, the measurements points from shear rate 49.1 s^{-1} to 1000 were considered to avoid the before-mentioned scatter at low shear rates. The results fit well with the above-stated observations: The power law index n is significantly smaller for the suspensions with 20, 15 and 9 wt%, which indicates the shear thinning behaviour of the suspensions. For the less concentrated dilutions, the index is also smaller than 1 but very close to 1, indicating Newtonian behaviour. Also, for water, the index is not exactly one. However, considering the measurement deviations, Newtonian behaviour is sufficiently shown.

CLP content	**K**	**n**	**R^2**
$wt\%$	$kg/(ms^{2-n})$	–	–
20	0.7500	0.4700	0.9968
15	0.0790	0.6000	0.9985
9	0.0130	0.7800	0.9993
6	0.0040	0.8900	0.9985
3	0.0023	0.9100	0.9978
0	0.0012	0.9700	0.9944

Table 5.1: Power law coefficient K, power law index n and the coefficient R^2 derived from an exponential curve fitting to the measurement points for the shear stress over the shear rate range 49.1 to 1000 s^{-1} for the suspension C220523 and its dilutions at 20°C

The obtained results for suspensions C220329 and C220523 show good accordance with the literature cited in subsection 3.3.1. The addition of particles to a suspending liquid like

water leads to an increase in viscosity. At higher concentrations, a deviation from Newtonian behaviour is noticeable [14]. A shear thinning flow behaviour is often typical for dispersions as the particles are oriented into flow direction during the shearing process. Therefore, the interactive forces between particles are reduced, and the resistance to the flow is less [52].

As the suspension C220523 showed the highest CLP concentration with 20 wt%, this suspension was further analyzed by determining the density at 20°C to calculate the kinematic viscosity. The density measurement results can be found in Table 5.2.

pyknometer mass		**suspension mass**	**density suspension**
empty	**full**		
g	g	g	g/cm^3
36.0168	86.3065	50.2897	1.0065
36.0097	86.3126	50.3029	1.0068
36.0079	86.3130	50.3051	1.0068

Table 5.2: Results for the pyknometer measurements for suspension C220523 at 20°C

The mean density of the three measurement runs leads to a final density of 1.0067 g/cm^3 at 20°C. Compared to the density of water at the same temperature (0.9981875 g/cm^3 [68]), the density of the suspension is only slightly higher. The kinematic viscosity is the ratio of dynamic viscosity to the density, as shown in Equation 5.1) [68] and has the unit m^2/s. Table 5.3 shows the calculated kinematic viscosities for some of the shear rates in the measurement range.

$$\nu = \frac{\eta}{\rho} \tag{5.1}$$

Shear rate	**Kinematic viscosity**	**Standard deviation**
s^{-1}	m^2/s	m^2/s
1.15	1.12E-03	1.43E-04
11	2.57E-04	1.60E-05
105	6.22E-05	1.62E-06
391	3.06E-05	7.02E-07
1000	1.98E-05	5.07E-07

Table 5.3: Calculated kinematic viscosities for a selection of shear rates for suspension C220523 at 20°C

These rheological results were then related to the pumpability of suspensions by using centrifugal pumps as an example as they cover a substantial part of all pump requirements [60]. As mentioned in section 3.2, the properties of a fluid are important to consider when selecting a pump. The pump manufacturer determines the performance of centrifugal pumps using

water. Therefore, changing fluid properties like the viscosity, can significantly influence the pump's operation [2]. At higher viscosities, rotodynamic/centrifugal pumps show increased parasitic losses, reducing the pump's performance and efficiency [60]. Experimental data showed that for fluids with viscosities up to $2.0 * 10^{-5} m^2/s$, the performance of centrifugal pumps is nearly the same as for water. This also applies to fluids having a similar density and viscosity to water. Up to a viscosity of $1.0 * 10^{-4} m^2/s$, the head and efficiency of the pump decrease noticeably, and for viscosities higher than that, both are significantly reduced [2]. According to Vliet and Lyklema, typical shear rates during pipe flow when pumping lay between 10 s^{-1} and 1000 s^{-1} [88]. Comparing the results for the kinematic viscosity in Table 5.3 for this shear rate range, one can see that at shear rates above 1000 s^{-1}, the viscosity of the 20 wt% C220523 suspension should not influence the centrifugal pumps performance. However, below 1000 s^{-1}, the kinematic viscosity indicates a significant influence, which can manifest as a substantial increase in energy consumption of the pump as well as a reduction in efficiency and head [2]. This is schematically shown for a centrifugal pump at constant speed in Figure 5.5, taken from Pumping Machinery Theory and Practice [2], including the performance characteristics efficiency, power consumption and head depending on the flowrate. These influences are also noticeable in characteristic pump curves, which need to be corrected using correction factors for the head, capacity and efficiency of the pump at higher viscosities.

Figure A.2 in the appendix, shows an example for correction factors for a centrifugal pump with radial impellers by KSB to convert the characteristic curves pumping water to characteristic curves for pumping viscous fluids [38].

As seen from the results discussed in section 5.1.1, the viscosity of suspensions increases with higher CLP concentration, making the concentration step during the CLP production the primary focus for pumpability issues. The production of the colloidal particles as described in [3] is followed by a downstream process step using membrane separation to concentrate and remove impurities in the suspensions [54]. In this filtration step, a flow rate Q of 3500 l/h is reached, and the suspension passes through four membrane modules with DIN32. As shown, the suspension displays shear thinning behaviour and the viscosity changes with the shear rate. To find a representative shear rate at the flow rate of interest, the Rabinowitsch-Mooney equation is used (see Equation 5.2) [68]. The equation gives the shear rate on a pipe wall for a steady laminar flow of any time-independent non-Newtonian fluid with velocity v and pipe diameter D. With the available process data and the results shown in Table 5.1, the wall shear rate can be calculated to 388.09 s^{-1}.

$$\dot{\gamma}_w = \frac{8 * v}{D} \left(\frac{1 + 3n}{4n}\right) \tag{5.2}$$

Using this shear rate as a reference, the kinematic viscosities shown in Table 5.3 indicate that during the concentration step, there is a significant reduction in pump efficiency and head as the suspension concentration increases. Also, the energy consumption of the pump

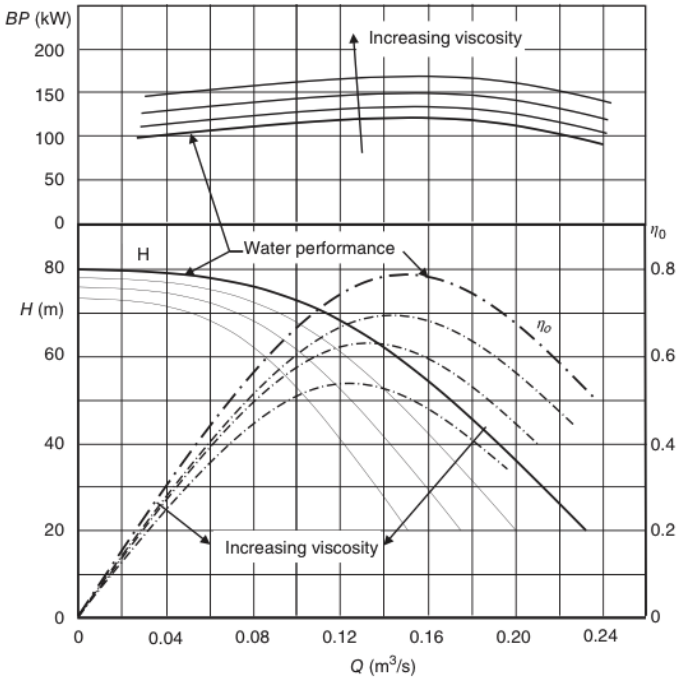

Figure 5.5: Effect of viscosity on the performance of a centrifugal pump at a constant speed, taken from [2]

will intensify. While a diluted suspension can be handled more efficiently in terms of transportability, less particles can be processed, and the process productivity is not as high [65]. Transportability is, however, an essential factor to consider when the concentration of the suspensions should be increased in future productions, as it could result in less process yield.

Figure 5.6 shows the dynamic viscosity of the suspensions C220329, C220523 and C220601 and a shear rate of 391 s^{-1}. The data shows a clear increase in viscosity for each suspension, with the highest concentration showing the highest viscosity. C220523 has the highest value, followed by C220601 and C220329. Assuming the density of the different suspensions does not vary significantly, this order stays the same for the kinematic viscosity. This further suggests the concentration of CLPs is critical for the pumpability of the suspension.

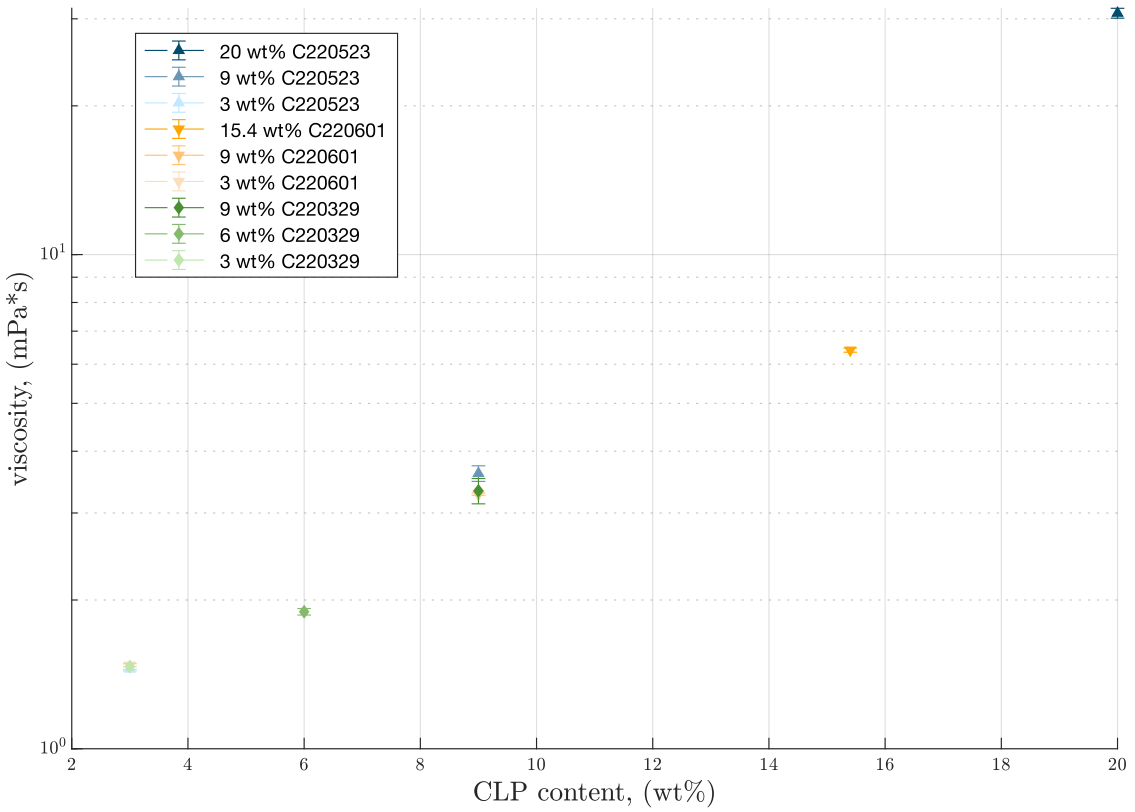

Figure 5.6: Dynamic viscosity of each suspension at a shear rate of 391 s^{-1} at 20°C

Influence of temperature

The influence of temperature on CLP suspensions is represented in the following figures for the suspensions C220523 and C220601.

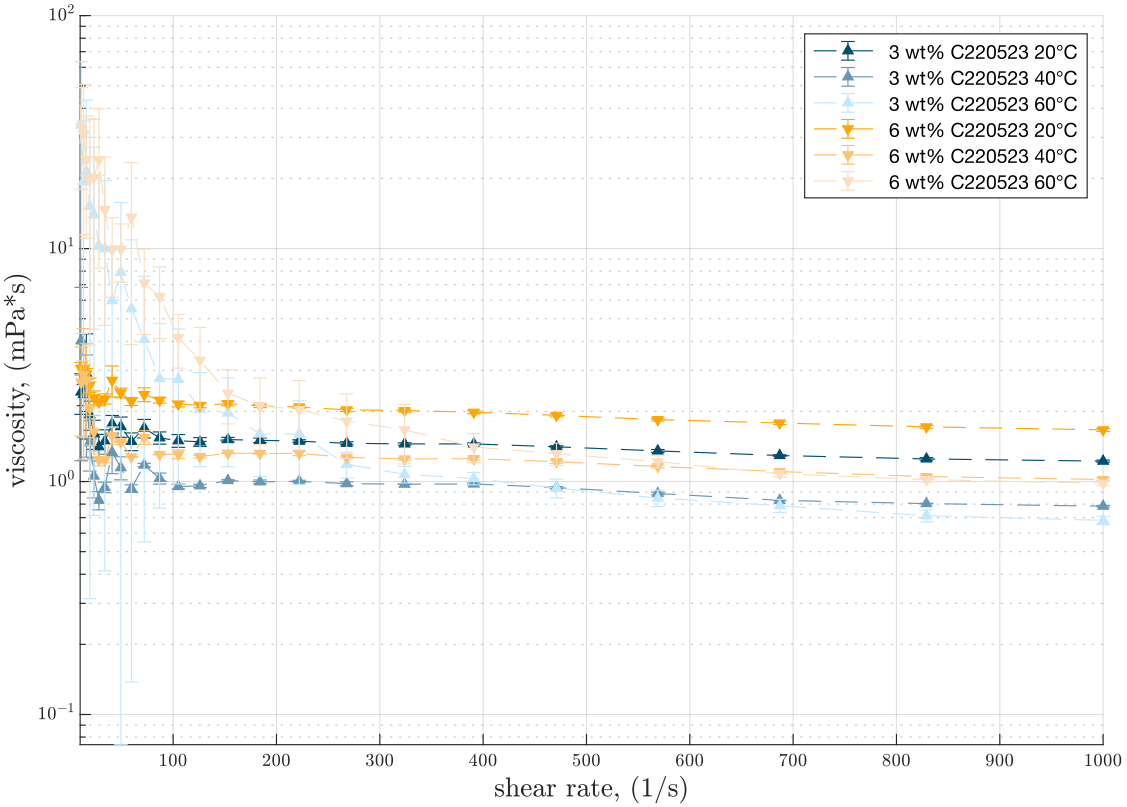

Figure 5.7: Dynamic viscosity η over the shear rate range 10-1000 s^{-1} for the 3 and 6 wt% dilutions of the suspension C220523 at 20°C, 40°C and 60°C

Figure 5.7 shows the dynamic viscosity values of the suspension C220523 at 3 and 6 wt% at temperatures of 20°, 40° and 60°C for shear rates from 10 to 1000 s^{-1}. For the 3 wt% suspension, represented in the blue colour, the viscosity values at 20°C are higher than the ones at 40°C. This is also true for the suspension with 6 wt% at 20°C and 40°C. This is in good accordance with the literature, which states that an increase in temperature leads to a decrease in viscosity for Newtonian fluids [82]. As stated in the previous subsection section 5.1.1, suspensions with a low CLP concentration show similar behaviour to water, a Newtonian fluid. The results for the dilutions with 3 and 6 wt% CLPs at 60°C show a slight deviation from this pattern. At lower shear rates, the dynamic viscosity at 60°C is higher than at 20° and 40°C. At shear rates higher than 100 s^{-1}, the viscosity of the two suspensions at 60°C falls to a similar value than at 40°C, which is lower than at 20°C. Also, the viscosity of the two suspensions shows signs of non-newtonian behaviour at elevated temperatures, as the viscosity decreases sharply with increasing shear rate (shear thinning). This may suggest a breakdown of the temperature-induced aggregate structures at higher shear rates [82]. For

suspensions, the viscosity change is not solely determined by the continuous phase but also by the disperse system itself [82]. As stated in section 2.3, CLPs are sensitive to increased temperatures, leading to the aggregation of the colloidal particles. Higher temperatures can cause more vigorous Brownian motion, increasing the chance for inter-particle interactions, which can increase viscosity as the chances for particle collisions are higher [44].

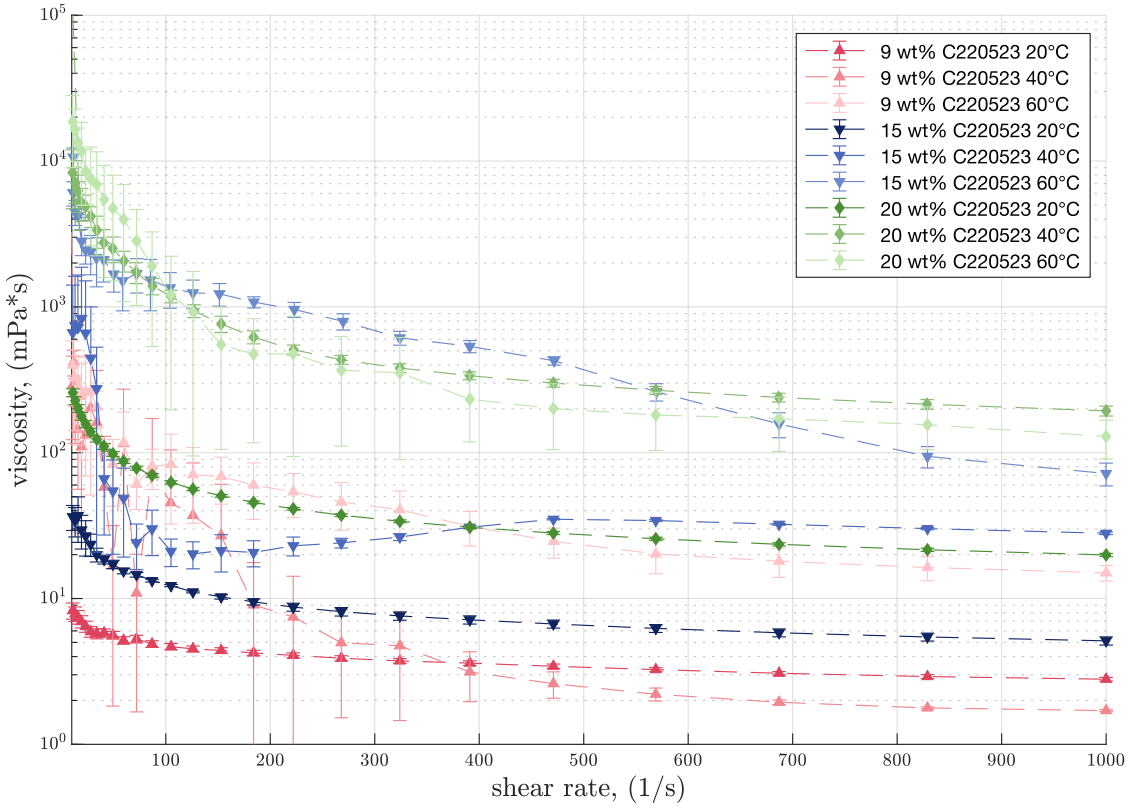

Figure 5.8: Dynamic viscosity η over the shear rate range 10-1000 s^{-1} for the suspension C220523 and its 9 and 15 wt% dilutions at 20°C, 40°C and 60°C

Figure 5.8 shows the dynamic viscosity values of the suspension C220523 at 9, 15 and 20 wt% at temperatures of 20°, 40° and 60°C for shear rates from 10 to 1000 s^{-1}. At 20°C, the viscosity values for the more concentrated suspensions are higher than the ones with fewer CLPs. All suspensions show a general decrease in viscosity with higher shear rates, indicating shear-thinning behaviour. Also, all suspensions at 60°C show higher viscosities than at 20°C, confirming an increase in viscosity with higher temperature. Looking at the suspension with 20 wt%, one can assume that at higher particle concentration, a temperature of 40°C already leads to a significant viscosity increase as the values for 40°C and 60°C are similar. This is not the case for the suspension with 9 and 15 wt% of CLPs, where the values at 60°C are the highest. As shown in section 5.1.1, an increase in CLP concentration generally leads to an increase in viscosity. As mentioned, higher temperatures increase particle interactions, especially at increased CLP concentrations, causing aggregates to form

more easily. According to Mewis et al., [48], even a small amount of aggregates can have pronounced effects on the rheology with a particular viscosity increase at low shear rates. Also, the data at higher temperatures show an uneven course of the curve and increased standard deviations, which can be a result of the breakdown of aggregates at higher shear rates into smaller units.

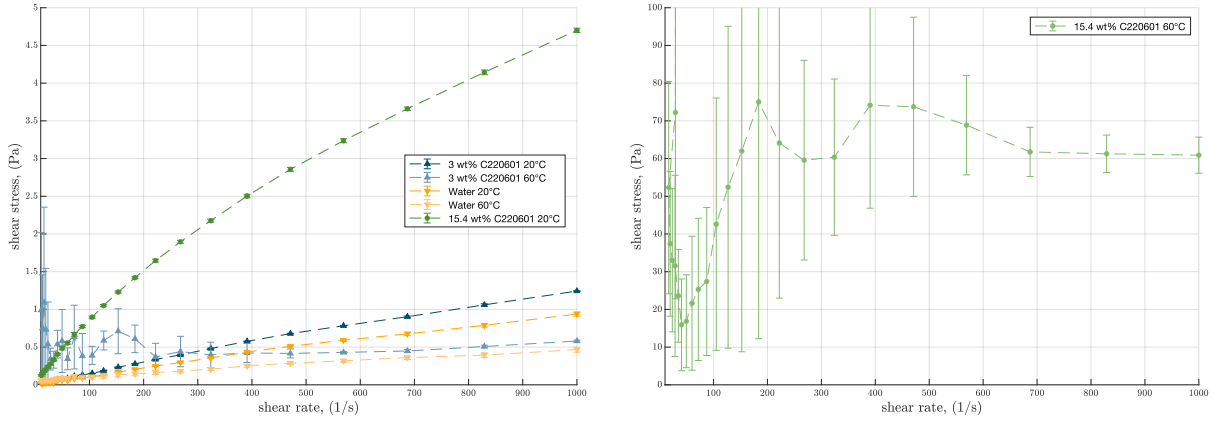

(a) (b)

Figure 5.9: Shear stress over the shear rate range 10-1000 s^{-1} for the suspension C220601 and its 3 wt% dilutions at 20°C, 40°C and 60°C

Figure 5.9 shows the shear stress over a shear rate range of 10 to 1000 s^{-1} for the suspensions C220601 and the 3 wt% dilutions at 20°C and 60°C, as well as water. Here one can see that at low temperatures and concentrations, a linear relationship between the shear stress and shear rate is appreciable for all suspensions. This is also the case for water at both 20° and 60°C. Therefore, both show Newtonian behaviour. On the other hand, shear stress for the suspension with 15.4 wt% at 20°C increases exponentially. Comparing it to Figure 3.5, this curve indicated shear thinning behaviour. At 60°C, the relationship between shear rate and shear stress changes for the suspensions: For C220601 at 3 wt% the shear stress seems to stay nearly even after a small peak and only increases slightly with higher shear rates. At 60°C, the values for the suspension C220601 with 15.4 wt% show significant deviations between the measurements, as indicated by the large error bars. The course of the curve only moderately follows an exponential fit, as the values dip between 270 to 570 s^{-1} after a sharp increase, followed by a decrease at higher shear rates. The values are far higher than at lower CLP contents and show significant scatter, making it difficult to determine the nature of the flow at more elevated temperatures. For the suspension C220601, the observations made above for C220523 can be confirmed. At the low CLP concentration of 3 wt%, an increase in temperature leads to a decrease in viscosity, as the relationship between shear stress and rate shows a behaviour similar to Newtonian fluids such as water. At the highest particle concentration, the viscosity is much higher at 60°C than at 20°C, which can also be seen from the higher shear stress values for 15.4 wt% C220601.

Relating the influence of temperature on CLPs back to the pumpability of the suspensions, the apparent deviation in behaviour compared to Newtonian liquids is a crucial aspect to consider. To make the pumping of high-viscosity liquids easier or, in some cases, even possible, a common industrial practice is heating the liquid to be pumped [59]. While this may lead to the desired effect of lowering the viscosity for some, usually Newtonian fluids, the results show that it is not the case for CLP suspensions where the viscosity is increased at high CLP content and can lead to the destruction of the suspension in the worst case. Also, at high temperatures, the appearance of agglomerates or changes in the CLPs leads to significant scatter in the values, making it hard to predict the flow and pumpability of the suspensions.

Influence of the particle size

As mentioned in section 3.3, the size of the particles can influence the rheology of colloidal suspensions [88]. To investigate this for the CLP suspensions C220329, C220523 and C220601, the 9 wt% dilutions of all three suspensions were compared at three different shear rates. Results are shown in Table 5.4. Generally, the viscosity decreases for all suspensions, with C220523 displaying the highest values at shear rates of 391 and 569 s^{-1}. At 829 s^{-1}, the viscosity of C220329 is highest. The decrease of the viscosity with the increase in the shear rate indicates shear thinning behaviour for all suspensions.

	C220523		**C220601**		**C220329**	
Shear rate	**Viscosity**	**Standard deviation**	**Viscosity**	**Standard deviation**	**Viscosity**	**Standard deviation**
s^{-1}	$mPas$	$mPas$	$mPas$	$mPas$	$mPas$	$mPas$
391	3.607	0.131	3.277	0.019	3.327	0.196
569	3.253	0.103	3.003	0.017	3.167	0.180
829	2.917	0.090	2.707	0.009	2.963	0.160

Table 5.4: Viscosity values for C220523, C220601, and C220329 at 9 wt% and 20°C for shear rates 391, 569 and 829 s^{-1}

The viscosity values of all suspensions were evaluated at the same dilution of 9 wt%, with the only difference being the CLP particles. Table 5.5 shows the particle sizes of the undiluted suspensions. From the SEM data, the size of the singular colloidal particles can be seen, indicating that the suspensions C220601 show the largest primary particle size, while C220329 has the smallest primary particle size. The measured hydrodynamic diameters are nearly double the values for the primary particles. Here the suspensions C220523 shows the largest particle size, followed by C220601 and C220329. Comparing the SEM data with the hydrodynamic diameters, suggests that the particles occur as agglomerates of singular particles in the suspension.

As established, the addition of particles to the fluid increases its viscosity [59]. According to the research of Liu et al. concerning colloidal SiO_2 particles, smaller-sized particles display a better viscosity-increasing effect as the distance between particles decreases, leading to higher inter-particle forces [44]. Also, they exhibited a stronger aggregate structure, leading

Suspension	Primary particle size from SEM			DLS	
	Median	Mean	Stand. Deviation	HD	Stand. Deviation
	nm	nm	nm	nm	nm
C220329	54.00	56.74	19.49	106.11	2.01
C220523	60.00	61.67	13.19	223.33	3.74
C220601	70.00	71.12	15.42	167.62	0.81

Table 5.5: Primary particle size and hydrodynamic diameter, including standard deviations for each result, measured with the SEM and DLS, respectively, for all suspensions

to a significant viscosity increase and improved anti-shear capability. Comparing the primary particle sizes and the corresponding viscosity of the suspensions at a shear rate of 829 s^{-1} in Table 5.4 shows that the suspension with the smallest primary particles, C220329, also exhibits the highest viscosity.

Figure 5.10 shows the viscosity curves for the suspensions at 6 wt% over a shear rate range from 1 to 1000 s^{-1}. Here, C220329 and C220523 show very similar viscosity values, while the suspension C220601 displays nearly double the values. Analogizing this with the values for the 9 wt% CLP dilutions obtained, it is not always the case that the smaller primary particles lead to a higher viscosity since C220329 shows the lowest viscosity. As can be seen from the hydrodynamic diameters, larger particle agglomerates might influence the viscosity, leading to a viscosity increase [33]. For example, at the lower shear rates, the suspension C220523 displays the highest viscosity values for the suspensions in Table 5.4.

SEM images used to determine the size of the primary particles for the suspensions are shown in Figure 5.11. They not only reveal the size but also the shape of the particles. One can see that the primary particles in C220329 are more round-shaped than the others. The CLPs for C220601 show some more elongated particles, which look like two or more particles are attached. When the particles are not entirely spherical, rotation and orientation of the particles significantly influence the rheology [50]. Rod-shaped particles can increase the viscosity even more than disc-shaped ones [88]. While the particles shown in the SEM pictures are not perfectly spherical, most are more or less roundly shaped, making the influence of the particle shape on the suspension's rheology negligible.

Regarding pumpability, the transported particles' size can influence the flow across the pipe. For suspended particles smaller than 50 μm, like the considered suspensions, the fluid can be called a homogeneous mixture, as the particles distribute themselves evenly without a concentration gradient [58]. Particle sedimentation is common in suspensions due to the density difference between particles and suspending fluid [81]. A critical flow velocity should be reached to avoid sedimentation in the pipe, which in turn influences the pump sizing [58]. However, for particles smaller than 1 μm no sedimentation occurs, as the Brownian diffusion is enough to overcome gravity [81]. Therefore, as all the suspension particles are below the size of 1 μm, the sedimentation of particles should not influence their pumpability.

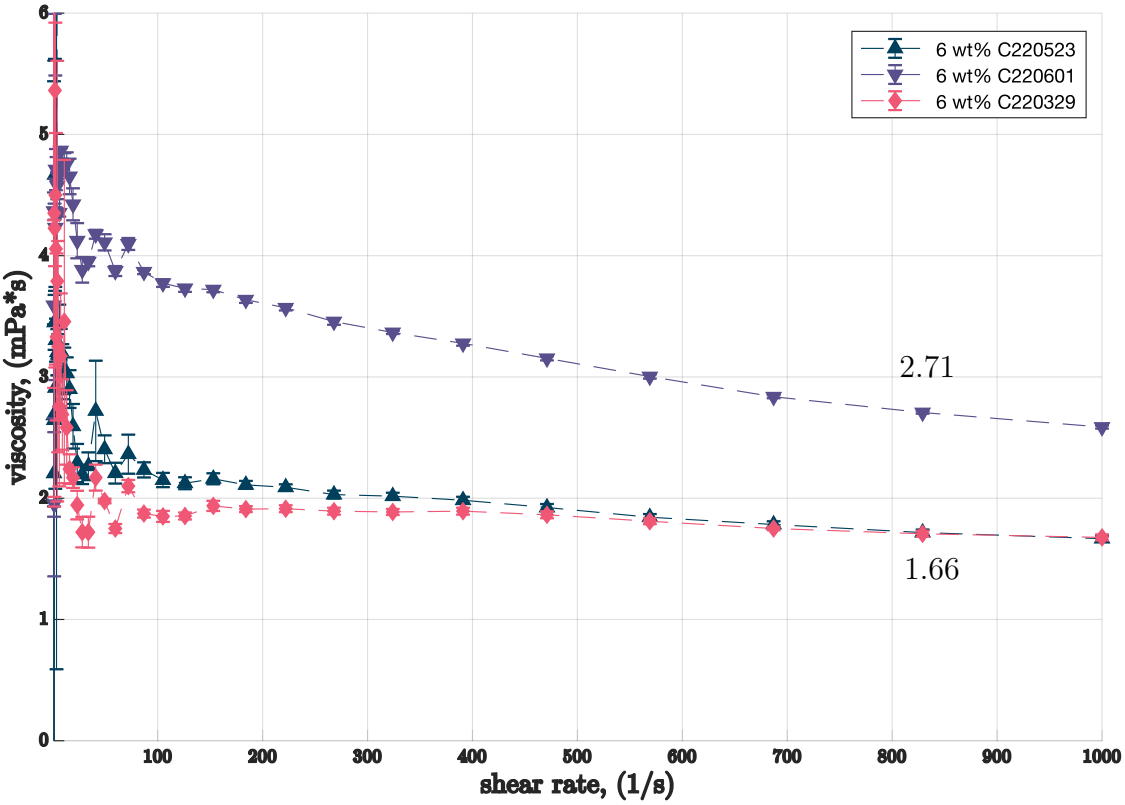

Figure 5.10: Dynamic viscosity over the shear rate range 1-1000 s^{-1} for the suspensions at 6 wt% at 20°C

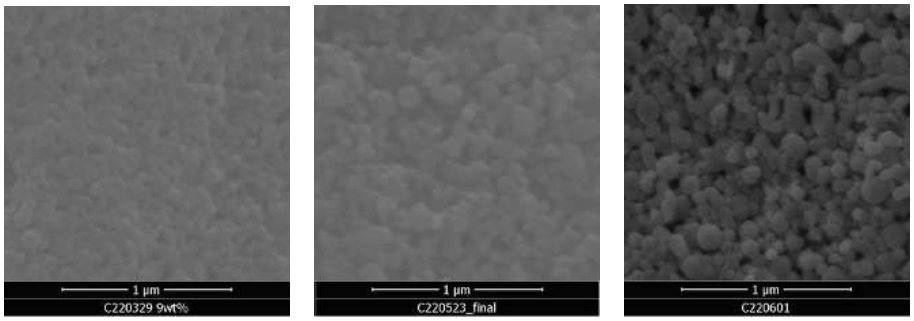

(a) (b) (c)

Figure 5.11: SEM pictures of suspensions (a) C220329 (b) C220523 and (c) C220601

Generally, since the particles' size and shape were considered to have negligible influence on the viscosity, the pumpability of suspensions seems to show little dependence on the size of the particles.

Influence of additives and contaminations

Another influence on the pumpability of CLP suspensions that was investigated was the presence of additives and contaminations. For example, pentylene glycol is added to the suspensions for preservation purposes. Also, the presence of charged particles like salt can heavily influence the viscosity of suspensions by causing flocculation [50]. It is, therefore, essential to investigate the influence of contaminations in the form of charged particles present in the pipes or pump on the CLP suspension and, consequently, its pumpability.

0 g NaOH / g suspension				
	C220329 9 wt%	**C220329 6 wt%**	**C220329 3 wt%**	**water**
Shear rate	**Viscosity**	**Viscosity**	**Viscosity**	**Viscosity**
s^{-1}	$mPas$	$mPas$	$mPas$	$mPas$
391	3.327	1.893	1.467	1.117
569	3.167	1.810	1.380	1.037
829	2.963	1.707	1.283	0.951
0.0001 g NaOH / g suspension				
	C220329 9 wt%	**C220329 6 wt%**	**C220329 3 wt%**	**water**
Shear rate	**Viscosity**	**Viscosity**	**Viscosity**	**Viscosity**
s^{-1}	$mPas$	$mPas$	$mPas$	$mPas$
391	11.967	5.630	1.507	1.090
569	9.317	4.963	1.423	1.013
829	7.410	4.313	1.333	0.928
0.001 g NaOH / g suspension				
	C220329 9 wt%	**C220329 6 wt%**	**C220329 3 wt%**	**water**
Shear rate	**Viscosity**	**Viscosity**	**Viscosity**	**Viscosity**
s^{-1}	$mPas$	$mPas$	$mPas$	$mPas$
391	42.500	13.200	3.767	1.087
569	31.633	10.380	3.210	1.009
829	23.833	8.247	2.743	0.934

Table 5.6: Dynamic viscosity values for selected shear rates for the suspension C220329, its dilutions and water with 0.0001 and 0.001 NaOH g/g at 20°C

Table 5.6 shows dynamic viscosity values at selected shear rates for the suspension C220329, its dilutions and water, before and after the addition of salt. Here, a significant difference between the viscosity values at 0, 0.0001 and 0.001 g/g NaOH can be noted for the suspensions, with at least double the values for the viscosity at the higher salt concentration. Compared to the viscosities of C220329 and its dilutions, one can see that the increase in viscosity is larger for higher CLP concentrations. For example, the suspension with 3 wt% has a dynamic viscosity of 1.283 $mPa \cdot s$ at 829 s^{-1}, which is only slightly smaller than for the corresponding suspension with 0.0001 g/g NaCl. After the addition of 0.001 g NaOH, the dynamic viscosity of C220329 is even higher at 2.743 s^{-1}. For the suspension with 9

wt% and 0.0001 g/g salt, the viscosity is nearly three times higher than at the same shear rate without salt.

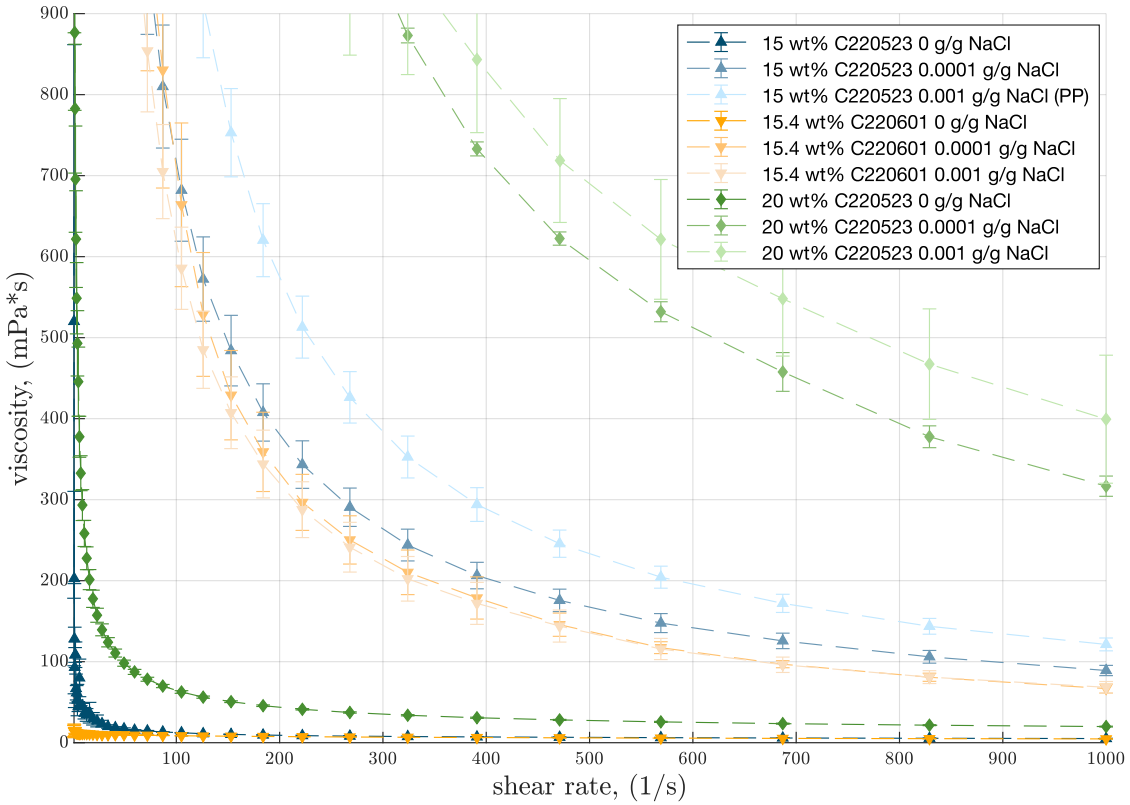

Figure 5.12: Dynamic viscosity over the shear rate range 1-1000 s^{-1} for the suspension C220601 and C220523 at 15 wt% with the addition of 0, 0.0001 and 0.001 g/g NaOH at 20°C

Figure 5.12 shows the dynamic viscosity of the suspension C220601 and C220523 with the addition of 0, 0.0001 and 0.001 gram NaOH per gram suspension at 20°C, as well as water. In order to rule out the influence of concentration when comparing the suspensions, the suspension C220523 was examined at 15 wt%, as well. Looking at the suspensions with no salt added, one can see that the dynamic viscosity values for C220523 at 15 wt% are higher than the ones for C220601 (15.4 wt%) at lower shear rates. At higher shear rates, the values overlap. For suspension C220523 at 20 wt% they were even higher. A strong increase in viscosity can be noted for all suspensions after adding salt, with the suspensions C220523 showing higher viscosities than the C220601 ones. Suspension C220523 showed the most heightened viscosity values after adding 0.001 g/g of salt, followed by the same suspensions with a lower salt concentration. All suspensions generally show shear-thinning behaviour, as the viscosity decreases with the shear rate. For suspension C220601, both viscosity curves for the samples with salt are several magnitudes higher than those without salt. For example, just adding NaOH in a concentration of 0.0001 g/g results in a dynamic viscosity of 66.8

$mPa \cdot s$ at a shear rate of 1000 s^{-1} compared to 4.7 $mPa \cdot s$ without salt. Interestingly, the added salt amount does not seem to be related to the increase in viscosity. The data shows that the addition of 0.0001 and 0.001 g/g led to a similar increase in viscosity in both suspensions, as the standard deviation of both suspensions with salt overlap. For the suspension C220523 this is not the case: The viscosity of the suspension with 0.0001 g NaCl shows lower viscosity values compared to the one with 0.001 g NaCl. The amount of salt also seems to influence the viscosity increase for the suspension C220329 and its dilutions, as shown in Table 5.6. Similar to these results, the suspension C220523 at higher concentrations also exhibits a stronger reaction to the addition of salt than the same suspension at 15 wt%.

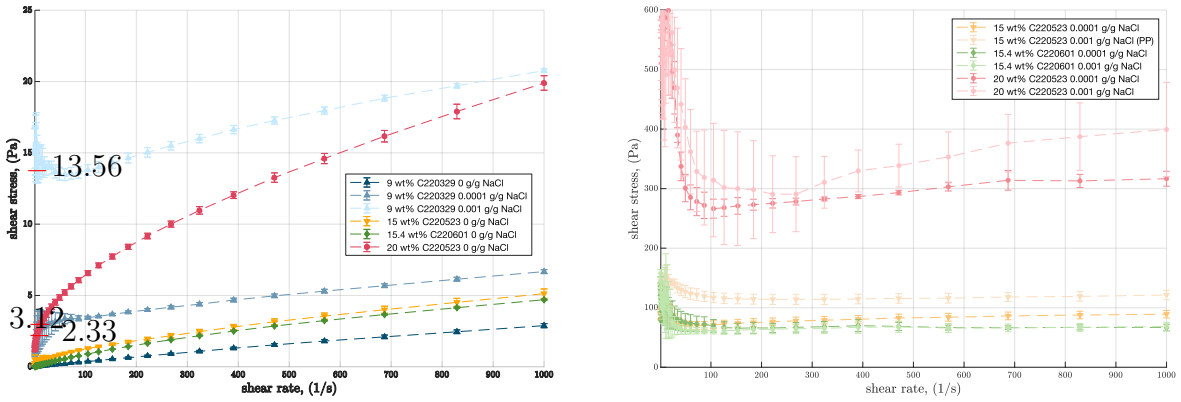

(a) (b)

Figure 5.13: Shear stress over the shear rate range 1-1000 s^{-1} for the suspensions C220329, C220523 and C220601 with water, 0.0001 and 0.001 NaOH g/g at 20°C. The yield stress is marked by a red line.

Figure 5.13 shows the flow curves of the suspensions C220329 with 9 wt%, C220523 with 15 and 20 wt% and C220601 with 15.4 wt%, with and without added salt. The shear thinning behaviour of the suspensions without salt can also be seen from their flow curves: The shear stress increases exponentially with the shear rate. All suspensions with added salt display larger values than those without. Same as for the viscosity, the addition of NaCl leads to an increase in the values, especially with higher CLP concentrations. The suspensions with added salt as well as C220523 with 20 wt% all show plastic flow behaviour, where an initial stress limit must be overcome for the suspension to start flowing. This point is marked by a flow limit or yield point τ_y, after which the structure collapses [14].

As already mentioned in before, the suspension C220523 with 20 wt% can be described by a power law model. The power law (Equation 3.9) can also be extended by the addition of a yield point τ_y. This point is marked at 2.33 Pa in Figure 5.13a.

For the suspensions C220329 with NaCl, the flow curve can be approximated using the Bingham model (see section 3.3). A Bingham fluid is the simplest model to describe a liquid with a yield stress, meaning a finite stress is needed before deformation occurs [68]. The

Bingham yield point τ_B can be determined by the intersection of the curve's linear course with the shear stress axis [52]. Using linear curve fitting the Bingham yield point τ_B for the suspension with 0.0001 g/g NaCl is 3.12 Pa, and for 0.001 g/g NaCl it results in 13.56 Pa. The yield points are indicated by arrows in the figure. Here, a higher salt concentration leads to a bigger yield point, which was not present in the same suspension without salt.

The shear stress values for C220601 with salt do not show a distinct Bingham curve. After a sharp decrease at lower shear rates, the shear stress increases again for shear rates > 100 s^{-1} at both salt concentrations. The high standard deviations make determining a flow curve similar to the ideal models challenging. This can also be said for the flow curves of C220523 shown in Figure 5.13b. The same sharp drop in shear stress can also be seen for all suspensions at shear rates below 100 s^{-1}. A more or less exponential increase in shear stress with shear rate can be noted at higher shear rates, confirming the shear thinning behaviour shown in Figure 5.12. In this case, the flow can be described as non-linear plastic flow with a τ_y and shear-thinning flow as the non-linear flow [14].

The change in rheological behaviour after adding salt can be explained using the DLVO theory presented in subsection 3.1.1. The addition of salt leads to a change in the ionic strength of the suspension so that the electrostatic repulsion between the particles is diminished, destabilizing the suspension and leading to the formation of agglomerates [57]. The increase in ionic strength causes the Debye length, which indicates the thickness of the electrical double layer, to shrink to zero, allowing the formation of van der Waals and hydrophobic interactions between the particles. According to Nakamura et al. [57], this led to a substantial viscosity increase for negatively charged silica particles in aqueous media with the addition of 0.1 mol/l NaCl and a larger shear-thinning gradient. This observation fits well with the data collected for the colloidal suspensions C220329. For the other suspensions, the viscosity increase can also be noted, as well as a change in the flow curve. The addition of salt also leads to the appearance of a yield point. The shrinking of the double layer and increased attractive forces between the particles allow the agglomerates to be held in a strong structure [14]. The network remains stable if the deformation rate does not rise above the yield stress, which increases with the inter-particle bond strength. After the breakdown of the structure, the fluids showed shear-thinning behaviour [14]. This can also be seen for the suspensions in Figure 5.13. As the yield value is higher for the suspensions C220523 after the addition of salt, this seems to suggest the yield stress increases with the present CLP concentration.

The agglomeration of particles can also be seen from Table 5.7, showing the results of the suspensions' DLS measurements. The hydrodynamic diameter measurements for the suspensions without salt can be found in Table 5.4. However, for the suspensions with added salt, this value was not representative of the particle sizes present in the suspension. For this reason, the peak values of the measured size distributions were used. This shows that the particle size augments significantly with salt addition, leading to some agglomerates of ten times the size of the original hydrodynamic diameter. In this context, the sedimentation of particles becomes relevant when pumping.

Suspension	**Salt content**	**Peak 1**	**Peak 2**	**Peak 3**
	g NaCl / g Suspension	*nm*	*nm*	*nm*
C220329	0.0001	282.046	10281.3726	34.929
9 wt%	0.001	671.969	4247.053	
C220523	0.0001	319.000	16056.000	
20 wt%	0.001	279.600	10152.000	
C220601	0.0001	631.300	5677.000	
15.4 wt%	0.001	270.200	7876.000	
Suspension	**Salt content**	**Hydrodynamic diameter**		**Standard deviation**
	g NaCl / g Suspension	*nm*		*nm*
C220329	0	103.042		0.395
C220523	0	223.333		3.743
C220601	0	163.170		0.421

Table 5.7: Hydrodynamic diameters and DLS peak values of all four suspensions with 0, 0.0001 and 0.001 NaOH g/g at 20°C

As explained in the section about particle sizes, particle sedimentation can be an issue for particles larger than 1000 nm. To avoid sedimentation in pipes, the fluid flow has to be at least the same as the so-called critical velocity v_{cr}, making v_{cr} an important factor for pump sizing. v_{cr} marks the velocity at the start of turbulent flow, for which the head loss of homogeneous mixtures is the same as for water [58]. With particles smaller than 50000 nm, the suspension can still be considered a homogeneous suspension [58]. A commonly used velocity calculation for solid-liquid mixtures is the so-called conveying velocity for settling slurries by Durand: Equation 5.3. Above this velocity, there is no deposit, moving or stationary, on the bottom of the pipe [68].

$$v_{cr} = F_L \sqrt{2 \cdot g \cdot D_p (\frac{\rho_s}{\rho_l} - 1)} \tag{5.3}$$

The Durand factor F_L is determined empirically and depends on the particle diameter and volume fractions. For conservative designs, it is common practice to use a value of 1.5 [68]. Using the data from the density measurement of suspension C220523 with 20 wt% CLPs from section 5.1.1, the particle density for this suspension can be calculated and results to 1.04216 g/cm^3.Assuming the pipe diameter D_p is identical to the diameter of the membrane modules used in the concentration step (see section above: Influence of concentration), the critical velocity v_cr = 1.2144 m/s. As the flow rate during the concentration step results in 3500 l/h (v=1.2433), the flow velocity in the pipe should be enough to avoid sedimentation when the same pipe diameter as the one for the membrane modules is assumed. The membrane module diameter represents the largest diameter in the system, as the modules themselves consist of several hollow fibre membranes with much smaller diameters, through which the fluid flows faster. The flow velocity would have to be increased for larger pipe diameters to meet the critical velocity.

Sedimentation is not the only issue regarding the pumpability of the suspensions, but also the substantial viscosity increase. As already explained in section 5.1.1, higher viscosities can lead to increased energy consumption in centrifugal pumps as well as a loss in efficiency and head [2]. Using the density of C220523 with 20 wt% the results for the dynamic viscosity can be used to calculate the kinematic viscosity. Table 5.8 shows the kinematic viscosities for selected shear rates. For both salt concentrations, the values are higher than $1.0 * 10^{-4}$ m^2/s, at which the efficiency loss and head reduction are considerable [2]. As adding salt or other additives causing flocculation is not part of the process design, caution has to be taken that no contamination of this kind is present in the solutions. The agglomerates also lead to the development of yield stress, which can make the manipulation and processing of the suspensions more difficult as the energy consumption for transfer and mixing increases [65]. The results of the rheological tests showed that adding salt, even in minimal concentrations, can increase viscosity significantly. This makes the presence of salt and other charged particles an essential parameter to be controlled for the pumpability, especially during the concentration step, since with the increased concentration of CLPs, the increase in viscosity after salt addition also becomes more pronounced.

	0.0001 g NaOH / g suspension		**0.001 g NaOH / g suspension**	
Shear rate	**Viscosity**	**Standard deviation**	**Viscosity**	**Standard deviation**
1/s	m^2/s	m^2/s	m^2/s	m^2/s
391	7.28E-04	8.58E-06	8.38E-04	8.96E-05
569	5.28E-04	1.22E-05	6.17E-04	7.34E-05
829	3.75E-04	1.34E-05	4.64E-04	6.78E-05
1000	3.15E-04	1.24E-05	3.97E-04	7.85E-05

Table 5.8: Kinematic viscosity values for selected shear rates for the suspension C220523 at 20 wt% with 0.0001 and 0.001 NaOH g/g at 20°C

The deliberate addition of substances to the suspension can also influence the rheological properties. For example, pentylene glycol is added as a preservative to the suspensions after the production. Figure 5.14 shows the effect the addition of PG has on the viscosity and shear stress of suspension C220601 over the shear rate from 10 to 1000 s^{-1} and at 20°C.

Figure 5.14a displays the viscosity measurements of the suspensions C220601 and C220601PG. As already seen in the section on the concentration influence, the higher the concentration of the CLPs, the higher the viscosity. The viscosity values at 3 wt% are nearly the same for both C220601 with and without pentylene glycol. The 9 wt% suspensions do show a difference after the addition of PG: the non-preserved suspension has a viscosity more than half of the preserved one. The difference is even more striking for the highest concentrated suspensions C220601 and C220601PG, even though the first suspension has a higher concentrations of CLPs. All suspensions also show shear thinning behaviour, with the higher concentrated suspensions presenting the clearest reduction in viscosity over the shear rate range. This behaviour can also be seen in Figure 5.14b. While all suspensions but C220601PG at 14.6

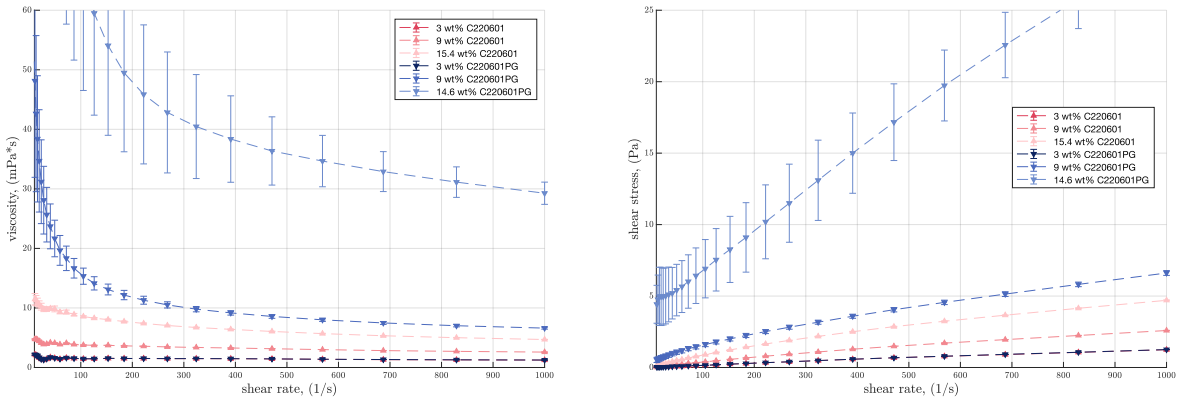

(a) (b)

Figure 5.14: Dynamic viscosity over the shear rate range 10-1000 s^{-1} for the suspensions C220601 and C220601PG and their 3 and 9 wt% dilutions at 20°C

wt% show an exponential rise, the flow curve for C220601PG at 14.6 wt% can be described by the Bingham model. Using linear curve fitting from the measured shear stress values beginning at a shear rate of 1.15 s^{-1} places the Bingham yield point τ_B at 3.667 Pa.

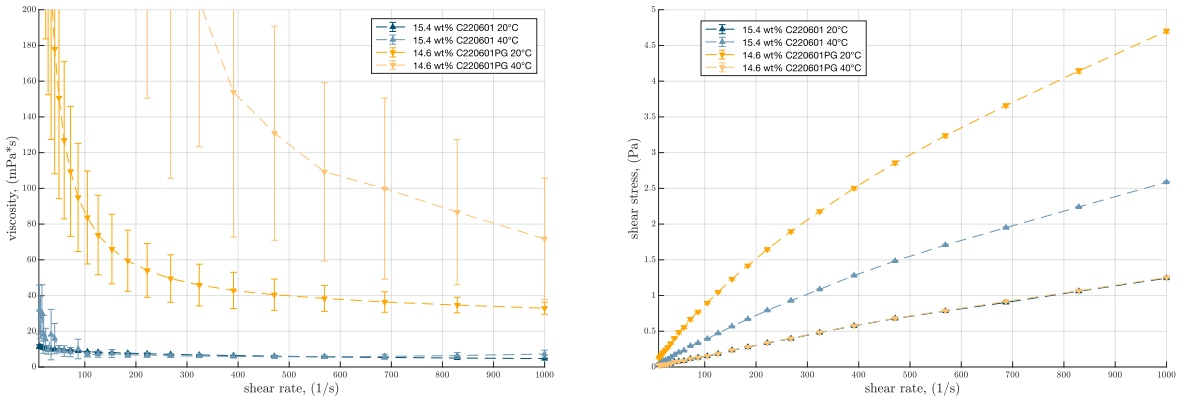

(a) (b)

Figure 5.15: Dynamic viscosity over the shear rate range 10-1000 s^{-1} for the suspensions C220601 and C220601PG at 20°C and 40 °C

The viscosity increase after the addition of pentylene glycol is even more striking at higher temperatures. No measurement data could be collected for the suspension C220601PG with 14.6 wt% at 60°C since the rheometer could not perform the measurement cycle before the sample was destroyed. The sample lost its structure and turned liquid, creating agglomerates looking like burned residues at the outer corners of the measurement stamps. Since the suspension could not be measured at 60°C, the values for 40°C were used for for the comparison. The viscosity displayed in Figure 5.15 is much higher at 40° than at 20°C, fitting with the observations made above. Figure 5.15b shows the shear stress over a shear rate range of 10

to 1000 s^{-1} for the suspensions C220601 and C220601PG at 20°C and 40°C. For C220601 the shear stress seems to stay nearly the same and only increases slightly with higher shear rates. For C220601PG at 40°C, the relationship between shear rate and shear stress changes in comparison to 20°C. The measured shear stress values are several magnitudes higher than at 20°C and they show large scatter and standard deviations. The curve does not follow a Bingham fluid course but is more of an exponential one. This results in a decreasing viscosity with increasing shear as well.

The measurements prove that the addition of pentylene glycol can influence the rheological behaviour of the suspensions at higher concentrations as well as enhance the effect of temperature has on the suspensions viscosity and shear stress. However, the exact interactions of pentylene glycol with the CLPs are not yet clear and subject of further examinations. Still, the results highlight the necessity of the rheological measurements when additives are used together with the CLP suspensions, since the addition of pentylene glycol can be critical for the pumpability of the suspension due to the increased viscosity. However, in process terms, the addition of the preservative is carried out after the concentration step and before the suspension filling. Keeping this in mind, adding the preservative might be a critical step for transferring the suspension after production via pumps but not during the concentration step. The presence of salt or charged particles seems to be a more determining influence on pumpability for that process.

5.1.2 Temperature stability

As mentioned in section 2.2 and section 2.3, temperature can lead to condensation reactions and aggregation of lignins and CLPs in aqueous medium, respectively. Temperature stability is a significant characteristic of CLPs and is essential for further processing and product development, making it an important aspect to investigate.

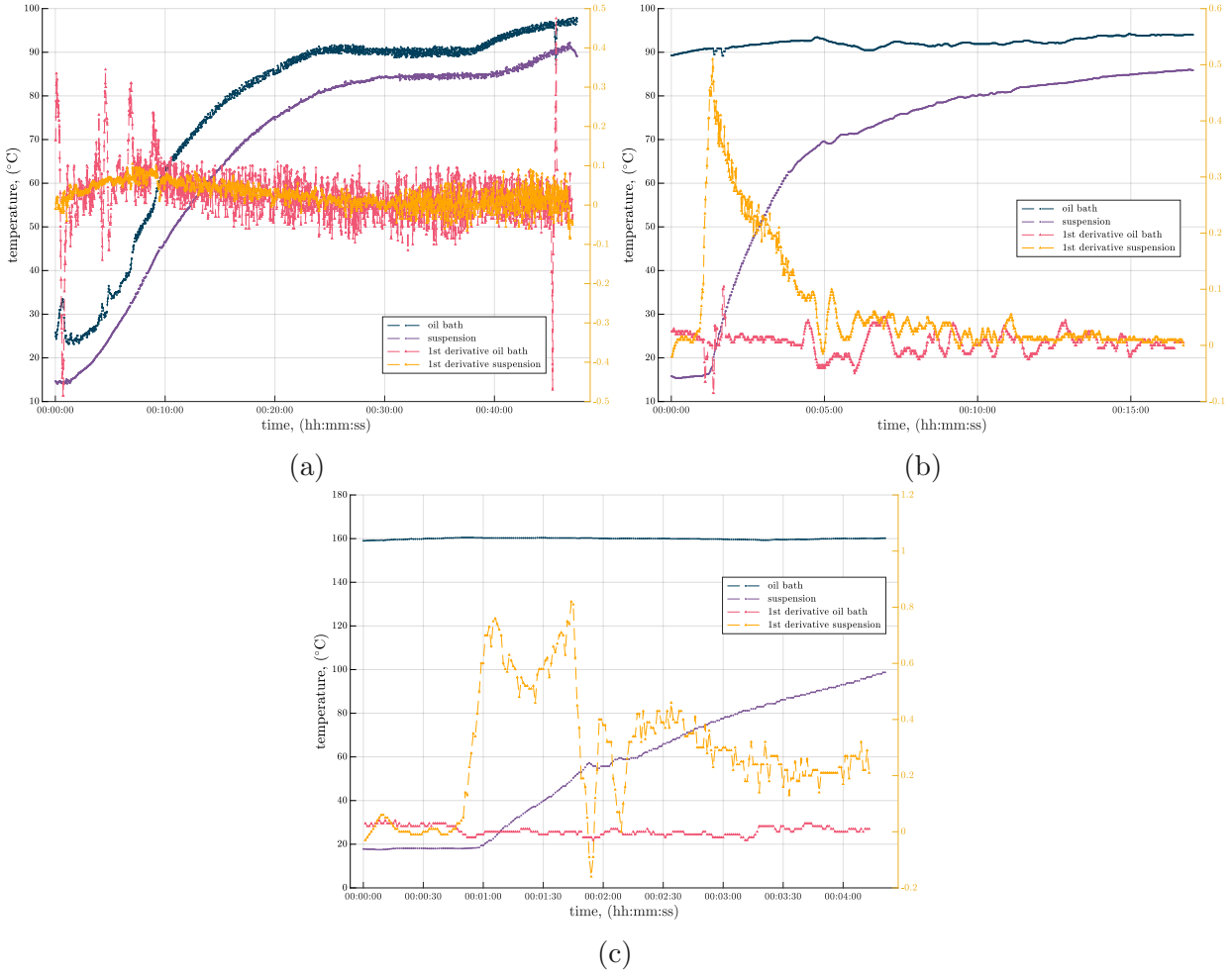

Figure 5.16: Temperature course and the first derivative over time: (a) Trial S_1, (b) Trial S_2 and (c) Trial S_3

The subfigures in Figure 5.16 show the recorded temperature of the suspensions over the heating time, as well as the first derivative of the temperature curves of each trial. All suspension temperature curves show a similar temperature increase. However, the time to reach over 90°C shortens with each trial. Figure 5.16a shows the slow heating of the suspension and oil bath, reaching 90°C at around 23 minutes. When looking at the functions of the first derivative, the general increase in temperature over time can be seen for both suspension and oil bath, as the values are mostly greater than 0. While there is a clear scatter

in the data, the maximum values for the derivative are relatively small compared to the other temperature curves. For Figure 5.16b, the suspension quickly heats up to 70°C, where a kink in temperature is visible, and then the heating commences slower. The first derivative of the suspension sharply increases, then decreases less steeply. It shows primarily positive values, reflecting the temperature increase. The oil bath temperature was not held perfectly constant at 90°C but around temperatures of 93°C, causing the first derivative to fluctuate. The course of the temperature of the suspension during S_3 also shows a bend at around 60°C. The heating process at 160°C is reduced to nearly one-third of the time compared to S_2. The course of the first derivative over time is also mostly positive, reflecting the increase in temperature. At the mentioned kink in the temperature course, the derivative curves for both Trial S_2 and S_3 show a quick fall, followed by a peak value. This indicates points of inflection and further highlights the oddity in the temperature course.

(a) (b) (c)

Figure 5.17: Remaining aggregates in the round-bottom flask after (a) Trial S_1, (b) Trial S_2 and (c) Trial S_3

The suspensions were then further analyzed using analytical methods. While the dry matter of each heated suspension showed no significant reduction in lignin content from the original 9.06 wt% (see Appendix B: Table B.1), there was a difference in the remnants after the decanting of the round-bottom flask used to heat the suspensions. The figures in Figure 5.17 show the residual aggregates for the different trials. Optically, all three trials led to the appearance of visible precipitated agglomerates, with Figure 5.17c for Trial S_3 showing the most significant amount compared to the others, followed by Trial S_2. The pictures seem to indicate an increase in aggregates with faster heating methods. Fritz et al. [23] showed that temperatures up to 70°C led to the appearance of agglomerates in solutions of hardwood and softwood kraft lignins detectable by turbidity measurements. However, macroscopic precipitation was only detected for the softwood colloidal particles at higher concentrations (above 0.3%). Since the suspension C220329 has a much higher dry matter content of 9.06 wt%, the appearance of larger, visible and heat-induced aggregates at temperatures up to 90°C fits well with this literature, even though the suspension raw material is hardwood.

The results for the DLS measurement of the original suspension and the temperature-treated ones are listed in Table 5.9, which shows an increase in HD of around 20 to 30 nm for each suspension. The particles in S_1 seem to be increased the most. This also fits well with the results found by Fritz et al. [23], where higher temperatures promote lignin aggregation

Trial	Hydrodynamic diameter *nm*	Standard deviation *nm*	Polydispersity index -
original	103.04	0.40	17.49
S_1	135.84	2.14	12.97
S_2	126.60	1.10	16.38
S_3	131.36	0.86	15.76

Table 5.9: Results for hydrodynamic diameter and polydispersity index for the suspension C220329 before and after the different heating trials

in solution. Leskinen et al. [41] also exposed CLPs from softwood kraft lignin to higher temperatures as part of a post-treatment to increase the resistance of CLPs to known solvents. They reached nearly double the temperatures used in this work but did not report any precipitating agglomerations or an increase in particle size. This seems to indicate that the thermal behaviour of CLPs is dependent on many parameters since the particles in both works differ in several characteristics from the ones in this thesis, such as the extraction process of the raw materials.

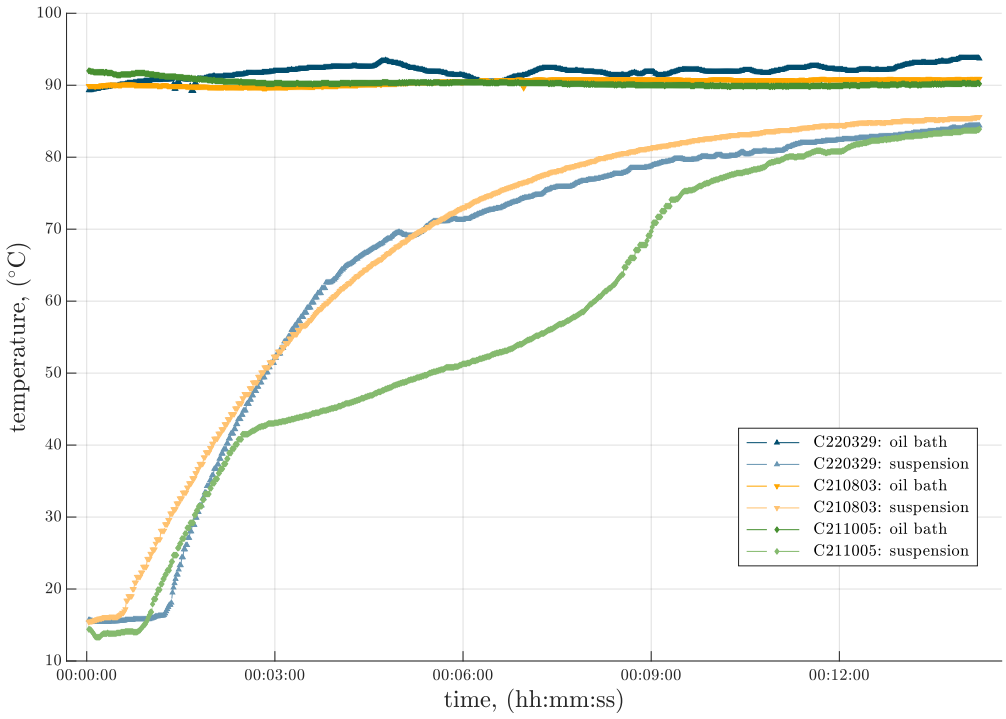

Figure 5.18: Temperature curves for the suspensions C220329, C210803 and C211005 after being heated in an 90°C oil bath

The influence of differing raw materials for the CLPs on their temperature behaviour was further investigated in this work. As the processing of CLPs for Pickering emulsions in

personal care products is one relevant application of the suspensions and is often linked to higher process temperatures (subsection 6.1.2), the heating pattern of Trial S_2 was repeated for three different suspensions in order to depict the possible worst-case in the production process of cosmetic emulsions. Figure 5.18 shows the recorded temperature curves for the suspensions C220329, C210803 and C211005. The suspensions differ in the raw material used as well as its extraction method: C220329 was extracted by enzymatic hydrolysis from hardwood, C210803 also but from softwood, and C211005 is Soda lignin from wheat straw. The course of the curve is similar for both C220329 and C210803: after a steep ascent, the curve flattens out. C220329 shows a slightly steeper temperature increase. The curve for the soda lignin CLPs (C211005) shows a very different course. While the temperature of the suspension also rises steeply at the beginning, at around 40°C, the temperature increase flattens out. At around 60°C, the temperatures start to rise faster again.

(a) (b) (c)

Figure 5.19: Remaining aggregates for the suspensions (a) C220329, (b) C210803 and (c) C211005 after being heated in an 90°C oil bath

The suspensions' heating also led to precipitating aggregates in the suspensions C210803 and C211005. Figure 5.19 shows the remnants in the round bottom flask after decanting the suspension. When comparing Figure 5.19a to Figure 5.17b, there seem to be slightly bigger aggregates, which are also more spread out on the flask walls. The softwood lignin CLP suspension in Figure 5.19b showed comparatively the least amount of aggregates. Also, they are smaller sized. The third suspension, on the other hand, did not only differ in the temperature course but also in the amount and colour of the aggregates. Figure 5.19c shows many small, fine and blackish aggregates.

	Mean dry matter *wt%*	**Stand.dev.** *wt%*	**DM 1** *wt%*	**DM 2** *wt%*	**DM 3** *wt%*
C220329	4.847	0.007	4.842	4.841	4.857
C210803	4.846	0.003	4.841	4.849	4.848
C211005			3.894		
C211005 supernatant fluid			0.458		

Table 5.10: Dry matter content for the suspensions C220329, C210803 and C211005 after being heated in an 90°C oil bath

The difference can also be noted in the dry matter content after heating, shown in Table 5.10, where there is a notable reduction from the original 4.85 wt% to 3.89 wt%. The lignin content for the suspensions C220329 and C210803 does not significantly change, similar to the heating trials discussed before. For C211005, the liquid sample showed precipitated agglomerates after a week. Therefore, the dry matter content of the supernatant liquid was also determined. Here, the dry matter content was reduced to 0.45 wt%, marking a considerable change from the first measurement. This indicates some agglomerates in the heated suspension, which need time to settle. Another possibility is the potential association of smaller aggregates to larger conglomerates, which then settle.

Table 5.11 shows DLS measurement results for the original and treated suspensions. For the suspension C220329, there is again a 20 *nm* increase, which fits well with the data for Table 5.9. For the other two suspensions, the increase is more significant. For C210803, the hydrodynamic diameters increased by nearly 50 *nm*, while for C211005, it was nearly double that. Comparing the original particle sizes with the agglomeration remnants in Figure 5.19, the amount of agglomerates seems to increase with the particle size. Interestingly, the polydispersity of both C220329 and C210803 decreased after the heating process, most significantly for the first. This was also the case in the previous temperature experiments with C220329 (Table 5.9), indicating a reduction in the particle size heterogeneity.

	original			***heating in 90°C oil bath***		
	HD	**Standard deviation**	**Polydisp.index**	**HD**	**Standard deviation**	**Polydisp.index**
	nm	*nm*	-	*nm*	*nm*	-
C220329	103.04	0.40	17.49	124.83	1.39	15.13
C210803	72.65		16.14	120.83	0.64	15.91
C211005	308.73		20.45	398.10	8.46	26.63

Table 5.11: Results for hydrodynamic diameter and polydispersity index for the suspensions C220329, C210803 and C211005 before and after being heated in an 90°C oil bath

In order to determine if the heating processes and the subsequent appearance of agglomerations also led to changes in the chemical structure of the considered CLPs, UV spectroscopy and FTIR were used. Due to the aromatic structure of lignin, it can absorb UV radiation in a light range from 250 to 400 nm [74]. A change in UV absorption of the CLPs could therefore be an indication of a change in structure. The results of the UV measurements for the original and heat-treated suspensions from the trials S_1, S_2 and S_3 can be found in Figure 5.20a. The figure shows no difference between the heated and untreated samples. All show a sharp decrease in absorbance up to 260 *nm*, then after a peak between 270 to 290 *nm*, the absorbance slowly decreased again. This indicates that no drastic changes to the chemical structure of the suspensions took place during the heating process, as the course of the curve is the same for all samples. The peak between 280 to 290 *nm* results from the free and etherified phenolic groups in the lignin structure, while the absorption between 300 to 400 nm can be attributed to the present double bonds and carbonyl groups conjugated with a phenyl group [87]. Figure 5.20b shows similar behaviour for the suspension C211005 and the aggregates: All curves show the same UV absorption curve. The wavelengths of the

peak values also align for both suspension types and the dissolved agglomerates. In order to make sure no potential structural differences could be credited to the drying process of the agglomerates, they were dried in the oven at 120°C as well as in the air. The results presented in Figure 5.20 show that the heat treatment does not affect the absorption capacity of the CLPs, even though it led to aggregation, and the chemical structure responsible for the absorption capacity was not changed.

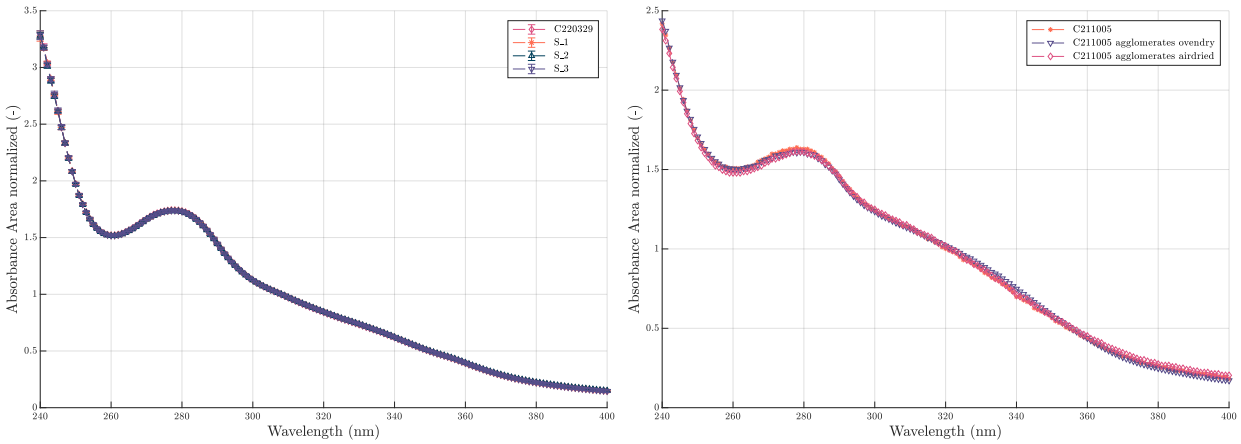

(a) (b)

Figure 5.20: Area normalized UV absorbance for (a) C220329, Trial S_1, Trial S_2 and Trial S_3 and (b) C211005 and C221005 agglomerates from 240 to 400 nm

As the suspension C211005 showed the most substantial temperature-induced instability, the suspension supernatant and the agglomerates were analyzed using FTIR. The full spectrum can be found in Appendix B: Figure B.1. The range from 1800 to 800 cm^{-1} can be described as the "fingerprint" region, containing bands characteristic of cellulose, hemicellulose and lignin [69].

Figure 5.21 shows the FTIR spectra for the suspension C211005 and the suspension supernatant and agglomerates. The spectra all show the same peaks in the fingerprint region. The marked peaks are similar to those reported in the literature [69, 95, 34, 75]. The peaks at 1031 cm^{-1} result from the stretching of bonds between oxygen and hydrogen of primary alcohols [34, 69, 95], while the peaks at 1120 cm^{-1} appear due to the plane deformation of C-H bonds in syringyl units [34, 69, 75]. The 1215 cm^{-1} peaks result from C-O bonds in syringyl and guaiacyl units. The stretching of C-C bonds in aromatic structures with deformation C-H stretching in plane leads to the peaks at 1425 cm^{-1} [34, 69, 95]. The peaks between 1417 and 1511 cm^{-1} can be credited to C-C and C-H stretchings of the aromatic skeletal and C-H deformations of methyl groups [95]. The peaks at 1597 cm^{-1} can also be credited to C-C stretching of the aromatic structures present in lignin [34, 69].

Windeisen and Wegener [90] used FTIR measurements to monitor the changes in hardwood and softwood samples after thermal treatments. The measurements revealed changes in the

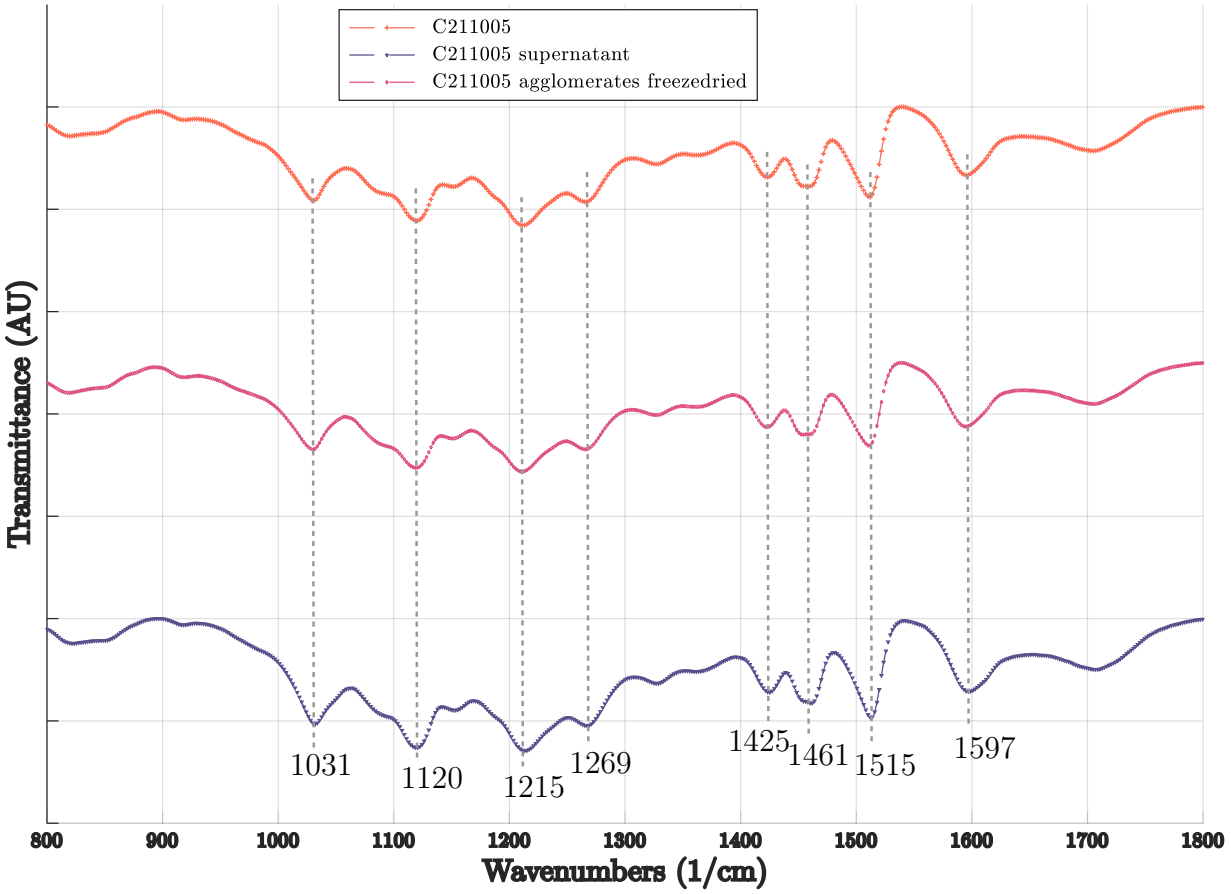

Figure 5.21: FTIR spectra for the untreated suspension C211005 and the suspension supernatant and agglomerates after being heated in a 90°C oil bath

lignin structure due to condensation reactions after the samples were treated at temperatures above 130°C: The peaks at 1330 cm^{-1} intensified as well as the vibrations of the aromatic skeletal resulting in the peaks at 1600 and 1505 cm^{-1}. This was not the case for the results in Figure 5.21, indicating that the temperatures up to 90°C did not lead to structural changes in the CLPs. Together with the results of the UV measurements (Figure 5.20), it seems that temperatures up to 90°C do not lead to structural changes or reduce the UV absorbing function of CLPs. However, the aggregations resulting from the temperature treatments might bring about difficulties in using the suspensions, especially as an ingredient in personal care products.

Chapter 6

CLP applications

6.1 Results and Discussion

Emulsions are a widely applied system in personal care and cosmetic products. Besides the medical safety of the ingredients, the formation, storage stability and rheology of emulsions are important characteristics to consider for these products [83]. The knowledge of the rheological properties of cosmetic materials is essential for the development of products, as the application and customer acceptance depend on it [39]. Initial skin feel and spreadability are just some characteristics strongly tied to rheology. Also, the temperature stability of the added CLP suspensions is an important characteristic for the manufacturing process of the emulsions.

6.1.1 Rheological behaviour

Rheology of emulsions with varying concentrations

Figure 6.1 shows samples of the produced emulsion containing CLPs. The labels below the samples indicate the suspension concentration used to make the emulsions. For easier comprehension, the emulsions will be referred to by the concentration of the suspension used to produce the emulsion. The lowest concentrated emulsion on the left side of the figure shows the lightest colour, while the other creams darken progressively in colour with the increase of CLP concentration. The reference is not shown in the image but is white.

Figure 6.2 displays the measured viscosity over the shear rate for all four emulsions. Shear thinning can be observed for all emulsions: the viscosity decreases with increasing shear rate. The presence of CLPs raises the viscosity. For example, the emulsion prepared with the 9.7 wt% suspension shows η around three times higher than the reference cream without CLPs for most of the measured shear rate range. The viscosity for the emulsion with 14.6 wt% CLPs is even higher. However, the course of the curve deviates at shear rates around 20. Then, the viscosity falls to the levels of the one with 9.7 wt% and continues to fall

Figure 6.1: Samples of the emulsions containing varying amounts of CLPs. The weight percentages shown refer to the concentration of the CLP solution used to prepare each emulsion.

below the others for higher shear rates. At low shear rates $\dot{\gamma} < 2s^{-1}$, a slight plateau-ing of the viscosity curves is visible. Also, at higher shear rates, the viscosity of the emulsions containing 0 wt%, 4.85 wt% and 9.7 wt% of CLP suspension seems to reach a similar value.

The shear stress τ over the measured shear rate $\dot{\gamma}$ range for the emulsions in a logarithmic scale at 25°C is presented in Figure 6.3. The graph shows that all emulsions experience a significant increase in the shear stress at shear rates below 0.5 s^{-1}. Here, the values for the shear stress are highest for the emulsion prepared with 14.6 wt% CLP suspension and decrease for each emulsion with less concentration of CLPs. The lowest shear stress values were measured for the cream containing no CLPs for shear rates between 0.01 and 200. The 0 wt% and 9.7 wt% emulsions show little change in the shear stress value over the range of 0.5-10 s^{-1} and 0.5-30 s^{-1}, respectively. A nearly exponential rise can be noted for both emulsions for the subsequent shear rates, ending at a value of around 450 Pa at the final measurement point. This final shear stress magnitude is also noticeable for the emulsion prepared with 4.85 wt%. However, this emulsion does not show a distinct plateau in the curve as the other two emulsions, but rather a constant increase. Over most of the curve's course, the shear stress values lay closer to those for the emulsion with no CLPs.

A striking difference can be seen for the cream prepared with 14.6 wt% CLP suspension. Here, the course of the curve significantly deviates compared to the others at shear rates higher than 0.5 s^{-1}. After reaching a maximum value for the shear stress of 361 Pa at 1.9 s^{-1}, the shear stress decreases for the next 15 measurement points. As mentioned before, the other emulsions show an increase in the shear rate until reaching a similar shear stress at the end of the measurement. This behaviour is not the case for the 14.6 wt% emulsion, where the shear stress values only increase by around 60 for shear rates after 21.9 s^{-1}. Looking at the error bars for each measurement point, which display the standard deviation from the mean of the three measurements done for each emulsion, larger deviations can

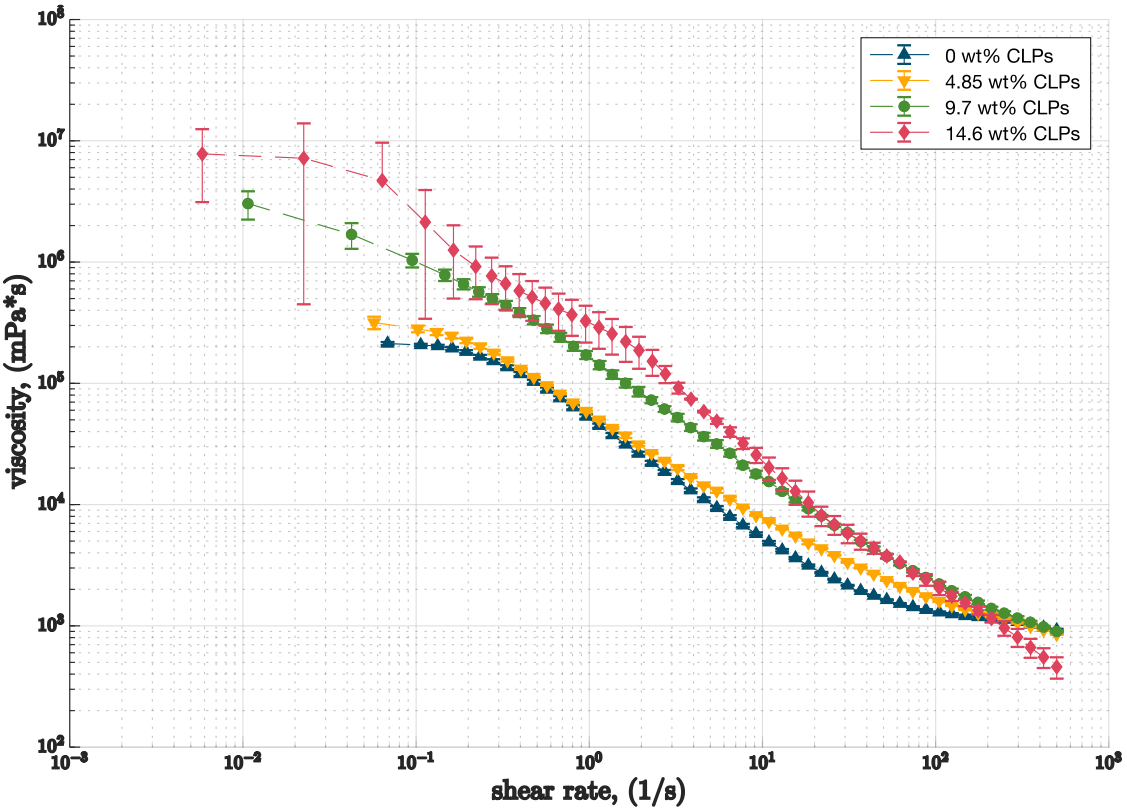

Figure 6.2: Viscosity as a function of the shear rate for the four emulsions at 25°C

be seen for this emulsion in comparison to the others: The relative standard deviation for these measurements lay mostly above 10%. For the other emulsions, the relative standard deviation remains below 5% for at least half of the measurement points.

Figure 6.4 presents the viscosity η as a function of the shear stress in a logarithmic scale. Since both the shear stress and viscosity resulted from the measurement, horizontal and vertical error bars indicate the standard deviation derived from the three measurements per emulsion. The curves generally show a slight decrease in viscosity for low shear stresses, then a sharper decline in viscosity for higher shear stress values. For even higher stress values, the reduction in viscosity is less substantial. The viscosity for the emulsion prepared without CLPs is lowest and increases with the concentration of the suspension used for the emulsion production. At the higher shear stresses, the viscosity for the emulsions prepared with 0%, 4.85% and 9.7 wt% of CLP suspension seem to lay close together. Similar to Figure 6.3, the course of the curve for 14.6 wt% shows a significant difference compared to the others as well as the most considerable standard deviations for each measurement point.

Figure 6.2 shows that all emulsions display non-ideal flow, as the viscosity does not remain constant over the shear rate [52]. The curves of the four emulsions in Figure 6.4 and Figure 6.2 also allow them to be characterised as having a shear-thinning region, as the viscosity

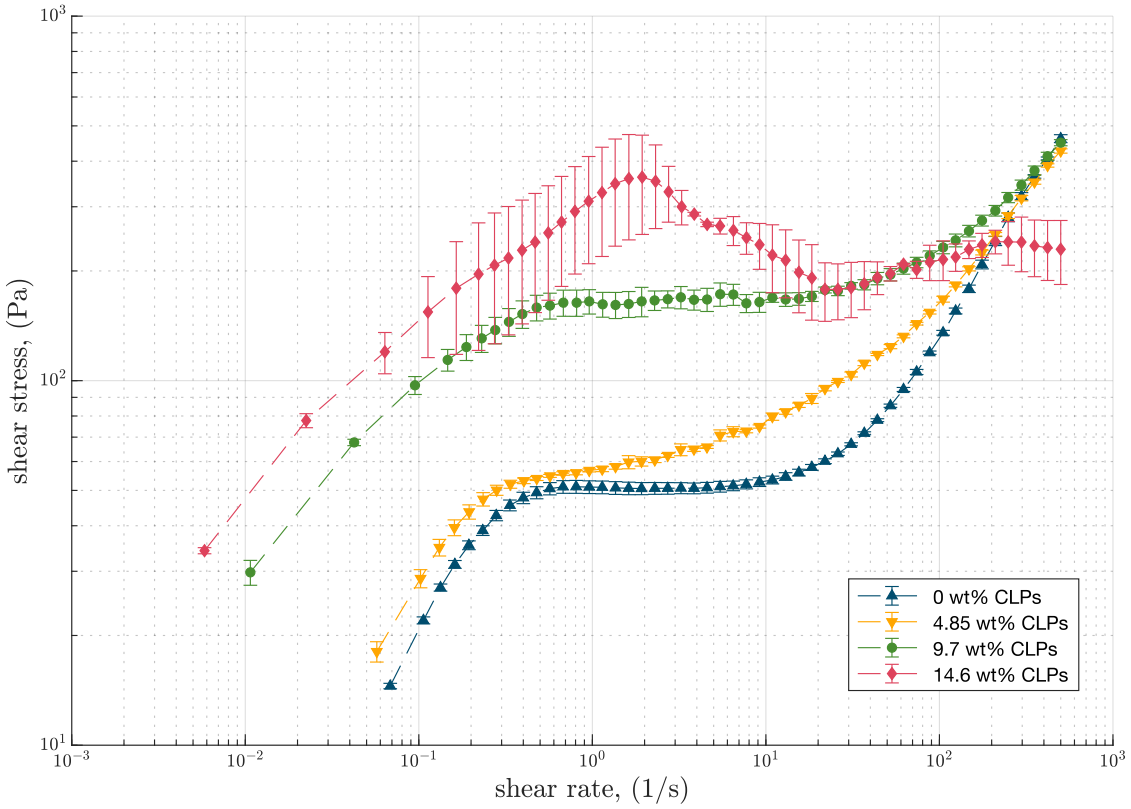

Figure 6.3: Shear stress τ as a function of shear rate $\dot{\gamma}$ for the four emulsions at 25°C

decreases in parts of the curve with increasing shear load (shear stress and shear rate). The curves of the emulsions containing no CLPs and 9.7 wt% display a typical shear-thinning course. Also, at very low shear stress, the viscosity of all emulsions seems to reach a high limiting value. This plateau value is usually referred to as the residual or zero shear viscosity [83]. According to Tadros [83], this flow behaviour is typical for emulsions. Using a method suggested by Stokes et al. [79], the apparent yield stress τ_0 can be estimated from Figure 6.4 by finding the point of intersection between the extrapolated zero-shear plateau and the shear-thinning region. Since there are differing views on the concept of yield stress and the determination of it as a natural material constant, the term apparent yield stress is used.

In this context, the apparent yield stress is equal to the critical stress of a shear-thinning flow curve, where the behaviour of the emulsion changes from solid-like at low shear rates to liquid-like at higher shear rates [79]. Looking at the course of the curves in Figure 6.4, the critical stress characterises the point where a high zero-shear viscosity yields to a viscosity several decades lower [79]. The critical stresses of the four emulsions vary with the concentration of CLPs: the lowest is reached by the 0 wt% cream and seems to increase with increasing wt% of CLPs. Approximating the apparent yield stress for the creams containing 9.7 wt% and 14.6 wt% proved difficult, as the data shows no distinct shear-viscosity plateau. Still, an estimation can be made: the critical stress of the 9.7 wt% emulsion is three times the

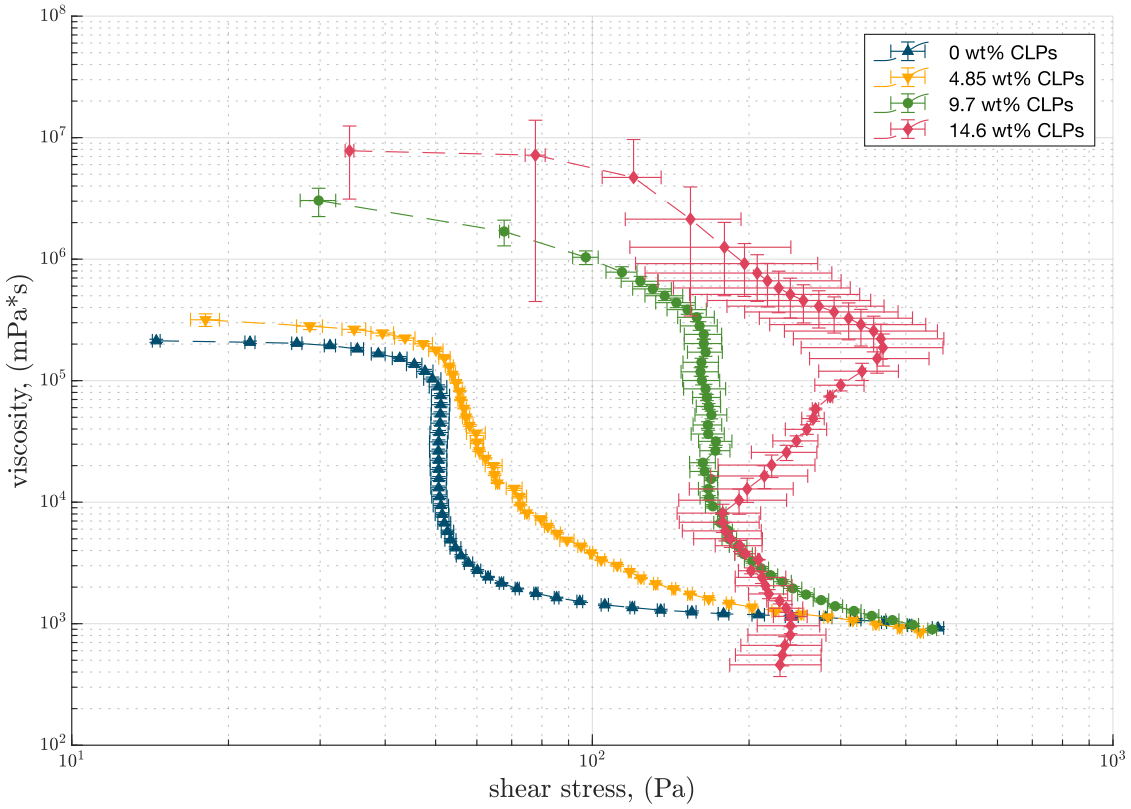

Figure 6.4: Viscosity η as a function of shear stress τ for the four emulsions at 25°C

magnitude of the emulsion containing no CLPs and that of the 14.6 wt% emulsion four times. This suggests that the apparent yield stress increases with the concentration of CLPs added to the emulsion. For the experimental emulsions, the higher yield can marginally be felt when first putting the emulsions on the skin: the creams containing more CLPs keep better consistency before being spread.

Figure 6.2 also showed plateauing of the viscosity values at very high shear rates (above $\dot{\gamma} > 100$ to $500s^{-1}$). This is called the infinite shear-viscosity [52]. According to Mezger [52], at this point, all macromolecules are oriented in the flow direction, and the flow resistance reaches a minimum value, resulting from the molecules gliding off each other. A flow range showing the typical shear-thinning behaviour between very low and high shear rates can be found. Here, the dispersed droplets of the emulsion are deformed from spheres to ellipsoids and oriented in the flow direction [52]. In their work on the rheology of Pickering emulsions, Boostani et al. attributes the shear thinning behaviour to a shear-induced down-break of the emulsion network [7]. While a disrupted network can recover, after a certain point, the disruption rate becomes more significant than the recovery rate [7]. They argue that a higher concentration of particles leads to an increased viscosity in Pickering emulsions, as higher interactions between smaller droplets reinforce the emulsion network, leading to stronger resistance to flow. This fits well with the measured viscosity values in Figure 6.2.

The rheological behaviour of emulsions is an important aspect of Pickering emulsions as cosmetic applications. According to Tadros [83], the critical stress and the zero shear viscosity are helpful parameters in using emulsions for cosmetic purposes. The zero shear viscosity can indicate the emulsion's stability: the lower its value, the higher the chance for creaming or sedimentation of the emulsion. Therefore, adding CLPs to the emulsion could be beneficial, as the zero shear viscosity for the emulsions with CLPs was higher. The yield stress can be used to estimate the true yield stress, which is significant for long-term stability and application purposes [83]. Kwak et al. [39] also describe the yield stress as a measure of the initial sensory feeling the consumer experiences when using the product. For one, it can give an idea of the minimal force required to pour the emulsion from its container, and it should therefore be large enough so that the contents do not flow out. At the same time, the yield stress should not be too great to prevent the emulsion from spreading on the skin. Minor yield stress suggests that the emulsion can be applied more easily on the skin. However, for values too low, the cream might flow down immediately.

Shear thinning behaviour is also a critical factor for the spreadability of cosmetic products and, therefore one of the key aspects of consumer acceptance. When spread on the skin, the product should form a thin and even layer, which is a direct result of a decreasing viscosity with increasing shear [39]. Especially in the context of sunscreens, shear thinning flow is essential, as the formulation can break down easily while spreading and regain viscosity to form a protective film with evenly distributed UV filters. A coherent protective film is linked to a higher and consistent SPF, which makes this flow property an important factor for the efficiency of a sunscreen [25, 21]. Recalling the critical stress mentioned above, a higher yield stress prevents the cream from immediately flowing off the skin, which allows it to be spread evenly. The UV-filtering emulsions with CLPs might therefore be more efficient than the emulsion without, even though all display shear-thinning behaviour, however, the critical stress of the CLP emulsions is higher.

As previously mentioned, the course of all the curves for the emulsion containing the 14.6 wt% suspension showed striking differences from the other emulsions as well as larger standard deviations, such as Figure 6.3. An explanation for this can be the occurrence of slip between the walls of the measuring geometry, where a low-viscosity film forms on the shearing surface [79]. Slip behaviour can be identified by the appearance of a plateau or shoulder in the viscosity curve at intermediate shear stresses, as was the case for the 14.6 wt% emulsion in Figure 6.2 [79, 29]. To avoid this, measurement plates with roughed surfaces might be used for future investigations. The measurement of the rheological properties of structured fluids is generally difficult as a number of parameters can influence it [79]. Besides the already mentioned wall slip, other reasons like the loading process or the presence of large particles can lead to micro-structure alteration or breakage. The chosen PP setup also has some drawbacks. Within the gap, the shear strain increases from zero in the centre to a maximum value at the rim, exposing the sample to a non-uniform shear rate and shear stress [40]. As all these parameters are difficult to avoid, an IUPAC Technical Report on viscosity measurements in rotational rheometers sets the typical experimental error to 1-10% [40].

Therefore the measured rheological values can still be considered somewhat representative since the relative standard deviations of the other three emulsions lie inside this error margin.

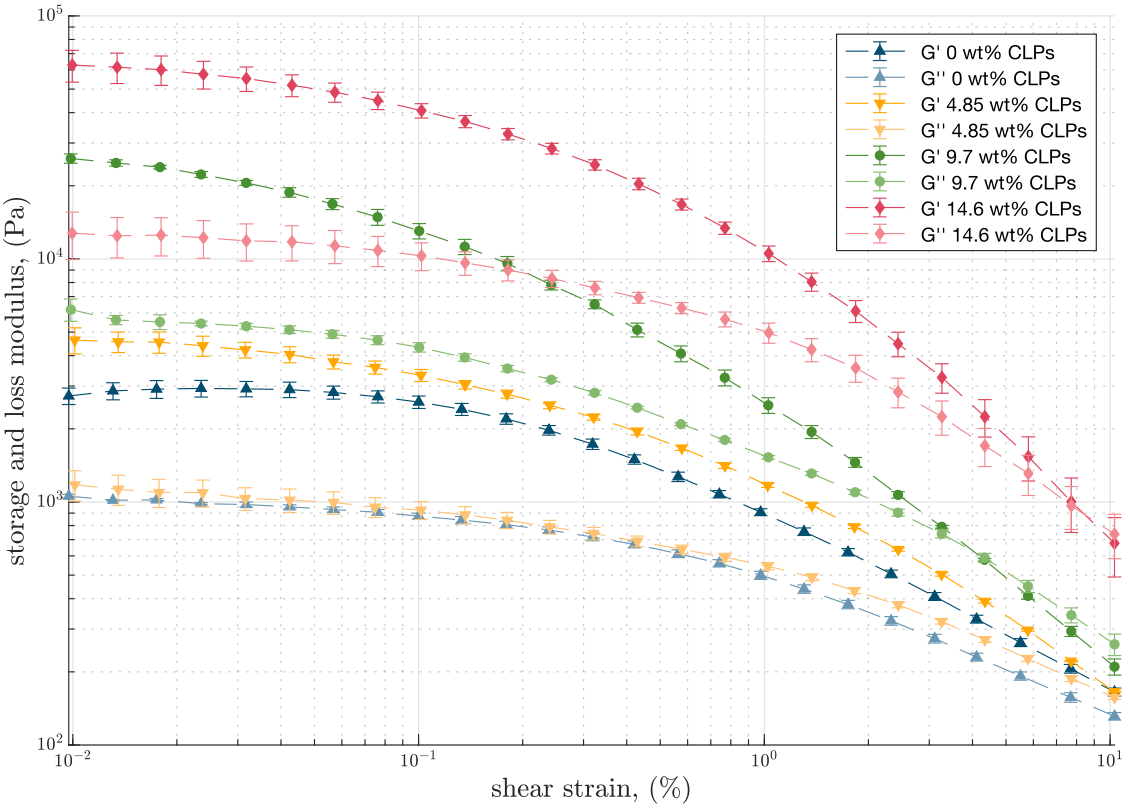

Figure 6.5: Result of the amplitude sweep with storage and loss modulus (G' and G") for the four emulsions at 25°C

Oscillatory measurements In addition to the shear stress and viscosity measurements which were discussed up until now, the rheology of the emulsions was also analysed by performing oscillatory tests. Figure 6.6 and Figure 6.5 present the results for the amplitude tests carried out over a strain rate from 0.01-10%. Amplitude sweeps are a part of oscillatory tests where the amplitude varies, while the frequency is set at a constant value [52]. In all oscillatory tests, the frequency was set to 10 rad/s. The measurement provides values for the storage modulus G' and loss modulus G", which, in simple terms, represent the elastic and viscous behaviour of the sample, respectively. The results are shown in Figure 6.5. For all samples, the curve of the storage modulus G' is higher than the curve of G" up until 0.1% strain. Until then, elastic behaviour is stronger than the viscous behaviour in all samples, indicating a gel- or solid-like state [52]. The point of intersection between G' and G" (G' = G") is called the flow point. It represents the rupture of the internal structure, and a solid-to-liquid-like transition takes place [16]. For the emulsions with 0% and 4.85 wt%, the flow point lies outside the measured range. The values for each emulsion's flow point can

be found in Table 6.1 together with the critical strain. For the emulsion with 9.7 wt% of CLP suspension, the curves intersect at around 4%. Then the curve for G" is higher. From then onwards, the viscous behaviour is stronger than the elastic one, and the sample shows characteristics of a liquid [52].

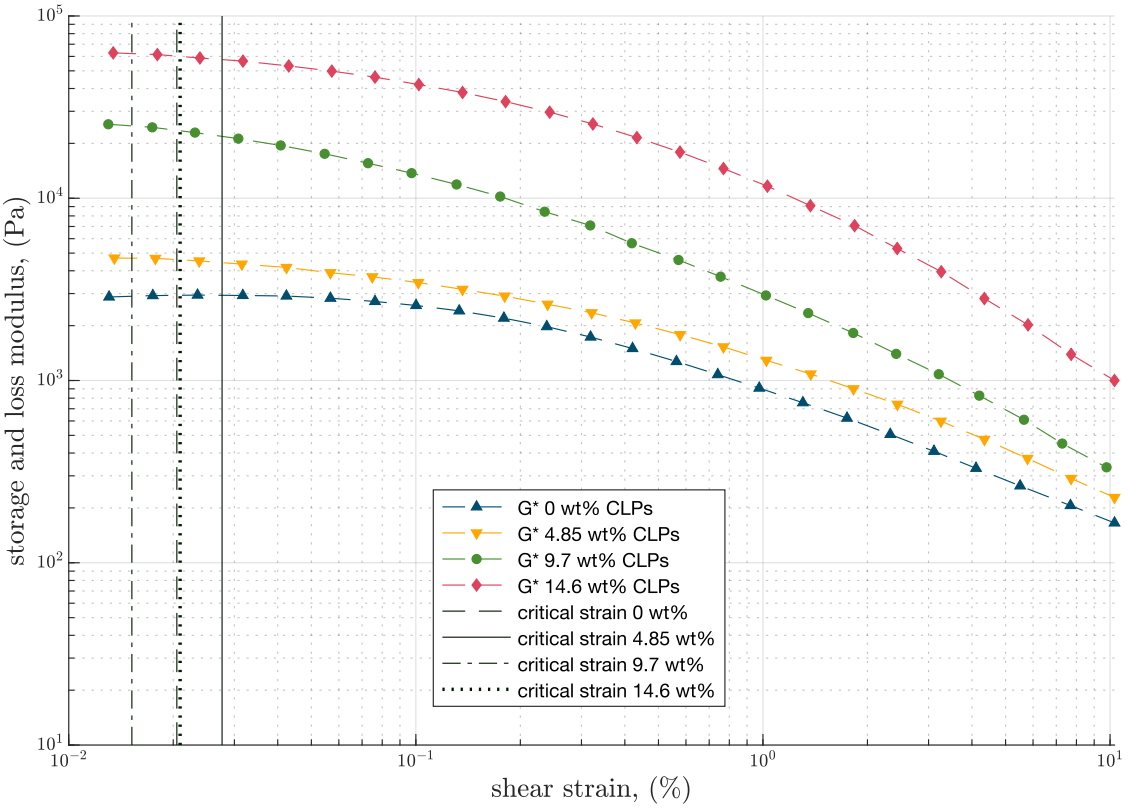

Figure 6.6: Complex modulus G* as a function of strain γ and the critical strains γ_{crit} for the four emulsions at 25°C

The measured storage modulus G' and loss modulus G" were brought into relation via the Cox-Merz analogy Equation 3.10 and used to calculate the complex modulus G* [50]. The result is shown in figure Figure 6.6 together with the values for the critical strain. The latter's value (γ_{crit}) was found by firstly determining the strain value at which a more than 10% deviation of the storage modulus G' from the plateau value occurred [52]. This plateau value was calculated using the mean of the first three storage modulus values. Using the value for the strain at which the deviation was first higher than 10%, the critical strain was calculated as a mean value between it and the preceding measured strain value. The results can be found in Table 6.1.

Knowing the critical strain is necessary for the oscillation frequency test, as it marks the end of the Linear Visco-elastic (LVE) region and the fixed amplitude strain should be below that [52]. When the critical strain value is surpassed, the structure of the sample has been changed and micro-structural properties can no longer be related to it.

Emulsion (-)	critical strain γ_{crit} (%)	flow point γ_f (%)
with 14.6 wt% CLPs	0.0209	8.5
with 9.7 wt% CLPs	0.0152	3.9
with 4.85 wt% CLPs	0.0277	-
with 0 wt% CLPs	0.0205	-

Table 6.1: Calculated critical strain γ_{crit} and flow point γ_f for the emulsions at 25°C

The values fit with the estimated limiting value of $\leq 1\%$ for the strain described by Mezger for materials with a network such as emulsions [52]. Comparing these values also with the data shown in Figure 6.5 and Figure 6.6, all samples display gel-like behaviour in the LVE-region. Based on the results in Table 6.1, the strain value for the following frequency tests was set at 0.01% to ensure the results lay inside the LVE for each emulsion.

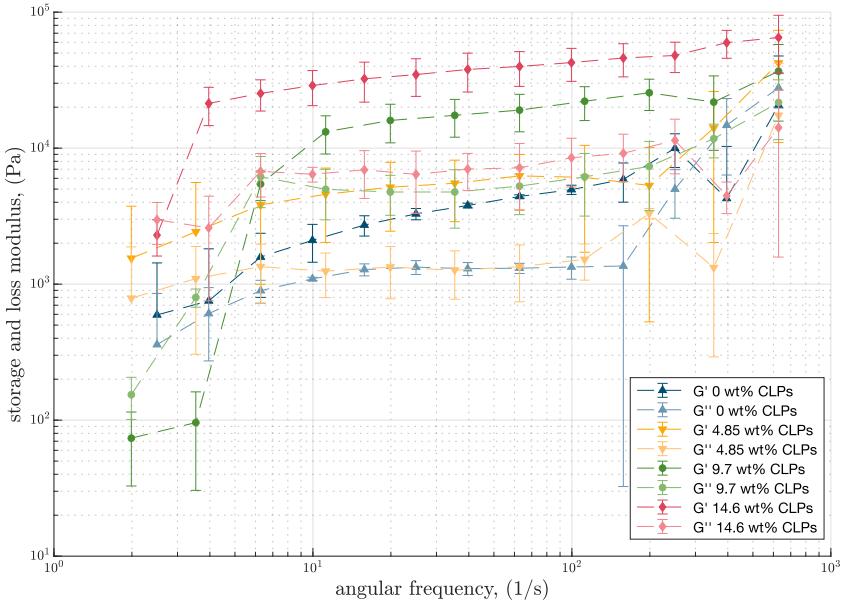

Figure 6.7: Storage and loss modulus G' and G" as a function of the angular frequency ω for the four emulsions at 25°C

The result of the frequency sweeps, the second oscillation tests that were carried out, can be found in Figure 6.7. These measurements can be used to show if the elastic or viscous response predominates in a visco-elastic material and indicates the presence of network structures [33]. All measurement points are higher than 10 Pa and the data shows that the values for storage modulus G' and loss modulus G" are higher with more CLPs present in the emulsion. Mezger [52] suggests that, as a rule of thumb, a storage modulus G' higher than 10 Pa is an indication of certain dispersion stability in an emulsion. This is the case for all of the considered emulsions. The graph in Figure 6.7 also show that, for the emulsions

containing no and 9.7 wt% CLPs the curve of G' starts out lower than the one for G" for the first 2 and 3 measurement points respectively. Then, the storage modulus G' proceeds to be higher than the loss modulus G". For the other two emulsions this is not the case over the measured angular frequency range: Just for the emulsion containing 14.6 wt% the first measurement point of G" is slightly higher than G'. The dominance of the storage modulus G' indicates that the behaviour of the emulsions is primarily of elastic and not viscous nature [39].

As mentioned above, these measurements also indicate if a network structure is present in the sample. If G' is greater than G" and the course of the curve is independent of frequency, meaning it stays unchanged over the varying frequency, then a network formation is present. On the other hand, little to no network structure and a viscous liquid-like system exist if the moduli are dependent on the frequency and the loss modulus is greater than the storage modulus [86]. Comparing the course of the storage modulus G' of the cream containing no CLPs over the range of 10-100 ω, it shows a more substantial increase than the other emulsions. This indicates a stronger dependency on the frequency. The creams containing CLPs only increase slightly and show less dependence on the frequency. Therefore, it can be assumed, that the presence of colloidal particles generally supports a network formation between dispersed droplets. Torres et al. [86] back this claim, arguing that colloidal particles provide an important stabilising mechanism for the built network. Expanding on this idea, Figure 6.7 shows a more linear course of the curve for the 9.7 and 14.6 wt% emulsions at higher frequencies than the emulsions with 0 and 4.85 wt%, implying a more stable network formation with higher CLP concentrations. If both criteria of G' > G" and frequency-independence of the moduli are met, then an emulsion can be regarded as physically stable [86]. As mentioned above, the emulsions with 0 wt% and 9.7 wt% CLPs show a different behaviour at low frequencies, as the loss modulus G" is higher than the storage modulus G'. This suggests that, at low frequencies, the response of the systems is more viscous than elastic. As the frequency is a reciprocal value of time, low frequencies correspond to longer timescales than high frequencies. The behaviour of the two emulsions is not uncommon for visco-elastic samples and results from characteristic relaxation times of the build network [86].

Another way to interpret the results of the frequency tests is via the so-called loss factor $\tan(\delta)$, which can be calculated by Equation 6.1. As the ratio of the lost and stored deformation, the loss factor allows for a characterisation of the viscous and elastic share of the visco-elastic deformation. A $\tan(\delta)$ lower than 1 indicates a gel-like or solid-like visco-elastic state [52]. The smaller the value, the more elastic the system is since G" is smaller than G' [80]. On the other hand, if $\tan(\delta)$ is larger than 1, then a more fluid or liquid state is reached.

$$tan(\delta) = \frac{G''}{G'} \tag{6.1}$$

Figure 6.8 shows the results for the loss factor of all four emulsions. The obtained curves show

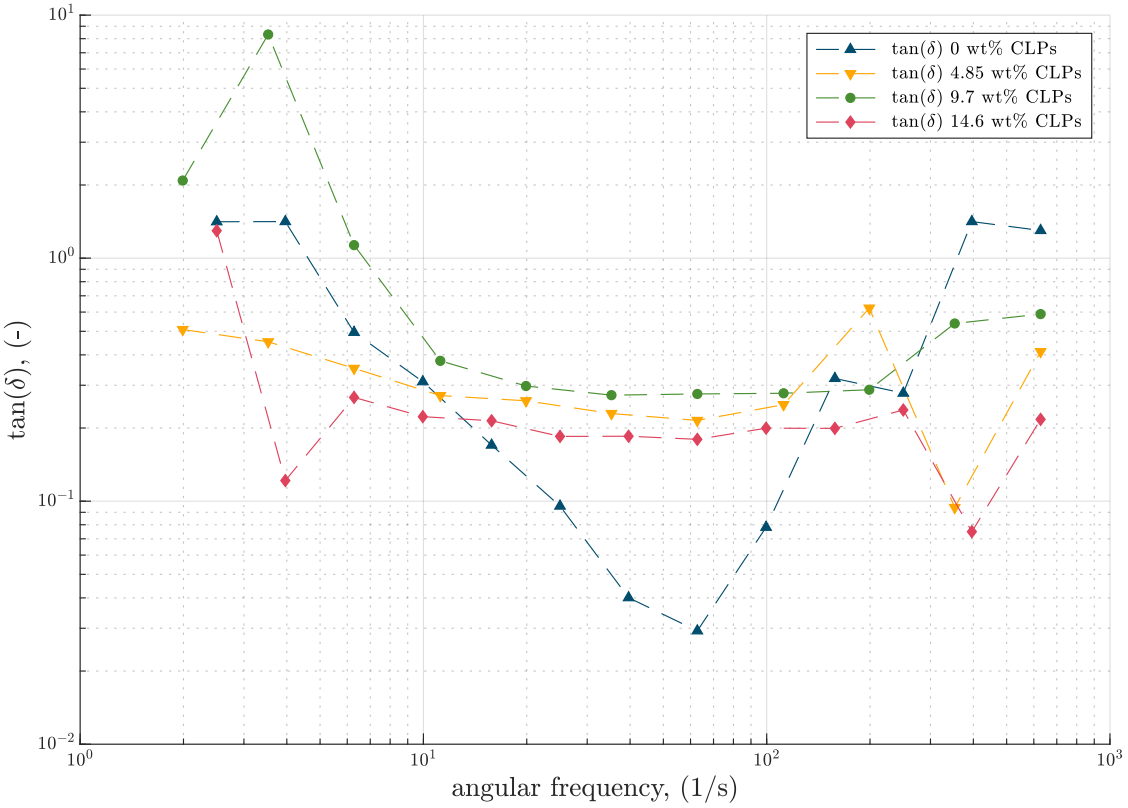

Figure 6.8: Tan(δ) as a function of angular frequency ω at 25°C

good accordance with the conclusions that were drawn from Figure 6.7 presented above. For most of the frequency range, the emulsions show gel-like behaviour. As a tan(δ) smaller than one results of G' > G", the behaviour of the material is more elastic than viscous. At low frequencies, the loss factor of the emulsion containing 0 wt% and 9.7 wt% is bigger than 1, suggesting more fluid-like behaviour, and decreases to below one at higher frequencies. This fits well with the viscosity curves of the two emulsions in Figure 6.4, as systems behaving this way often show distinct zero-shear viscosity plateaus [52]. For angular frequencies between 10 and 100 s^{-1}, the loss factor of the emulsions containing CLPs remains fairly constant, while the one for the reference emulsion without CLPs shows a strong dependence on the frequency. According to Hohl et al. [33], an emulsion can be considered kinetically stable if G' > G" and the loss factor shows little dependency on the angular frequency. This seems to suggest, that the presence of CLPs positively influences the stability of the emulsions. While the emulsion without CLPs also exhibits a gel-like character in this frequency range, a strong dependence on the angular frequency can be observed. Kwak et al. [39] present these linear visco-elastic features as helpful criteria to assess the stability of cosmetic products at rest: A gel- or solid-like elastic behaviour is to be preferred, as the shape and structure of the product remain preserved for longer.

Rheology of emulsions with varying pH

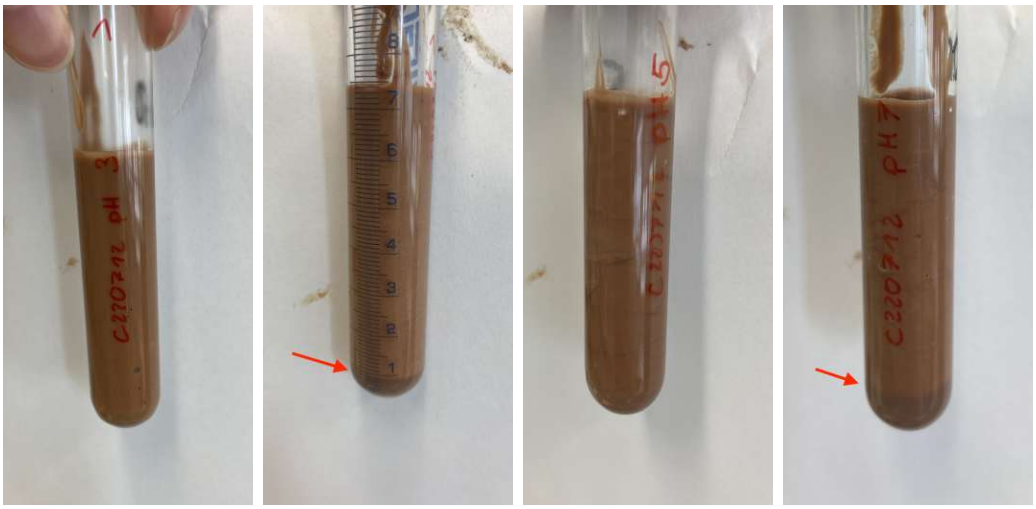

(a) (b) (c) (d)

Figure 6.9: Sample of emulsions with (a) pH 2.5, (b) pH 3.4, (c) pH 5.5 and (d) pH 7.2 after 24 hours at room temperature

The above pictures in Figure 6.9 show the emulsions after 24 hours at room temperature. The emulsions with pH 5.5 and 2.5 remained stable. The emulsions with pH 3.4 and 7.2 show some instability in the form of a segregated water phase at the bottom of the centrifuge tube below a stable emulsion phase. The segregated water phase is around 10 vol% for both emulsions. The segregation of just water and not oil indicates the formation of a stable droplet network resistant to coalesence [85].

Figure 6.10 shows the results for the measured viscosity over the shear range. For easier comprehension, the emulsions with different pH values will be referred to by the set pH value. Figure 6.11 is an excerpt of the measurement range from 1 to 100 s^{-1} that was included for better visibility, as the values for pH 3.2, 5.5 and 7.2 lay closely together. Both graphs show the shear thinning behaviour of the MCT emulsions, as the viscosity decreases with the increasing shear rate. At low shear rates, an indication of a zero-shear plateau can be observed. For shear rates up to 10 s^{-1}, the viscosity of the emulsion with pH 2.5 is significantly lower than the other three emulsions. At $\eta \geq 10\ s^{-1}$, the curve's course starts to level before decreasing again. This slight shoulder indicates that wall slip occurred [29]. Looking at Figure 6.11 for more detail, one can see that the viscosity of the emulsion with pH 5.5 is the highest. The emulsion with pH 3.4 shows nearly identical viscosity values to the one with pH 5.5 at higher shear rates. In this shear rate range, the emulsion with pH 7.2 shows the third-highest viscosity. Therefore the measured viscosities of the emulsions can be ranked from highest to lowest by their pH-value: 5.5, 3.4, 7.2 and 2.5. Looking at Table 4.7, this ranking fits with the concentrations of the suspensions used to prepare the emulsions, since the addition of the acid and base led to small concentration differences.

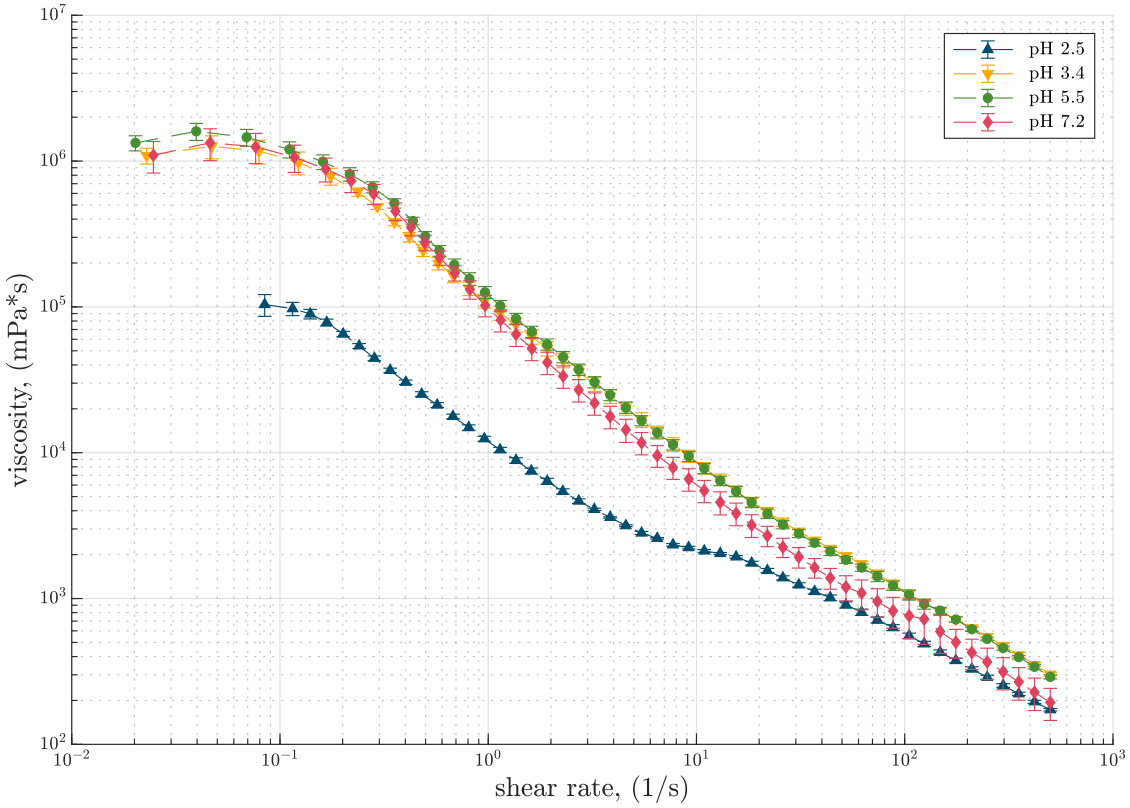

Figure 6.10: Viscosity as a function of shear rate γ_{crit} for the four emulsions at 25°C

Only the emulsion with pH 5.5 and 3.2 switched positions. Still, as the concentrations only differ by max. 2.1%, the influence of the concentration difference on the viscosity might be neglected. Therefore the viscosity seems to increase with increasing pH, probably reaching the highest values between pH 3 to 6 and decreasing again at more neutral and alkaline pH values.

In Figure 6.12, one can see that the emulsions with pH 3.4, 5.5 and 7.2 show a similar course of the shear stress function. All three curves show a maximum for the stress values at 0.3 s^{-1}, followed by a decrease of the stress values and another increase at shear rates higher than 20 s^{-1}. At lower shear rates, the shear stress is highest for the emulsion with pH 5.5. At shear rates around 5.5 s^{-1}, the values for τ for pH 3.4 become nearly equal to the ones of pH 5.5. The emulsion with pH 7.2 shows lower stress values than the before mentioned emulsions, especially in the higher shear rate range. Here, the values lie lower by an order of magnitude of around 30 Pa. On the contrary, the course of the curve for pH 2.5 is very different from the others, and the measured shear stress values are smaller. The shear stress increases at a lower shear rate, but the subsequent decrease is not as pronounced here. The increase after $\dot{\gamma} \geq 20$ is more drastic, and the values for the shear rate rise to 86.5 Pa for $\dot{\gamma} = 500\ s^{-1}$.

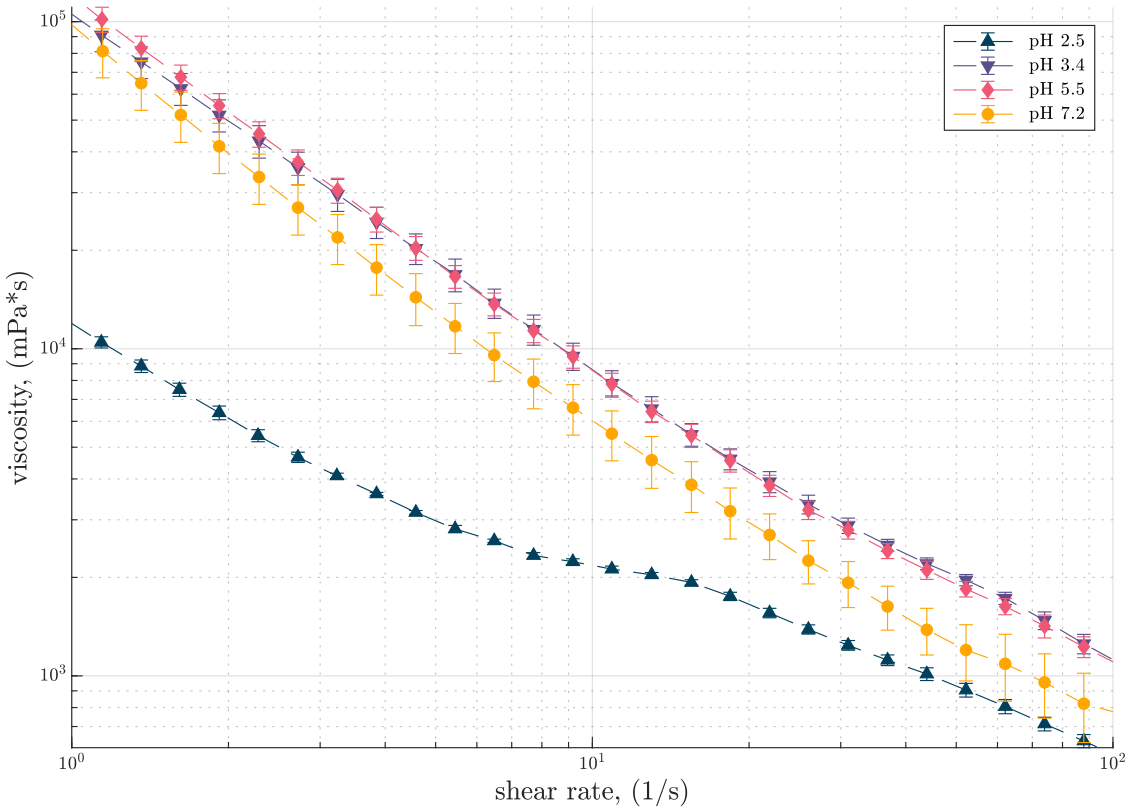

Figure 6.11: Close-up of the viscosity as a function of shear stress over 1 to 100 s^{-1} for the four emulsions at 25°C

Figure 6.13 displays the measured viscosity values over the shear stress. The horizontal error bars for the measured shear stress were omitted for better visibility. The graph shows shear thinning behaviour for all emulsions as the viscosity decreases with the shear stress. For the first measurement points of each emulsion, the viscosity shows a nearly constant value before the viscosity declines sharply. As already mentioned in section 6.1.1, this plateau value indicates the presence of a zero-shear viscosity, which is typical for emulsions [83]. In accordance with Figure 6.12, the zero-shear plateau for the emulsion with pH 2.5 shows lower viscosity values than the other emulsions. Then, the viscosity continuously decreases with the shear stress. For the other emulsion, the viscosity falls as well. However, the shear stress changes over the measurement from higher to lower values and back to higher ones. Still, a decrease in the viscosity takes place, showing the shear-thinning behaviour of the emulsions.

This non-newtonian behaviour can also be seen in Figure 6.12, as the relation between shear stress and shear rate is non-linear. Using the same method as for the emulsions with shea butter and babassu oil [79], the critical stress can be estimated from Figure 6.13. The critical stress for the emulsions with pH 2.5 is nearly ten times lower than those with pH 3.4, 5.5 and 7.2. A lower apparent yield stress suggests that the emulsion starts to flow earlier than the other emulsions, for example, making it easier to pour out of containers [39]. Also,

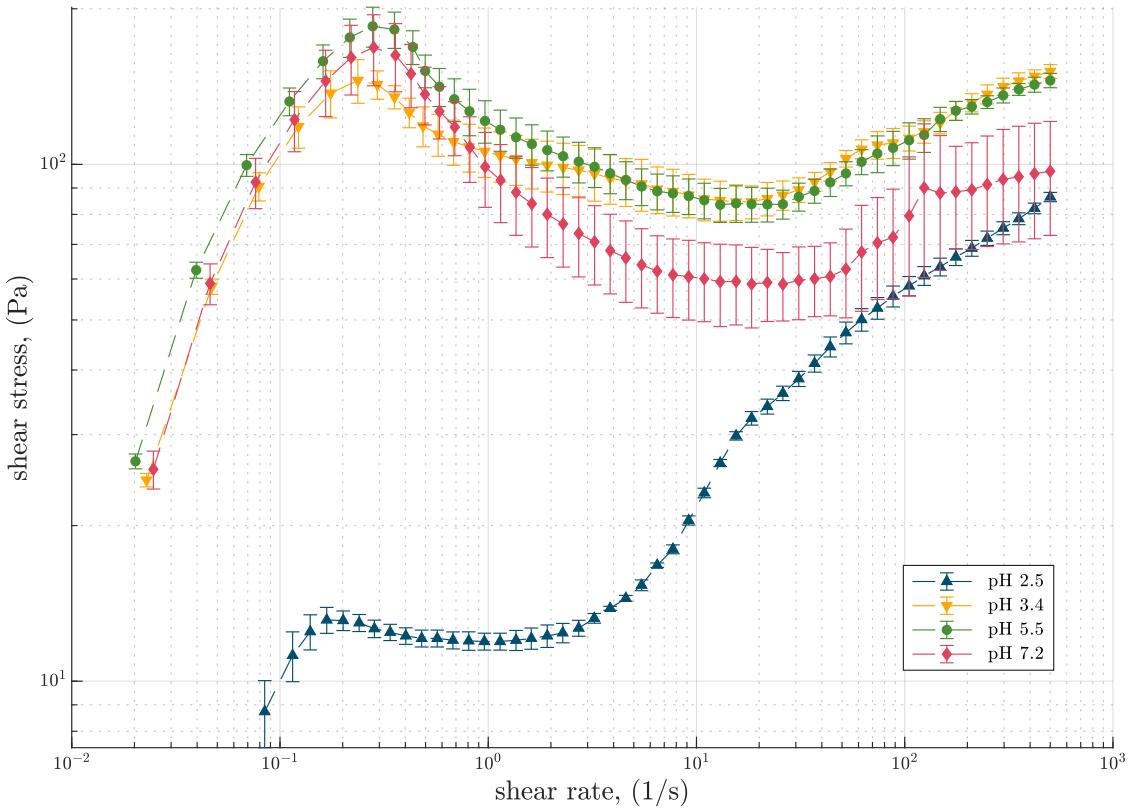

Figure 6.12: Shear stress as a function of shear rate for the four emulsions at 25°C

the zero-shear viscosity shows a lower value than for the other emulsions. As mentioned in the previous section, the zero-shear viscosity can indicate the emulsions' stability, with low values showing a higher chance of instability effects like creaming [83]. This seems to suggest that the emulsion with added H_2SO_4 is less stable than the emulsions with higher pH, which does not agree with the prior assessment of the stability at room temperature. Nonetheless, since the rheological measurements were carried out later than the optical evaluation, the stability of the emulsion might have changed in this period.

These results can be compared to shear viscosity flow tests carried out for Pickering emulsions stabilized by amphoteric lignin, and SiO_2 nanoparticles by Lu et al. [45]. They found that the viscosity of emulsions first increased with increasing pH up to a maximum value at pH values between 3 and 4, then decreasing again. While the peak value is lower than the results found in this work, the course of the viscosity over the pH value is similar. As mentioned above, the emulsions with pH 3.4 and 7.2 showed some instabilities after 24 hours at room temperature. This might have influenced the measured viscosities. Still, when looking at the zero-shear viscosities as an indication of the stability of the emulsions, the emulsions with pH 3.4, 5.5 and 7.2 can be regarded as more stable. Sipponen et al. found that CLPs generally stabilize emulsions over a broad pH range when the emulsions are not subjected to external forces. Stability tests, carried out in a centrifuge, for CLP Pickering emulsions

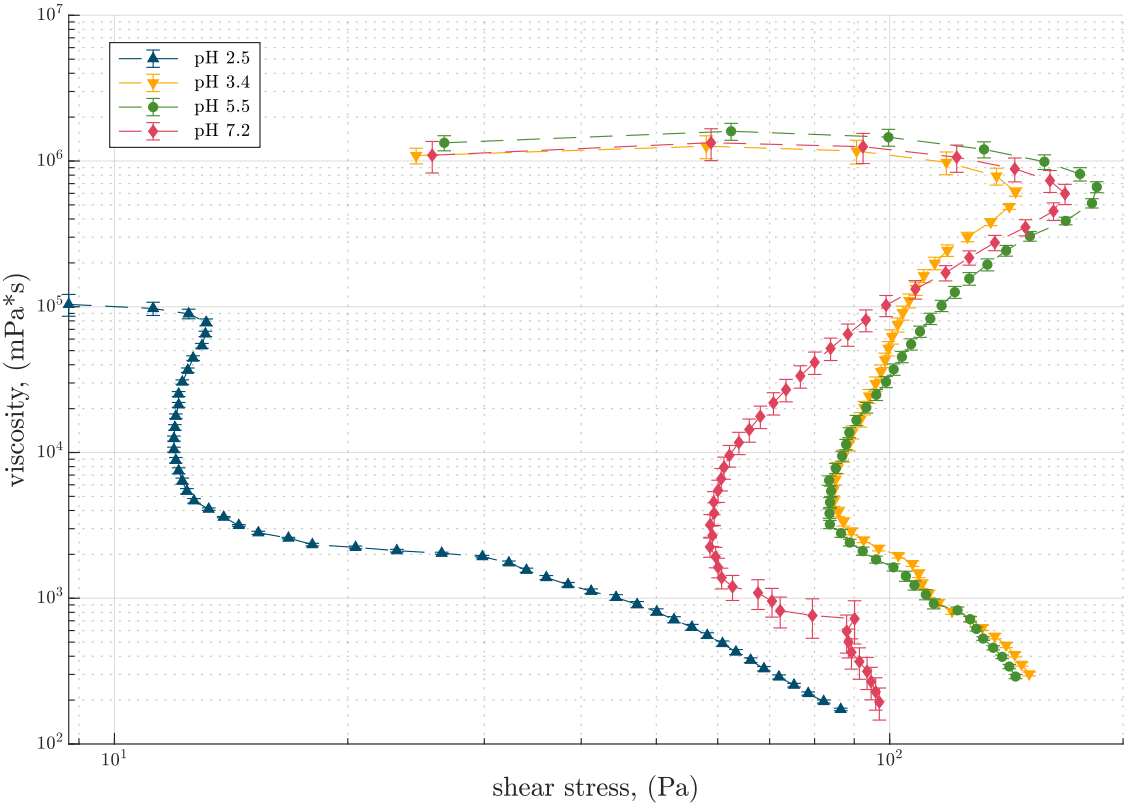

Figure 6.13: Viscosity as a function of shear stress for the four emulsions at 25°C

at different pH values showed the best results at neutral and alkaline pH [77]. The stability of Pickering emulsions over different pH values can be improved by modifications like the preparation of cationic-CLPs [77] or esterification of CLPs with long-chain fatty acids [45].

6.1.2 Temperature stability

The influence of temperature on lignin was not only evaluated for the suspensions but also for its application. For this, Pickering emulsions with lignin similar to sunscreens were produced at two different temperatures. The SPF value of the emulsions was then determined using an *in vitro* methodology.

The production of cosmetic emulsions conventionally involves the heating of both the oil and water phase before they are mixed together, in order to melt all of the oil phase ingredients and to hydrate gum that may be included in the aqueous phase respectively [12]. The product is called a hot process emulsion [17]. When temperature-sensitive ingredients are used, they must be added to the formulation once the emulsion has cooled [12]. Also, the processes' heating and cooling cycles are time-intensive. This can be avoided by the so-called cold processing, where both the oil and water phase should ideally be in a liquid state without the requirement of high temperatures before being mixed together. For cold process emulsions, the phase mixing by homogenization is more time-intensive and requires more agitation than for warm processes [17]. If parts of the emulsion ingredients do need melting, a combination of both hot and cold processes can be performed. Here, the non-heat-sensitive ingredients are processed at higher temperatures and added to the others, which are processed at room temperature.

Due to the temperature-sensitivity of colloidal lignin particles (see section 2.3) the production process of Pickering emulsions with heat can lead to the formation of aggregates. Therefore, a hot-cold process offers a practical production method for emulsions. However, hot processing options are widespread throughout the cosmetic industry [12]. In order to be able to use lignin as a valuable alternative active ingredient in personal care products, the possibility to use it in hot processing needs to be investigated. The results in subsection 5.1.2 showed the sensitivity of the CLPs to higher temperatures. By producing two emulsions similar to sunscreens with a hot and hot-cold processing method, the impacts of higher temperatures or aggregates on the functionality of CLPs as a UV blocker and Pickering emulsion component were investigated. This was realized by the methods described in section 4.3.2, where each production process was repeated three times, resulting in 9 emulsions in total. Each produced emulsion was evaluated by ten repeated UV spectroscopy measurements in the wavelength range 290 to 400 nm. The thirty measurements were then coverted into SPF values using the Equation 3.12 and interpreted with boxplots to diminish the influence of outliers. The SPF results of all measurements can be found in Appendix B (Table B.2).

The values show the large measurement uncertainty that is associated with the *in-vitro* measurement of the SPF values [78]. While not giving a precise SPF value for each cream, the measurement can be used to reveal trends. For example, the values of the creams with lignin are mostly higher than the ones without. An exception can be made for the creams from the hot-cold process: Here, the SPF results for emulsions 2 and 3 are lower than for 1. This can be explained due to the difference in production date for these two creams, which was two months later than for the first one. Since the suspension used (C220329) did not

have a preservative added, the decline in UV protection can be credited to microbial activity in the suspension. For this reason, the SPF measurements of the second and third repetition of the hot-cold process emulsion were disregarded in the following box plot Figure 6.14 of the *in-vitro* SPF results.

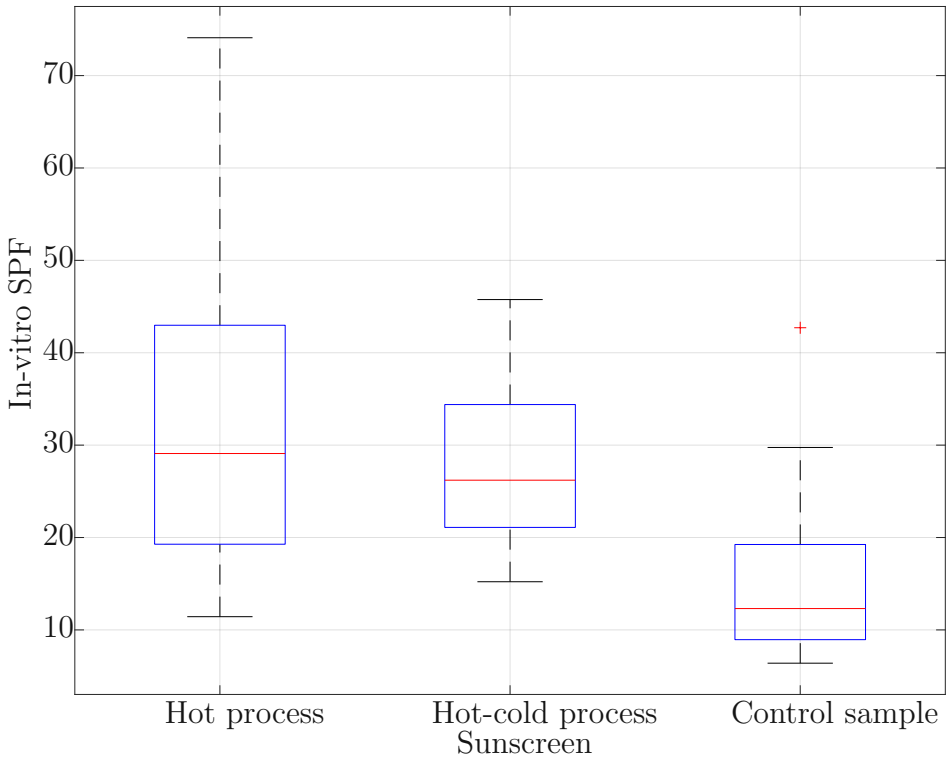

Figure 6.14: Box plots of the emulsions produced by a hot process, hot-cold process and a control sample produced for the first emulsion.

The box plot shows the emulsions median with a red line and the upper 75th percentile and the lower 25th percentile. The whiskers at the end of the box show the upper and lower adjacents, while the red crosses mark the outliers. The median for both emulsions with CLPs is higher than for the control sample without, with the highest median for the hot process emulsion. A difference in the box plot size is observable when comparing the hot-processed and hot-cold-processed creams. The first box is comparatively tall, showing a more significant deviation in the SPF values, which can also be seen from the more extensive box plot whiskers. As the upper quartile and upper whisker are longer than the lower half, the SPF values are more varied for values above the median. This applies to all emulsions but is most pronounced for the hot process emulsion. The hot-cold processed sunscreen's box plot is shorter in comparison, suggesting higher agreement in the SPF values. Its median value lies inside the first box plot, suggesting a significant difference between the two process

methods is less likely. This is not the case for the control sample. Here, the median is lower than for both box plots, indicating a more considerable difference between the sunscreens containing CLPs. The size of the box plot is the smallest, which suggests the least data scatter in comparison.

SPF	**Hot process**	**Hot-cold process**	**Control sample**
Mean	30.20	27.31	12.73
Standard deviation	7.57	5.60	3.30

Table 6.2: Mean values and standard deviations of the SPF values for the considered emulsions

Table 6.2 shows the mean values and standard deviations of the ten SPF values for each of the considered creams within the interquartile range. One can see that adding CLPs to the emulsions boosts the SPF values to more than double the control samples. Research by Qian et al. [71] also show a stark increase in SPF when 5 wt% of lignin were added to commercial sunscreens, highlighting lignin's capacity as a sunblocker. Same as for the medians in Figure 6.14, the mean SPF value for the hot processed emulsion is highest, followed by the hot-cold process sunscreen and the control sample. Also, the standard deviation is highest for the first one. This might result from the agglomerations formed during heating, which could affect the measured absorption values and, in turn, the calculated SPF values. Still, the UV absorption capacity of lignin does not seem to be affected by the processing method, as the hot-processed sunscreen's mean SPF value is close to the hot-cold processed one and more than double the one of the control samples. This evaluation of the temperature stability of the CLP Pickering emulsions can be seen as a positive outcome for the use of CLP suspensions in hot process applications. However, agglomerations are a drawback for use in personal care and cosmetic applications, not only due to consumer acceptance but the possible inconsistency in the protective SPF film due to the uneven distribution of the particles.

Figure 6.15a and Figure 6.15d show two emulsions, the first produced with a hot process method and the last with a hot-cold process method. The agglomerations appear due to the heating process of the suspension during the hot process method. Figure 6.15c shows the residues remaining in the beaker after mixing the water phase. In contrast, Figure 6.15b shows the remnants of the finished emulsion including residual agglomerates. While not strongly noticeable in the bulk emulsion (Figure 6.15a), Figure 6.15b indicates, the agglomerates can be seen when the hot-process cream is spread on the skin. Leskinen et al. [41] found that thermal treatments can lead to a darkening in the colour of the dispersions. The resulting dark colour of lignin sunscreens due to the isolation and processing of the lignin is already a drawback for the application and feasibility of lignin-based sunscreens [87]. Further darkening in colour is therefore undesirable. Leskinen et al. [41] also describe the release of

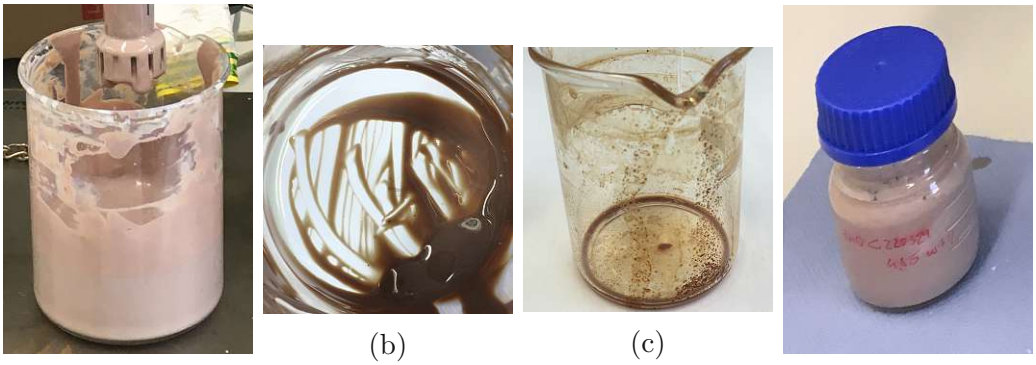

(a) (b) (c) (d)

Figure 6.15: (a) and (b) show an emulsion from a hot process method, (c) the remaining aggregates in the beaker that was used to heat the suspension and (d) shows an emulsion from a hot-cold process method

sulfur odour for heated CLP suspensions from kraft lignins, which is also not favourable for use in personal care products. Characteristics such as stability, skin feel, texture and appearance are essential to consumer expectations and buying practices and must be carefully considered by the manufacturers [39].

Chapter 7

Concluding remarks and outlook

The aim of this thesis is the exploration of the pumpability and temperature stability of colloidal lignin suspensions, as well as the rheological behaviour of colloidal lignin emulsions, and the temperature sensitivity of the contained CLPs.

The pumpability of suspensions was investigated using data obtained from the rheological measurements. The influence of different factors was considered and examined according to their importance for the pumpability. The data showed that increasing the CLP concentration increases the viscosity of the suspension, making the concentration step during CLP production the most critical for the pump performance. At low CLP concentrations, the flow behaviour of the suspensions is similar to water. Higher CLP contents lead to prominent non-Newtonian shear-thinning flow. An increase in viscosity greatly influences the pump performance, as higher viscosities lead to decreasing head and efficiency and increased energy consumption. Increased temperature and the presence of additives or charged particles like salt can also significantly alter the rheological behaviour of CLP suspensions. Both lead to aggregates of colloidal particles, which increase the suspension viscosity and make it difficult to determine the flow behaviour. These effects become even more critical at higher CLP content. Temperatures starting from 60°C can also lead to the destruction of the sample due to the temperature sensitivity of lignin. The influence of the particle size on the pumpability was shown to be negligible. However, if, for example, due to the presence of salt, changes in the particle size occur, sedimentation in the pipes might become an issue. Therefore, the ability to reach a critical velocity value must be considered in the pump design. The presence of charged particles in the suspension leads to higher viscosity and the appearance of a yield stress, which needs to be overcome for the suspension to start flowing. This can make manipulating and processing the suspensions more difficult as the energy consumption for transfer and mixing increases.
The temperature stability of the suspension was analyzed through experiments with different heating methods, revealing that temperatures up to 90°C cause significant amounts of precipitating agglomerations. Also, different raw materials for the CLP production led to different

temperature curves and agglomeration amounts. UV-absorption and FTIR measurements were used to compare the chemical structure of both the untreated and heat-treated suspensions, revealing to significant difference in the chemical structure due to the heating process.

Rheology is also an important aspect of colloidal lignin emulsions as it determines some key characteristics such as stability and texture when used in cosmetics [39]. The CLP concentration present in the evaluated Pickering emulsions influences the colour, flow behaviour and apparent yield stress. All emulsions showed a flow curve with a distinct shear-thinning region. With higher concentrations of CLPs the colour of the emulsion darkens and the apparent yield stress, needed to overcome before the shear-thinning behaviour occurs, increases. These properties positively influence the spreadability, skin-feel and long-term stability of the suspensions. The results of the oscillatory tests for the emulsions with varying CLP concentrations indicate that the CLPs provide an important stabilising mechanism for the emulsions. In addition to investigating the influence of concentrations, emulsions prepared with suspensions at the pH values 2.5, 3.4, 5.5 and 7.2 were evaluated. These emulsions also show shear-thinning behaviour. The zero-shear viscosities determined for the emulsions indicate higher emulsion stabilities for the emulsions with pH values between 3 - 7. The evaluated measurement results show the influence the concentrations and pH values can have on the emulsions and therefore their application in cosmetic and skincare products.
The production of these products is also often associated with elevated temperatures, making the evaluation of the application of the temperature-sensitive CLPs a necessary topic to be investigated. Comparing two different production methods of sunscreen like Pickering emulsions via *in vitro* SPF measurments showed that the median value of SPF was not significantely influenced by the higher temperatures. Still, as already seen from the suspensions, the appearance of agglomerations can be critical in personal care products and cosmetics, as it led to higher standard deviations in the SPF values in the hot process.

This work also highlighted some possible further research questions such as the a deeper look into the interactions of lignin with different chemical substances used as additives or more extensive research into the temperature stability of CLP suspensions using analytical methods such as Differential Thermogravimetrical Analysis or Differential Scanning Calorimetry, focusing on the temperature range from 20 to 160°C.

Bibliography

[1] Claire Albert et al. "Pickering emulsions: Preparation processes, key parameters governing their properties and potential for pharmaceutical applications". In: *Journal of Controlled Release* 309 (Sept. 2019), pp. 302–332. ISSN: 18734995. DOI: 10.1016/J.JCONREL.2019.07.003.

[2] Hassan M. Badr and Wael H. Ahmed. *Pumping Machinery Theory and Practice*. Vol. 9781118932087. Wiley, Dec. 2014, pp. 1–371. ISBN: 9781118932087. DOI: 10.1002/9781118932094.

[3] Stefan Beisl, Johannes Adamcyk, and Anton Friedl. "Direct Precipitation of Lignin Nanoparticles from Wheat Straw Organosolv Liquors Using a Static Mixer". In: *Molecules* 25.6 (Mar. 2020), p. 1388. DOI: 10.3390/molecules25061388.

[4] Stefan Beisl, Anton Friedl, and Angela Miltner. "Lignin from Micro- to Nanosize: Applications". In: *International Journal of Molecular Sciences* 18.11 (Nov. 2017), p. 2367. ISSN: 1422-0067. DOI: 10.3390/ijms18112367.

[5] Stefan Beisl, Angela Miltner, and Anton Friedl. "Lignin from Micro- to Nanosize: Production Methods". In: *International Journal of Molecular Sciences* 18.6 (June 2017), p. 1244. ISSN: 1422-0067. DOI: 10.3390/ijms18061244.

[6] Sharu Bhagavathi Kandy et al. "Temperature-Induced Aggregation in Portlandite Suspensions". In: *Langmuir* 36.36 (Sept. 2020), pp. 10811–10821. ISSN: 0743-7463. DOI: 10.1021/acs.langmuir.0c01798.

[7] Sareh Boostani et al. "The influence of emulsion parameters on physical stability and rheological properties of Pickering emulsions stabilized by hordein nanoparticles". In: *Food Hydrocolloids* 101 (Apr. 2020), p. 105520. ISSN: 0268-005X. DOI: 10.1016/J.FOODHYD.2019.105520.

[8] Anuj Kumar Chandel et al. "The path forward for lignocellulose biorefineries: Bottlenecks, solutions, and perspective on commercialization". In: *Bioresource Technology* 264 (Sept. 2018), pp. 370–381. ISSN: 0960-8524. DOI: 10.1016/J.BIORTECH.2018.06.004.

[9] Kai Chen et al. "State-of-the-Art: Applications and Industrialization of Lignin Micro/Nano Particles". In: (2021). DOI: 10.1002/cssc.202002441.

[10] Francesco Cherubini. "The biorefinery concept: Using biomass instead of oil for producing energy and chemicals". In: *Energy Conversion and Management* 51.7 (July 2010), pp. 1412–1421. ISSN: 0196-8904. DOI: 10.1016/J.ENCONMAN.2010.01.015.

[11] Giovana Colucci et al. "Development of colloidal lignin particles through particle design strategies and screening of their Pickering stabilizing potential". In: *Colloids and Surfaces A: Physicochemical and Engineering Aspects* 666 (2023), p. 131287. DOI: 10.1016/j.colsurfa.2023.131287.

[12] Russell Cox. *Cold Processing of Emulsions — Cosmetics & Toiletries*. URL: https://www.cosmeticsandtoiletries.com/research/methods-tools/article/21835518/cold-processing-of-emulsions#:~:text=Cold%20process%20emulsions%20are%20prepared,with%20an%20efficient%20mixing%20system.. *(Access date: 16/07/2023)*.

[13] Robinson C.D. Cruz et al. "Double layer electrical conductivity as a stability criterion for concentrated colloidal suspensions". In: *Colloids and Surfaces A: Physicochemical and Engineering Aspects* 520 (May 2017), pp. 9–16. ISSN: 0927-7757. DOI: 10.1016/J.COLSURFA.2017.01.059.

[14] Robinson C.D. Cruz et al. "Interpreting rheology and electrical conductivity: It all boils down to which particle size". In: *Journal of Colloid and Interface Science* 574 (Aug. 2020), pp. 97–109. ISSN: 0021-9797. DOI: 10.1016/J.JCIS.2020.04.046.

[15] Ayhan Demirbas. "Biorefineries: Current activities and future developments". In: *Energy Conversion and Management* 50.11 (Nov. 2009), pp. 2782–2801. ISSN: 0196-8904. DOI: 10.1016/J.ENCONMAN.2009.06.035.

[16] Svetlana R. Derkach. "Rheology of emulsions". In: *Advances in Colloid and Interface Science* 151.1-2 (Oct. 2009), pp. 1–23. ISSN: 00018686. DOI: 10.1016/J.CIS.2009.07.001.

[17] Elham Eghbali. *How to make a Hot Cold Process Emulsion - Formula Botanica*. URL: https://formulabotanica.com/make-hot-cold-process-emulsion/. *(Access date: 16/07/2023)*.

[18] *EN ISO 24444 Kosmetische Mittel – Untersuchungsverfahren für Sonnenschutzmittel – In-vivo-Bestimmung des Sonnenschutzfaktors (SSF)*. DIN Deutsches Institut für Normung e. V, 2022.

[19] Douglas H. Everett. "Manual of Symbols and Terminology for Physicochemical Quantities and Units, Appendix II: Definitions, Terminology and Symbols in Colloid and Surface Chemistry". In: *Pure and Applied Chemistry* 31.4 (Jan. 1972), pp. 577–638. ISSN: 1365-3075. DOI: 10.1351/pac197231040577.

[20] Muhammad Farooq et al. "Well-Defined Lignin Model Films from Colloidal Lignin Particles". In: *Langmuir* 36.51 (Dec. 2020), pp. 15592–15602. ISSN: 0743-7463. DOI: 10.1021/ACS.LANGMUIR.0C02970.

[21] V. T.P. Ferreira et al. "Application of Factorial Design and Rheology to the Development of Photoprotective Formulations". In: *AAPS PharmSciTech* 21.2 (Feb. 2020), pp. 1–8. ISSN: 15309932. DOI: 10.1208/s12249-019-1569-7.

[22] Patrícia Figueiredo et al. "Properties and chemical modifications of lignin: Towards lignin-based nanomaterials for biomedical applications". In: *Progress in Materials Science* 93 (Apr. 2018), pp. 233–269. ISSN: 00796425. DOI: 10.1016/j.pmatsci.2017.12.001.

[23] Consuelo Fritz et al. "Self-association and aggregation of kraft lignins via electrolyte and nonionic surfactant regulation: stabilization of lignin particles and effects on filtration". In: *Nordic Pulp & Paper Research Journal* 32.SPECIAL ISSUE ON LIGNIN (2017).

[24] Francisco García Calvo-Flores and JosØ A Dobado. "Lignin as Renewable Raw Material". In: *ChemSusChem* 3.11 (Nov. 2010), pp. 1227–1235. DOI: 10.1002/cssc.201000157.

[25] Lorena R. Gaspar and Patrícia M.B.G. Maia Campos. "Rheological behavior and the SPF of sunscreens". In: *International Journal of Pharmaceutics* 250.1 (Jan. 2003), pp. 35–44. ISSN: 03785173. DOI: 10.1016/S0378-5173(02)00462-3.

[26] Diego B. Genovese. "Shear rheology of hard-sphere, dispersed, and aggregated suspensions, and filler-matrix composites". In: *Advances in Colloid and Interface Science* 171-172 (Mar. 2012), pp. 1–16. ISSN: 0001-8686. DOI: 10.1016/J.CIS.2011.12.005.

[27] Sebastien Gillet et al. "Lignin transformations for high value applications: Towards targeted modifications using green chemistry". In: *Green Chemistry* 19.18 (2017), pp. 4200–4233. ISSN: 14639270. DOI: 10.1039/C7GC01479A.

[28] Oihana Gordobil et al. "Lignins from Agroindustrial by-Products as Natural Ingredients for Cosmetics: Chemical Structure and In Vitro Sunscreen and Cytotoxic Activities". In: *Molecules* 25.5 (Mar. 2020), p. 1131. DOI: 10.3390/molecules25051131.

[29] Joanne Gould, Guillermo Garcia-Garcia, and Bettina Wolf. "Pickering Particles Prepared from Food Waste". In: *Materials 2016, Vol. 9, Page 791* 9.9 (Sept. 2016), p. 791. ISSN: 1996-1944. DOI: 10.3390/MA9090791.

[30] Richard D. Handy et al. "The ecotoxicology and chemistry of manufactured nanoparticles". In: *Ecotoxicology* 17.4 (May 2008), pp. 287–314. ISSN: 09639292. DOI: 10.1007/S10646-008-0199-8.

[31] Cyril Heitner. *Lignin and lignans: advances in chemistry*. Ed. by Cyril Heitner, R. Donald Dimmel, and John A. Schmidt. Boca Raton: CRC Press, 2010. ISBN: 9781574444865.

[32] Maria Hingsamer and Gerfried Jungmeier. "Biorefineries". In: *The Role of Bioenergy in the Emerging Bioeconomy: Resources, Technologies, Sustainability and Policy* (Jan. 2019), pp. 179–222. DOI: 10.1016/B978-0-12-813056-8.00005-4.

[33] Lena Hohl et al. “Influence of Nanoparticles and Drop Size Distributions on the Rheology of w/o Pickering Emulsions”. In: *Chemie Ingenieur Technik* 88.11 (Nov. 2016), pp. 1815–1826. ISSN: 1522-2640. DOI: 10.1002/CITE.201600063.

[34] Mohamad Nasir Mohamad Ibrahim et al. “Synthesis of lignin based composites of TiO2 for potential application as radical scavengers in sunscreen formulation”. In: *BMC Chemistry* 13.3 (2019). ISSN: 2661801X. DOI: 10.1186/S13065-019-0537-3.

[35] Birgit Kamm and Michael Kamm. “Principles of biorefineries”. In: *Applied Microbiology and Biotechnology* 64.2 (Apr. 2004), pp. 137–145. ISSN: 01757598. DOI: 10.1007/S00253-003-1537-7.

[36] Joseph Kestin, H. Ezzat Khalifa, and Robert J. Correia. “Tables of the dynamic and kinematic viscosity of aqueous NaCl solutions in the temperature range 20 - 150 °C and the pressure range 0.1 - 35 MPa”. In: *Journal of Physical and Chemical Reference Data* 10.1 (1981), pp. 71–88. ISSN: 15297845. DOI: 10.1063/1.555641.

[37] Mauri Kostiainen et al. “As featured in: Closed cycle production of concentrated and dry redispersible colloidal lignin particles with a three solvent polarity exchange method”. In: *Green Chem* 20 (2018), p. 843. DOI: 10.1039/c7gc03465b.

[38] KSB SE & Co. KGaA. *Viscosity - KSB SE & Co. KGaA*. URL: https://www.ksb.com/en-global/centrifugal-pump-lexicon/article/viscosity-1117612. *(Access date: 04/05/2023)*.

[39] Min-Sun Kwak, Hye-Jin Ahn, and Ki-Won Song. “Rheological investigation of body cream and body lotion in actual application conditions”. In: *Korea-Australia Rheology Journal* 27.3 (Aug. 2015), pp. 241–251. ISSN: 1226-119X. DOI: 10.1007/s13367-015-0024-x.

[40] Martin Laun et al. “Guidelines for checking performance and verifying accuracy of rotational rheometers: Viscosity measurements in steady and oscillatory shear (IUPAC Technical Report)”. In: *Pure and Applied Chemistry* 86.12 (Dec. 2014), pp. 1945–1968. ISSN: 13653075. DOI: 10.1515/pac-2013-0601.

[41] Timo Leskinen et al. “Scaling Up Production of Colloidal Lignin Particles”. In: *Nordic Pulp and Paper Research Journal* 32.4 (Dec. 2017), pp. 586–596. ISSN: 20000669. DOI: 10.3183/NPPRJ-2017-32-04-p586-596.

[42] Jiebing Li, Gunnar Henriksson, and Göran Gellerstedt. “Lignin de-polymerization / re-polymerization and its critical role for de-lignification of aspen wood by steam explosion”. In: *Bioresource Technology* 98.16 (Nov. 2007), pp. 3061–3068. ISSN: 0960-8524. DOI: 10.1016/J.BIORTECH.2006.10.018.

[43] Miikka Lievonen et al. “A simple process for lignin nanoparticle preparation”. In: *Green Chemistry* 18.5 (Feb. 2016), pp. 1416–1422. ISSN: 1463-9270. DOI: 10.1039/C5GC01436K.

[44] Xiangyu Liu et al. "Viscosity modification of lubricating oil based on high-concentration silica nanoparticle colloidal system". In: *Journal of Dispersion Science and Technology* 38.9 (Sept. 2017), pp. 1360–1365. ISSN: 15322351. DOI: 10.1080/01932691.2016.1220319.

[45] Shuo Lu et al. "Pickering emulsions synergistic-stabilized by amphoteric lignin and SiO2 nanoparticles: Stability and pH-responsive mechanism". In: *Colloids and Surfaces A: Physicochemical and Engineering Aspects* 585 (Jan. 2020), p. 124158. ISSN: 0927-7757. DOI: 10.1016/J.COLSURFA.2019.124158.

[46] Alexander Ya. Malkin and Avraam Isayev. "Liquids". In: *Rheology*. ChemTec Publishing, Jan. 2017, pp. 129–232. ISBN: 978-1-927885-21-5. DOI: 10.1016/B978-1-927885-21-5.50009-6.

[47] Marilynne McKay. "Sun-associated Problems". In: *Travel Medicine: Second Edition* (Jan. 2008), pp. 423–427. DOI: 10.1016/B978-0-323-03453-1.10042-2.

[48] Jan Mewis and Norman J. Wagner. "Colloidal attractions and flocculated dispersions". In: *Colloidal Suspension Rheology*. Cambridge: Cambridge University Press, Nov. 2011. Chap. 6, pp. 180–227. DOI: 10.1017/CBO9780511977978.009.

[49] Jan Mewis and Norman J. Wagner. "Hydrodynamic effects". In: *Colloidal Suspension Rheology*. Cambridge: Cambridge University Press, Nov. 2011. Chap. 2, pp. 36–79. DOI: 10.1017/CBO9780511977978.005.

[50] Jan Mewis and Norman J. Wagner. "Introduction to colloid science and rheology". In: *Colloidal Suspension Rheology*. Cambridge: Cambridge University Press, Nov. 2011. Chap. 1, pp. 1–35. DOI: 10.1017/CBO9780511977978.004.

[51] Jan Mewis and Norman J. Wagner. "Rheometry of suspensions". In: *Colloidal Suspension Rheology*. Cambridge: Cambridge University Press, Nov. 2011. Chap. 9, pp. 291–324. DOI: 10.1017/CBO9780511977978.012.

[52] Thomas Mezger. *The rheology handbook: for users of rotational and oscillatory rheometers*. eng. 5th (revised). European coatings library. Hannover: Vincentz Network, 2020. ISBN: 386630532X.

[53] Michele Michelin et al. "Lignin from an integrated process consisting of liquid hot water and ethanol organosolv: Physicochemical and antioxidant properties". In: *International Journal of Biological Macromolecules* 120 (Dec. 2018), pp. 159–169. ISSN: 0141-8130. DOI: 10.1016/J.IJBIOMAC.2018.08.046.

[54] Martin Miltner et al. "Application of Membrane Separation for Cleaning and Concentration of Nanolignin Suspensions in a Biorefinery Environment". In: *Chemical Engineering Transactions* 76 (Oct. 2019), pp. 133–138. ISSN: 2283-9216. DOI: 10.3303/CET1976023.

[55] Taghi Miri. "Viscosity and Oscillatory Rheology". In: *Practical Food Rheology: An Interpretive Approach*. Wiley-Blackwell, Dec. 2010, pp. 7–28. ISBN: 9781405199780. DOI: 10.1002/9781444391060.CH2.

[56] Shohreh Nafisi and Howard I. Maibach. "Nanotechnology in Cosmetics". In: *Cosmetic Science and Technology: Theoretical Principles and Applications*. Elsevier, Jan. 2017. Chap. 22, pp. 337–369. ISBN: 978-0-12-802005-0. DOI: 10.1016/B978-0-12-802005-0.00022-7.

[57] Hiroshi Nakamura, Soichiro Makino, and Masahiko Ishii. "Effects of electrostatic interaction on rheological behavior and microstructure of concentrated colloidal suspensions". In: *Colloids and Surfaces A: Physicochemical and Engineering Aspects* 623 (Aug. 2021), p. 126576. ISSN: 0927-7757. DOI: 10.1016/J.COLSURFA.2021.126576.

[58] "Flow of liquids". In: *Handbook of Pumps and Pumping*. Ed. by Brian Nesbitt. Elsevier Science Ltd, 2006. Chap. 3, pp. 95–124. DOI: 10.1016/B978-185617476-3/50005-6.

[59] "Properties of liquids". In: *Handbook of Pumps and Pumping*. Ed. by Brian Nesbitt. Elsevier Science Ltd, Jan. 2006. Chap. 2, pp. 329–339. DOI: 10.1016/B978-185617476-3/50004-4.

[60] "Pump selection". In: *Handbook of Pumps and Pumping*. Ed. by Brian Nesbitt. Elsevier Science Ltd, 2006. Chap. 15, pp. 329–339. DOI: 10.1016/B978-185617476-3/50017-2.

[61] "Pump theory". In: *Handbook of Pumps and Pumping*. Ed. by Brian Nesbitt. Elsevier Science Ltd, 2006. Chap. 4, pp. 125–153. DOI: 10.1016/B978-185617476-3/50006-8.

[62] David Orentreich et al. "Sunscreens: practical applications". In: *Comprehensive Series in Photosciences* 3.C (Jan. 2001), pp. 535–559. ISSN: 1568-461X. DOI: 10.1016/S1568-461X(01)80063-6.

[63] Monika Österberg, Mika Henrikki Sipponen, and Gunnar Henriksson. "Editorial: From understanding the biological function of lignin in plants to production of colloidal lignin particles". In: *Nordic Pulp and Paper Research Journal* 32.4 (Dec. 2017), pp. 483–484. ISSN: 20000669. DOI: 10.3183/NPPRJ-2017-32-04-p483-484.

[64] Monika Österberg et al. "Spherical lignin particles: A review on their sustainability and applications". In: *Green Chemistry* 22.9 (May 2020), pp. 2712–2733. ISSN: 14639270. DOI: 10.1039/D0GC00096E.

[65] Akira Otsuki. "Rheology of colloidal particle suspensions". In: *Rheology of Polymer Blends and Nanocomposites: Theory, Modelling and Applications* (Jan. 2020), pp. 49–71. DOI: 10.1016/B978-0-12-816957-5.00004-5.

[66] Emilia Paone, Tommaso Tabanelli, and Francesco Mauriello. "The rise of lignin biorefinery". In: *Current Opinion in Green and Sustainable Chemistry* 24 (Aug. 2020), pp. 1–6. ISSN: 2452-2236. DOI: 10.1016/J.COGSC.2019.11.004.

[67] Sofia Peito et al. "Nano- and microparticle-stabilized Pickering emulsions designed for topical therapeutics and cosmetic applications". In: *International Journal of Pharmaceutics* 615 (Mar. 2022), p. 121455. ISSN: 0378-5173. DOI: 10.1016/J.IJPHARM.2022.121455.

[68] John H Perry, Don W Green, and Marylee Z Southard. *Perry's chemical engineers' handbook*. eng. Ninth edition. New York: McGraw-Hill Education, 2019. ISBN: 0071834087.

[69] Carmen Mihaela Popescu et al. "Spectral characterization of eucalyptus wood". In: *Applied Spectroscopy* 61.11 (Nov. 2007), pp. 1168–1177. ISSN: 00037028. DOI: 10.1366/000370207782597076.

[70] *Pumpability Definition & Meaning - Merriam-Webster*. URL: https://www.merriam-webster.com/dictionary/pumpability. *Access date: 15/06/2023*.

[71] Yong Qian, Xueqing Qiu, and Shiping Zhu. "Lignin: A nature-inspired sun blocker for broadspectrum Sunscreens". In: *Green Chemistry* 17.1 (Jan. 2015), pp. 320–324. ISSN: 14639270. DOI: 10.1039/C4GC01333F.

[72] Yuanqiao Rao. "Nanofluids: Stability, phase diagram, rheology and applications". In: *Particuology* 8.6 (Dec. 2010), pp. 549–555. ISSN: 1674-2001. DOI: 10.1016/J.PARTIC.2010.08.004.

[73] Guillaume Rivière. "Transformation of lignin and lignocellulose into nanoparticles: Structure-property relationship and applications". PhD thesis. Aalto: Aalto University, 2021. ISBN: 978-952-64-0306-9. URL: https://research.aalto.fi/en/publications/transformation-of-lignin-and-lignocellulose-into-nanoparticles-st.

[74] Hasan Sadeghifar and Arthur Ragauskas. "Lignin as a UV Light Blocker—A Review". In: *Polymers* 12.5 (May 2020). ISSN: 20734360. DOI: 10.3390/POLYM12051134.

[75] Saswata Sahoo et al. "Characterization of industrial lignins for their utilization in future value added applications". In: *Biomass and Bioenergy* 35.10 (Oct. 2011), pp. 4230–4237. ISSN: 0961-9534. DOI: 10.1016/J.BIOMBIOE.2011.07.009.

[76] Sanghamitra Sen, Shradha Patil, and Dimitris S. Argyropoulos. *Thermal properties of lignin in copolymers, blends, and composites: a review. Green Chemistry*. ISSN: 14639270. DOI: 10.1039/c5gc01066g.

[77] Mika Henrikki Sipponen et al. "All-lignin approach to prepare cationic colloidal lignin particles: stabilization of durable Pickering emulsions". In: *Green Chemistry* 19.24 (Dec. 2017), pp. 5831–5840. ISSN: 1463-9270. DOI: 10.1039/C7GC02900D.

[78] Myriam Sohn et al. "Calculation of the sun protection factor of sunscreens with different vehicles using measured film thickness distribution — Comparison with the SPF in vitro". In: *Journal of Photochemistry and Photobiology B: Biology* 159 (June 2016), pp. 74–81. ISSN: 1011-1344. DOI: 10.1016/J.JPHOTOBIOL.2016.02.038.

[79] Jason R. Stokes and Julia H. Telford. "Measuring the yield behaviour of structured fluids". In: *Journal of Non-Newtonian Fluid Mechanics* 124.1-3 (Dec. 2004), pp. 137–146. ISSN: 0377-0257. DOI: 10.1016/J.JNNFM.2004.09.001.

[80] Tharwat Tadros. "Application of rheology for assessment and prediction of the long-term physical stability of emulsions". In: *Advances in Colloid and Interface Science* 108-109 (May 2004), pp. 227–258. ISSN: 00018686. DOI: 10.1016/J.CIS.2003.10.025.

[81] Tharwat F Tadros. *Dispersion of Powders*. eng. Weinheim: John Wiley & Sons, Incorporated, 2012. ISBN: 9783527329410.

[82] Tharwat F Tadros. *Rheology of Dispersions: Principles and Applications*. Weinheim: Wiley-VCH, 2010. ISBN: 978-3-527-32003-5.

[83] Tharwat F. Tadros. *Emulsions: Formation, Stability, Industrial Applications*. Berlin / Boston: Walter de Gruyter, 2016. ISBN: 9783110290332.

[84] Tharwat F. Tadros. "Rheology of Suspensions, Emulsions and their Mixtures (Suspoemulsions)". In: *Colloids in Paints*. Vol. 6. Wiley Blackwell, Aug. 2010, pp. 165–192. ISBN: 9783527631193. DOI: 10.1002/9783527631193.CH72.

[85] Julia Tomasich, Stefan Beisl, and Michael Harasek. "Production and Characterisation of Pickering Emulsions Stabilised by Colloidal Lignin Particles Produced from Various Bulk Lignins". In: *Sustainability 2023, Vol. 15, Page 3693* 15.4 (Feb. 2023), p. 3693. ISSN: 2071-1050. DOI: 10.3390/SU15043693.

[86] Luis G. Torres et al. "Preparation of o/w emulsions stabilized by solid particles and their characterization by oscillatory rheology". In: *Colloids and Surfaces A: Physicochemical and Engineering Aspects* 302.1-3 (July 2007), pp. 439–448. ISSN: 0927-7757. DOI: 10.1016/J.COLSURFA.2007.03.009.

[87] My Ha Tran, Dieu Phuong Phan, and Eun Yeol Lee. "Review on lignin modifications toward natural UV protection ingredient for lignin-based sunscreens". In: *Green Chemistry* 23.13 (July 2021), pp. 4633–4646. ISSN: 1463-9270. DOI: 10.1039/D1GC01139A.

[88] Ton van Vliet and Hans Lyklema. "Rheology". In: *Fundamentals of Interface and Colloid Science*. Vol. 4. C. Academic Press Inc., 2005. Chap. 6. DOI: 10.1016/S1874-5679(05)80024-8.

[89] Hongliang Wang et al. "From lignin to valuable products–strategies, challenges, and prospects". In: *Bioresource Technology* 271 (Jan. 2019), pp. 449–461. ISSN: 0960-8524. DOI: 10.1016/J.BIORTECH.2018.09.072.

[90] Elisabeth Windeisen and Gerd Wegener. "Behaviour of lignin during thermal treatments of wood". In: *Industrial Crops and Products* 27.2 (Mar. 2008), pp. 157–162. ISSN: 0926-6690. DOI: 10.1016/J.INDCROP.2007.07.015.

[91] Yunqi Yang et al. "An overview of pickering emulsions: Solid-particle materials, classification, morphology, and applications". In: *Frontiers in Pharmacology* 8.MAY (May 2017), p. 235054. ISSN: 16639812. DOI: 10.3389/fphar.2017.00287.

[92] Srinivasa Rao Yearla and Kollipara Padmasree. "Preparation and characterisation of lignin nanoparticles: evaluation of their potential as antioxidants and UV protectants". In: *Journal of Experimental Nanoscience* 11.4 (Mar. 2016), pp. 289–302. ISSN: 1745-8080. DOI: 10.1080/17458080.2015.1055842.

[93] Luis Alberto Zevallos Torres et al. "Lignin as a potential source of high-added value compounds: A review". In: *Journal of Cleaner Production* 263 (Aug. 2020), p. 121499. ISSN: 0959-6526. DOI: 10.1016/J.JCLEPRO.2020.121499.

[94] Zhao Zhang, Vincent Terrasson, and Erwann Guénin. "Lignin Nanoparticles and Their Nanocomposites". In: *Nanomaterials* 11.5 (May 2021), p. 1336. ISSN: 2079-4991. DOI: 10.3390/nano11051336.

[95] Zhao Zhang et al. "The preparation of stable spherical alkali lignin nanoparticles with great thermal stability and no cytotoxicity". In: *International Journal of Biological Macromolecules* 222 (Dec. 2022), pp. 1830–1839. ISSN: 0141-8130. DOI: 10.1016/J.IJBIOMAC.2022.09.272.

List of Figures

List of Tables

Appendix A

Additional information for Chapter 4

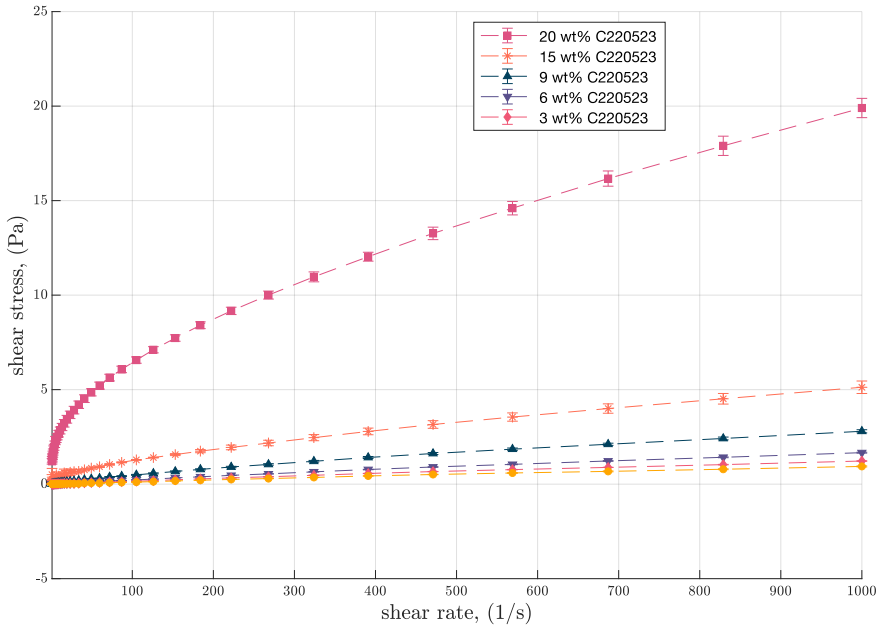

Figure A.1: Shear stress over the shear rate range 1-1000 s^{-1} for the suspension C220523, its dilutions and water at 20°C

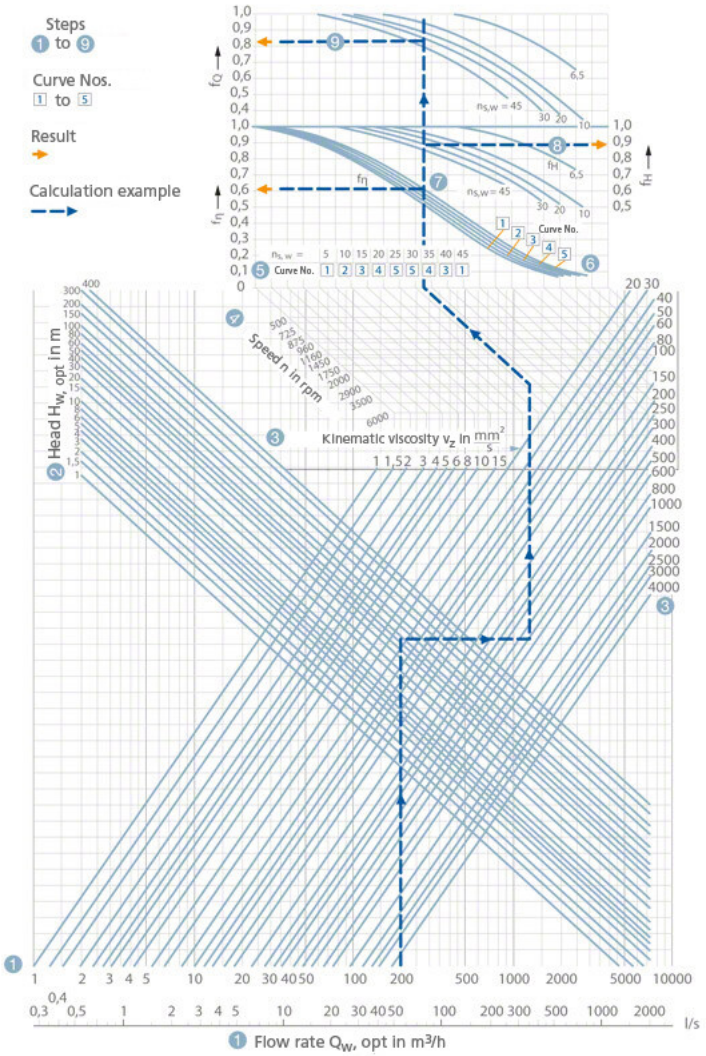

Figure A.2: Diagram for the conversion of characteristic curves of centrifugal pumps with radial impellers pumping water to characteristic curves for pumping viscous fluids, taken from KSB [38]

Appendix B

Additional information for Chapter 5

	Dry matter content *wt%*	**Standard deviation** *wt%*
Trial S_1	9.070	0.005
Trial S_2	9.062	0.029
Trial S_3	9.056	0.017

Table B.1: Dry matter measurements for Trial S_1, Trial S_2 and Trial S_3

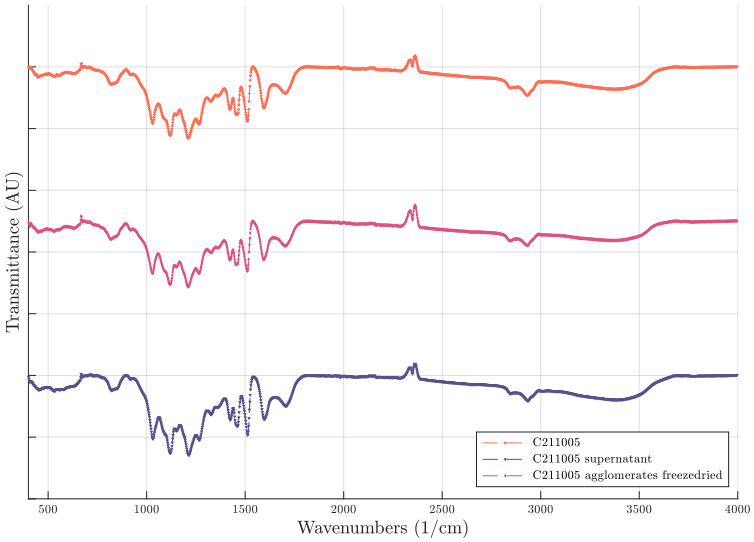

Figure B.1: Results for the FTIR measurment for the suspension C211005 and the temperature treated agglomerates and supernatant for a wavelength range from 400 to 4000 cm^{-1}

SPF			
Hot process			
Measurement	Emulsion 1	Emulsion 2	Emulsion 3
1	35.2370743	11.4316462	18.86
2	38.5003837	24.7455398	27.39
3	74.0956218	17.4574629	30.67
4	40.2808308	19.2753338	16.09
5	48.8009777	28.9123087	23.67
6	43.504322	28.0322178	29.27
7	19.1124717	32.1770229	26.64
8	35.1248113	11.7246423	45.21
9	15.1742322	20.2547907	43.97
10	58.5493515	42.9747467	42.97
Hot-cold process			
Measurement	Emulsion 1	Emulsion 2	Emulsion 3
1	29.14	22.29	13.53
2	21.10	18.87	15.28
3	45.76	9.35	15.34
4	17.14	6.88	10.83
5	26.32	11.85	8.08
6	26.09	25.71	17.43
7	34.39	13.14	11.80
8	37.36	13.26	19.73
9	15.21	14.78	8.87
10	21.79	11.60	17.24
Control sample			
Measurement	Emulsion 1	Emulsion 2	Emulsion 3
1	9.14	14.42	12.22
2	10.57	19.96	19.25
3	8.49	19.24	19.93
4	8.89	19.99	6.40
5	10.64	13.47	8.36
6	8.95	7.37	14.53
7	13.55	12.04	17.54
8	7.13	12.40	25.41
9	9.87	24.88	10.00
10	8.53	29.75	42.71

Table B.2: Results for the ten UV spectroscopy measurement for each emulsion type and its two repetitions